Development of Humidity Sensitive Polyaniline-Polytetrafluoroethylene Conducting Polymer based Split Ring Resonator Metamaterial Structure

Thesis submitted to the

UNIVERSITY OF CALICUT

by

Nees Paul

In partial fulfillment of the requirements
for the award of the degree of

DOCTOR OF PHILOSOPHY

RESEARCH AND POST GRADUATE DEPARTMENT OF PHYSICS,
CHRIST COLLEGE (AUTONOMOUS),
IRINJALAKUDA, THRISSUR - 680125.

NOVEMBER 2019

Format for plagiarism check certificate

UNIVERSITY OF CALICUT
CERTIFICATE ON PLAGIARISM CHECK

1	Name of the research scholar	NEES PAUL		
2.	Title of thesis/dissertation	DEVELOPMENT OF HUMIDITY SENSITIVE POLYANILINE - POLYTETRAFLUOROETHYLENE CONDUCTING POLYMER BASED SPLIT RING RESONATOR METAMATERIAL STRUCTURE		
3	Name of the supervisor	Dr. JOSEPH V. P.		
4	Department/Institution	Research & PG department of Physics Christ College, Irinjalakuda		
5	Similar content (%) identified	Introduction/ Review of literature	Materials and Methods	Result/ Discussion/Summary/ Conclusion
		0%	3%	1%
	Acceptable maximum limit (%)	25 /35	25	10
6	Software used	Urkund		
7	Date of verification	20/11/2019		

**Report on plagiarism check, specifying included/excluded items with % of similarity to be attached.*

Checked by (with name, designation & signature)

Dr. VINOD. V. M
Assistant Librarian(Sr.Scale)
University of Calicut

Name & Signature of the Researcher

Nees Paul

Name &Signature of the Supervisor

DR. V.P.JOSEPH
ASSOCIATE PROFESSOR
HEAD OF THE POST GRADUATE & RESEARCH DEPT. OF PHYSICS
CHRIST COLLEGE, IRINJALAKUDA

The Doctoral Committee* has verified the report on plagiarism check with the contents of the thesis, as summarized above and appropriate measures have been taken to ensure originality of the Research accomplished herein.

Name & Signature of the HoD/HoI (Chairperson of the Doctoral Committee)

DR.MATHEW PAUL UKKEN
PRINCIPAL
CHRIST COLLEGE (AUTONOMOUS)
IRINJALAKUDA

THESIS CERTIFICATE

This is to certify that the thesis titled **Development of Humidity Sensitive Polyaniline-Polytetrafluoroethylene Conducting Polymer based Split Ring Resonator Metamaterial Structure**, submitted by **Nees Paul**, to the University of Calicut for the award of the degree of **Doctor of Philosophy**, is a bona fide record of the research work done by her under my supervision. The contents of this thesis, in full or in parts, have not been submitted to any other institute or university for the award of any other degree.

Dr. V.P. Joseph
Research Guide
Associate Professor
Department of Physics
Christ College (Autonomous)
Irinjalakuda
680125

Place: Irinjalakuda
Date: 28/11/2019

DECLARATION

I hereby declare that the thesis entitled **Development of Humidity Sensitive Polyaniline-Polytetrafluoroethylene Conducting Polymer based Split Ring Resonator Metamaterial Structure**, is an independent work carried out by me and it has not been submitted to any other institute or university for the award of any other degree.

Nees Paul

Place: Irinjalakuda

Date: 28/11/2019

ACKNOWLEDGMENT

First and foremost I thank almighty for his unconditional love, mercy, compassion, blessings and grace for making this Ph D program fruitful and infinitely significant than what I believe to be probable. I would like to thank my guide Dr. V. P. Joseph for pushing me to continue my studies and advising me throughout the process. He gave me opportunities that have bettered myself not only as a researcher but as a human being. I specially take this moment to thank Fr. Dr. Jolly Andrews who joined our team with immeasurable blessings from Almighty to unfurl the research findings into an expression through this volume.

I would like to express my special gratitude to Dr. Mathew Paul Ukken, Principal, and to all my teachers of the Physics family at Christ College who gave me the golden opportunity to do this wonderful work. I am really thankful to them, I came to know about so many new things from them. I take this opportunity to thank the former Principal of Christ College Late Fr. Dr. Jose Thekkan, for being a great principal who builds character, inspires dreams and encourages creativity.

I would also like to thank Dr. Joy V. T. of Chemistry Department, Christ College, for the support and guidance rendered for synthesis of materials. I would also appreciate and honor Dr. Joyce Jose of St. Thomas' College for having this much goodness by spending her valuable time for correcting my papers and giving me constant guidance and support whenever I felt emotionally down.

I also take this moment to thank for the excellent support and earnest help rendered by the management, my colleagues of Physics Department and office staff's at St.Thomas' College, Thrissur throughout my research years.

My special thanks to all the research fellows at EMRL, Christ College for their friendship, encouragement, support and insightful comments. Thanks to all the memorable memories for those light moments in the midst of research life helped to maintain that affable environment necessary to boot my research skills.

Last but not least I would like to express my deepest gratitude to my parents, siblings and friends, without whose warm love, continued patience and endless support this dissertation would not have been possible.

And finally to my husband Linto K. L., who has been by my side throughout these years, living every single minute of it, and without whom, I would not have had the courage to embark on this journey in the first place and to my boys Alvin and Austin for being such good kids and making it possible for me to complete this journey successfully.

Nees Paul

Dedicated to

My beloved parents and my family

Contents

List of Tables

List of Figures

PREFACE

Chapter 1 is the introduction chapter which gives a small review and background for the present study. Starting from the history of metamaterials the classification of materials based on the electromagnetic parameters like permittivity and permeability with a brief note on different types of metamaterials is presented. The factors that result in the negative behaviour in a material like polarization, field distribution and conductivity are discussed further to understand the behaviour of each material in EM field. The theoretical explanation of metamaterials is presented using Drude-Lorentz model. Apart from the EM parameters like permittivity and permeability, the relevance of other material properties like flexibility, conductivity and humidity are discussed. The conventional method for the realization of metamaterials are presented using wire structure, Split Ring Resonators (SRRs) and negative refractive index media. In order to address the problem of present work, further section discusses the criteria for selection of material and the factors affecting the resonance in SRRs. The applications and recent development of metamaterials are mentioned in the last part of the chapter along with a special mention on the recent researches in the field of metamaterials.

Chapter 2 mainly discusses the different measurement techniques used for the physical and electromagnetic behavioural studies of prepared samples of Polyaniline-Polytetrafluoroethylene (PANI-PTFE) conducting polymer and silver thin films. Microwave characterization is mainly done using waveguides, slotted sections, monopole antennas and free space setup. The reflection and transmission coefficients are measured using the Vector Network Analyzer (VNA) in the frequency range of 3-9 GHz. Humidity studies of the sample are performed by placing the sample in a humidity chamber with atomizer-circulating fan setup. The conductivity studies are done using

standard four-probe method and Young's modulus, a measure of mechanical strength is analyzed from load-elongation plots. The structural and morphological studies are done from XRD and SEM images. For numerical simulation studies High Frequency Structure Simulation software is employed.

In **Chapter 3** the preparation and characterization of PANI-PTFE sheet is explained in detail. The Polyaniline (PANI) in powder form is prepared by following the standard chemical oxidation method. This is then rolled into sheet form by using isopropyl alcohol (IPA) and Polytetrafluoroethylene (PTFE) as adhesive and matrix respectively. The sheets of different thicknesses are prepared and their characterization by different methods (as discussed in **Chapter 2**) is explained in detail. Dielectric parameter studies of the sheet are done by measuring the transmission and reflection coefficients using VNA and by employing the Nicholson-Ross Algorithm and are verified using the Cavity Perturbation method. Humidity dependent microwave absorption studies of the sheet presented in this chapter propose its application as a flexible humidity sensitive microwave absorber in 3-9 GHz. For industrial applications, foam type microwave absorber using Polyaniline is also discussed.

Chapter 4 reports the fabrication of PANI-PTFE SRR and their magnetic resonance for metamaterial applications. The circular and square type SRRs show magnetic resonances which is verified using Closed Ring Resonators (CRRs) which have only electrical resonances. The studies carried out for single ring SRR and Broadside-Coupled SRR (BCSRR) using PANI-PTFE resonators are presented. The data is compared with the results from simulation studies. The humidity studies of the conducting polymer SRR is presented for sensor applications. The humidity studies are also done with wire SRR by filling the split region with PANI-PTFE sheet of uniform thickness. With increasing humidity, the conductivity of material increases and

SRR transforms to a CRR and the magnetic resonance disappears. The explanation for observance of wide band resonance for the PANI-PTFE SRR in comparison with equivalent LCR response is interpreted by analyzing the resonance curves of SRRs on lossy substrates and thin film silver SRRs.

With the introduction of thin film SRRs a new addition to the metamaterial resonators in microwave frequencies is reported. The preparation and resonance properties of metallic SRRs, ECSRRs and BCSRRs made with silver thin films of thickness below the skin depth are presented. The results verify LCR nature of SRRs as proposed using PANI-PTFE conducting polymer SRRs. The intense research in thin film technologies to meet the need for miniaturization and quality enhancement of devices and gadgets can be met using our proposed thin film metallic SRR.

In the last chapter which is **Chapter 5** the summary and future works are discussed along with the possible applications and outreach of the present work. Introduction of conducting polymers in the field of metamaterials brings up a new era of highly precise and efficient sensors and devices at microwave frequencies.

CHAPTER 1

REVIEW AND BACKGROUND

This chapter describes a brief history of metamaterials in relation to basic electromagnetic concepts. Classification of materials in terms of permittivity and permeability is presented to show the significance of metamaterial properties. The conduction mechanism involved in various types of materials is also briefed. Split Ring Resonators, which are the negative permeability metamaterial structures are also elaborated in this chapter.

1.1 Metamaterials - Historical perspective

Electric and magnetic forces have been known since antiquity, but they were regarded as separate phenomena for centuries. Scientific understanding into the nature of electric and magnetic forces grew throughout the 18^{th} and 19^{th} centuries with the works of researchers like Ampere, Coulomb, Faraday and Maxwell. It is in the middle of 19^{th} century, Scottish physicist James Clerk Maxwell developed twenty equations to explain electromagnetism, which has now been simplified to four basic formulas known as Maxwell's equations. All the four equations illustrate how an electric/magnetic field propagate through and interact with a particular medium.

The experimental validations of Maxwell's equations by the discovery of radio waves by Heinrich Hertz, led to a conceptual revolution in electrodynamics. Then onwards researchers started working on different techniques and materials for the generation and detection of electromagnetic (EM) waves for communication and for industrial, scientific and medical (ISM) applications. In order to meet the emerging demand for high speed networking and communication applications, intense research leading to technological innovations are pursued in radio and microwave regimes.

Metamaterials, a new class materials with negative properties, show unique electromagnetic properties which lead to a wide range of innovative applications. The conceptual and theoretical analysis of metamaterials commenced in 1967 by Soviet/Russian physicist V. G. Veselago with the publication of his paper entitled "The Electrodynamics of Substances with Simultaneously Negative Values of ε and μ" [1]. Working on this proposal English theoretical physicist J. B. Pendry realized the negative permittivity and negative permeability structures using thin wires and Split Ring Resonator (SRR) structures by the fag end of last millennium [2]. By combining the Pendry's

two structures the first negative index medium was successfully synthesized by D.R. Smith *et al.* in 2000 [3]. This crucial breakthrough in the realization of metamaterials which exhibits unique and exotic characteristics attracted many researchers to the field, thus opening up diverse possibilities in using these materials in emerging technologies. Immense research is taking place in this vibrant branch of electromagnetism where new and useful designs as well as materials are proposed, studied and fabricated for a wide variety of applications.

1.2 The world of metamaterials

Electromagnetic waves are ubiquitous in nature, and its interaction with matter can be represented in terms of Maxwell's equations which are given as,

$$\bigtriangledown \cdot \mathbf{E} = \frac{\rho}{\varepsilon} \tag{1.2.1}$$

$$\bigtriangledown \cdot \mathbf{H} = 0 \tag{1.2.2}$$

$$\bigtriangledown \times \mathbf{E} = -\mu \frac{\partial \mathbf{H}}{\partial t} \tag{1.2.3}$$

$$\bigtriangledown \times \mathbf{H} = \mathbf{J} + \frac{\partial \mathbf{D}}{\partial t} \tag{1.2.4}$$

where $\mathbf{E}$ and $\mathbf{H}$ are the electric field and magnetic flux density respectively, ρ is the volume electric charge density, $\mathbf{J}$ is the electric current density, ε is the permittivity of medium, μ is the permeability of medium and displacement vector $\mathbf{D} = \varepsilon \mathbf{E}$.

Since ε and μ are the deciding factors which determine the response of a material to an electromagnetic wave, based on the values of these two parameters, materials can be broadly classified using a $\varepsilon - \mu$ diagram as given in Fig. 1.1.

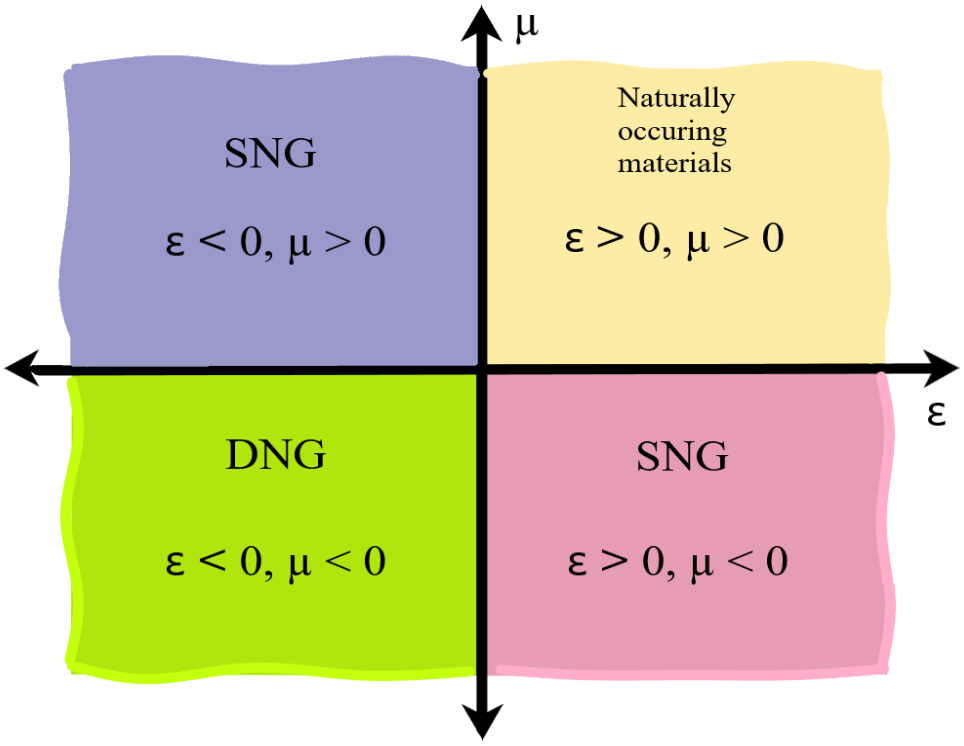

Figure 1.1: Classification of materials according to their permittivity and permeability showing the single negative metamaterials (SNG) and double negative metamaterials (DNG)

Most of the naturally occurring materials come under the quadrant 1 of $\varepsilon - \mu$ curve. The materials in other three quadrants have negative values for permittivity and permeability or at-least for one of them and are called metamaterials. If any one parameter is negative they are called single negative materials (SNG) and if both ε and μ are negative they are named as double negative materials (DNG). As it is evident from the Fig. 1.1 the 2^{nd} quadrant have negative values for ε. Natural plasmas and metals as well as artificially engineered plasma medium fabricated using thin conducting wires [2] and below their plasma frequencies will belong to this category. The materials in the 4^{th} quadrant have negative permeability as shown by certain chiral medium which can be realized using structures like Split Ring

Resonators (SRRs) [3]. The doubly negative materials in the 3^{rd} quadrant are commonly known as Left Handed Materials (LHM), since the propagation vector $\boldsymbol{k}$ is opposite to the energy Poynting vector $\boldsymbol{S}$ in these materials. They are realized by artificial means by combining both the negative permittivity wire structure and negative permeability SRRs to get a negative refractive index medium [4].

1.3 Interaction of EM field with matter - Conduction mechanism

When an EM field interacts with a medium, different currents developed in the material depend on factors like ε, μ and the ionic/electron conductivity. The ε related contribution to the current are due to polarization current and the displacement current whereas μ related current is due to magnetization current [5]. The conduction process in different materials is briefly explained below.

1.3.1 Metals

The conduction mechanism in metals is due to the presence of free electrons. In the presence of a *d.c.* field electrons move opposite to the field direction with an average drift speed, causing a *d.c.* current. On the other hand, when metals interact with an EM field, electrons try to oscillate in accordance with the frequency of the signal, causing an *a.c.* current which is a surface current mainly confined within the skin depth region [5].

1.3.2 Ionic crystals

Conduction in ionic crystals is by the movement of anions and cations from one site to another in an aqueous solution. Here conductivity is influenced by the carrier concentration and the carrier mobility. Intrinsic conduc-

tivity depends upon temperature of the crystal which in turn increases the carrier concentration, while the extrinsic conductivity of the crystal attained due to doping can be varied by changing the dopant and doping concentration. Here, free ions will contribute to induced current on interaction with the EM field [6].

1.3.3 Dielectrics

These are also called electrical insulators. In this type of materials the applied electromagnetic field will result in different types of polarization as explained below, which in turn produces the corresponding polarization currents [7, 8].

1. Electronic polarization: The displacement of the center of mass of electron cloud relative to the center of positively charged nucleus, under the influence of the electric field component of the applied EM field will cause electronic polarization.

2. Ionic polarization: This is caused by the displacement of cations and anions from their mean positions in opposite directions when the medium is placed in an EM field.

3. Orientation polarization: It is the characteristic of polar dielectrics like water arising due to the alignment of permanent electric dipole moment along the applied field direction.

4. Space charge polarization: This type of polarization is mainly observed in heterogeneous materials containing semiconducting impurities where the charges migrate within the impurity regions and get themselves stored at inter-phases. The charges trapped at grain boundaries will get displaced on interaction with the applied electric field.

1.3.4 Conducting polymers

Among different variants of organic polymers, conducting polymers gained special attention owing to their ability to conduct electricity mainly due to the existence of single-double bond conjugation (π bond). But the conductivity attained by the electron transfer mechanism [9] through the organic chain is relatively low and can be enhanced by different doping techniques [10].

The doping in conducting polymers will trigger electron-phonon interaction, which subsequently result in the formation of quasi-particle states like solitons, polarons and bi-polarons [11]. The two important doping methods of interest are acid doping and metallic doping. In acid doping the space charge oscillations in the attached anions and cations will enhance the current conductivity in a considerable manner [12]. In the case of metallic doping, the conductivity is still more enhanced owing to the presence of highly conducting metal nano particles. In the presence of the attenuating field, the above mentioned electronic as well as space charge currents will generate frequency dependent current effects [13, 14].

1.4 Theoretical model for EM wave interaction

In order to study the property/behaviour of a medium, its interaction with the EM wave in the microscopic levels has to be considered. The classical theory of electromagnetic interaction with metals and dielectrics is explained below using the Drude-Lorentz model [7].

1.4.1 Drude-Lorentz model

Atoms are considered to behave like a spring with stretching and compression forces existing between the heavy nucleus and the lighter electron of mass m. When an electric field ($\mathbf{E}$) interact with the atom it gets polarized

resulting in a net displacement vector ($\mathbf{D}$) inside the medium given by

$$\mathbf{D} = \varepsilon_0 \mathbf{E} + \mathbf{P} \tag{1.4.1}$$

ε_0 is the permittivity of free space, and $\mathbf{P}$ is the polarization vector which is given by

$$\mathbf{P} = \varepsilon_0 \chi \mathbf{E} \tag{1.4.2}$$

where χ is the electrical susceptibility [5]. The equation for $\mathbf{D}$ then changes to

$$\mathbf{D} = \varepsilon_0 (1 + \chi)\mathbf{E} = \varepsilon_0 \varepsilon_r \mathbf{E} \tag{1.4.3}$$

where ε_r is the complex permittivity .

The frequency (ω) dependent value of the complex permittivity of a lossy medium is given by [5, 15]

$$\varepsilon_r(\omega) = 1 + \frac{i\sigma}{\omega\varepsilon_0} \simeq 1 - \frac{\omega_p^2}{\omega^2} \tag{1.4.4}$$

where σ is the conductivity of the medium. The resonant plasma frequency ω_p is

$$\omega_p = \sqrt{\frac{ne^2}{m\varepsilon_0}} \tag{1.4.5}$$

where n is the electron density and e is the electronic charge.

The real and imaginary parts of the complex permittivity gives the measure of stored and dissipated energies respectively and can be written as

$$\varepsilon_r^{'}(\omega) = 1 + \omega_p \frac{\omega_0^2 - \omega^2}{(\omega_0^2 - \omega^2)^2 + \omega^2\gamma^2} \tag{1.4.6}$$

$$\varepsilon_r^{''}(\omega) = \omega_p^2 \frac{\omega\gamma}{(\omega_0^2 - \omega^2)^2 + \omega^2\gamma^2} \tag{1.4.7}$$

where γ is the damping factor.

Similarly the complex permeability can be evaluated from the magnetization produced as

$$\mu_r = 1 + \frac{\omega_{pm}^2}{\omega_{0m}^2 - \omega^2 - i\gamma_m\omega} \tag{1.4.8}$$

Here ω_{pm}, ω_{0m} and γ_m are the magnetic plasma frequency, magnetic resonance frequency and the magnetic damping factor respectively. For non-magnetic materials the value of μ_r is 1.

1.5 Realization of metamaterials

Metamaterials can be defined as promising artificial and engineered structures having unique properties consisting of nano and/or micro-scale metallic or dielectric resonant building blocks or particles with periodicity very much less than the interacting wavelength which support incoming strong EM field resonances in the optical and microwave frequencies. The three dimensional and large scale fabrication of metamaterials is one of the main challenges faced by the researchers in the realization of metamaterials. Another difficulty is in the realization of wide band negative μ structures since they are often of very narrow bandwidth.

The initial attempts for the realization of metamaterials were carried out in microwave regime. Artificial negative ε structures are usually realized in the form of low density plasma medium constructed using an array of thin conducting wires [2]. Its counterpart, negative μ structures are materialized using specially designed magnetically active resonating meta-molecule called Split Ring Resonator (SRR) [2, 3, 4, 15].

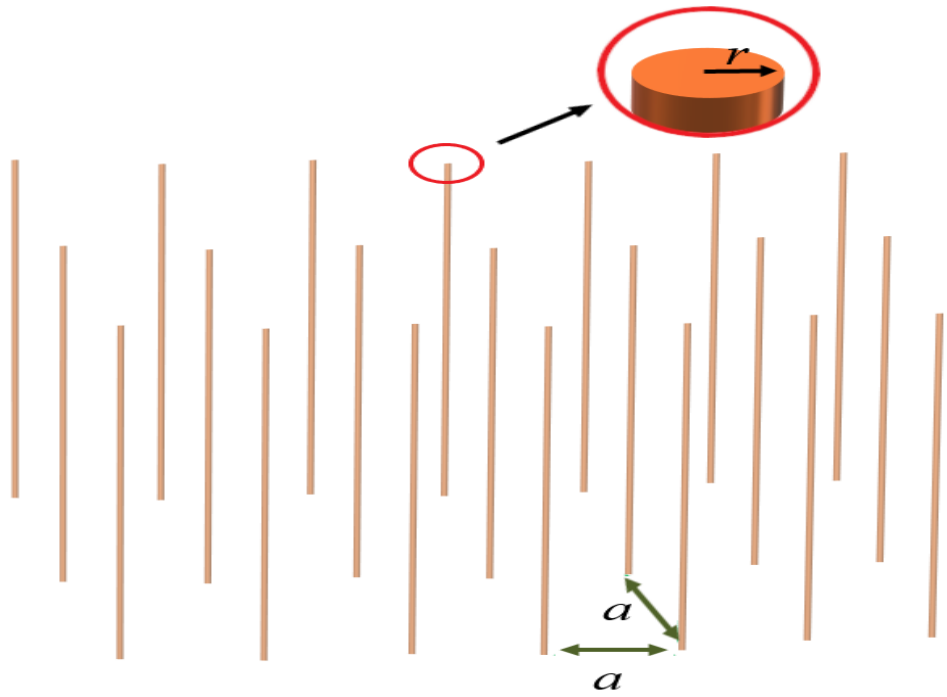

Figure 1.2: Schematic diagram of wire (radius r) structure showing lattice spacing a.

1.5.1 Wire structure

From the Drude-Lorentz model (Section 1.4.1) it is clear that if the resonant frequency is below plasma frequency (ω_p), the complex permittivity of the medium is negative (Eqn. 1.4.4). For realizing negative ε in the microwave frequencies, an array of conducting metallic thin wires with periodicity much less than the wavelength of applied EM wave is used and its plasma frequency is observed to be a function of effective mass and average electron density (Eqn. 1.4.5) [16]. A periodic array of wire structure is given in Fig. 1.2.

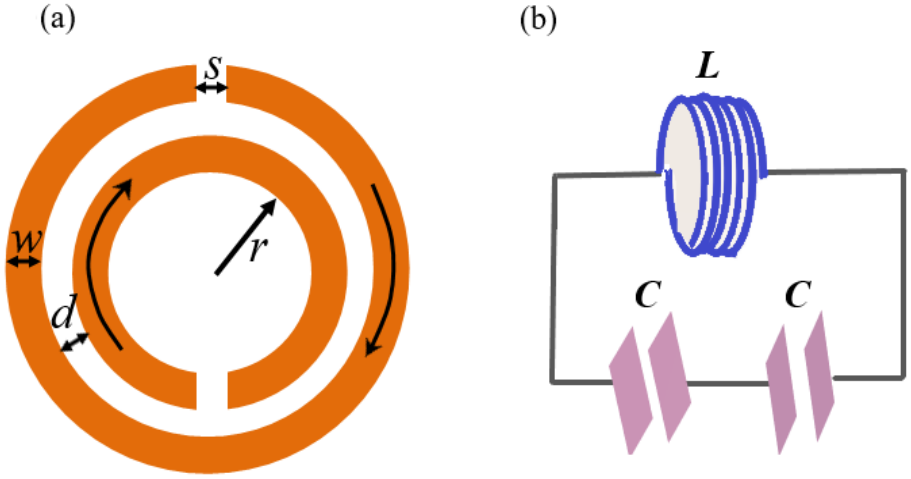

Figure 1.3: Schematic diagram of ECSRR and the corresponding equivalent circuit.

1.5.2 Split Ring Resonator (SRR)

The micro-structured Split Ring Resonator (SRR) medium proposed by Pendry *et al.* strongly respond to an incident alternating magnetic field near its magnetic plasma frequency (ω_{pm}) [2, 17]. The most popular such anisotropic structure, with enhanced non linearity, consists of two concentric metallic rings separated by a gap, both of which have splits at the opposite sides is depicted in Fig. 1.3(a). The split in the structure reduces most of the resonance related electrical activity due to the discontinuity in electrical path [18, 19].

The SRR meta-particle will have an intrinsic inductance (L) and capacitance (C) which can be explained as follows. Each ring will have contributions from its self inductance along with a mutual inductance, due to the mutual coupling. The value of effective inductance depends on the width and radius of rings and the spacing between them [20, 21].

The splits on the rings prevent the continuous flow of currents around

the rings which causes charge accumulation near the split ends leading to a capacitive effect. But the major contribution is from the mutual capacitance existing between the rings. The effective intrinsic capacitance is also seen to be strongly depending on the structural parameters of SRR [2, 22].

In the presence of an external electromagnetic field with its magnetic field component perpendicular to the plane of the rings, currents will be induced in the rings so that the SRR particle act as a LC oscillator. Figure 1.3(b) shows an equivalent circuit proposed for the analysis of SRR [23].

1.5.3 Negative refractive index medium

As devised by Pendry and realized by Smith, the negative refractive index medium can be constructed by periodic arrangement of wire structure and Split Ring Resonator structures (Fig. 1.4) [24, 25]. The basic unit cell size and periodicity should be much smaller than the applied wavelength for maintaining homogeneity of the medium. Bulk response will be entirely different from the response of constituent unit cells [26, 27, 28]. Metamaterials with negative refractive index show unique and remarkable properties like reversal of Snell's law and inverse Doppler effect [29].

1.6 Trends in applications of metamaterials

The developments in the field of metamaterials and their immense applications have contributed much to the disciplines of Physics and Engineering. The research breakthroughs so far and the vision for future can be consolidated as given below.

1. Sensing systems: Easy and rapid detection of signal by metamaterials due to the enhancement and localization of fields make it a highly selective and sensitive sensor for real time applications compared to conventional ones [30, 31]. Since the resonance of SRRs, the nega-

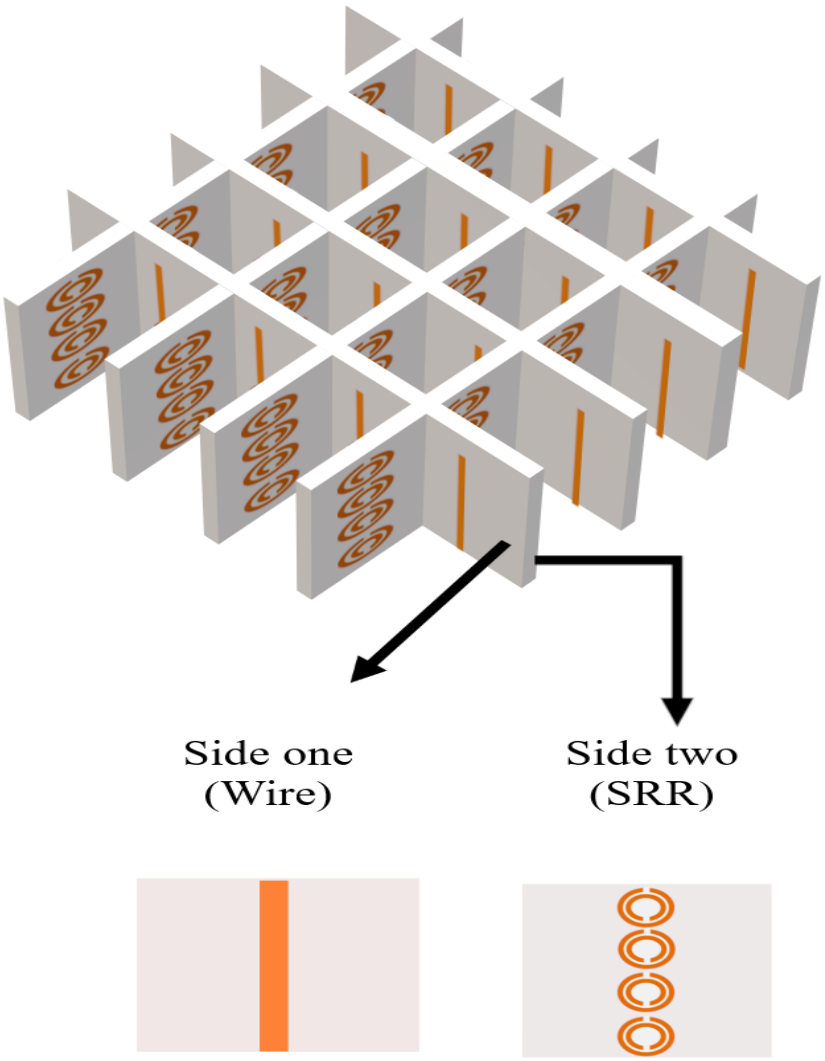

Figure 1.4: Schematic representations of the arrangement of wire and SRR structures on the opposite sides of the substrate to form a 2-Dimensional negative index medium

tive permeability meta-structures, depend strongly on geometrical parameters, the variation in physical parameters like humidity [32, 33], temperature [34, 35, 36] and pressure [37] can be easily monitored.

2. Communication systems: The entry of the novel metamaterials have initiated the modernization of the field of communication by bringing in miniaturization, better efficiency and high speed into the scenario [38, 39, 40].

3. Super lenses: Since metamaterial based flat lens will converge the evanescent waves, researches in the enhancement of image quality is progressing in a rapid manner so that in the near future a 'perfect lens' may be a reality [41, 42, 43, 44].

4. Super resolution: By using metamaterial inspired techniques, attempts have been made to break the diffraction limit by which a super resolution technique is expected to be realized in the near future [45, 46].

5. Cloaking: By channelizing the wave guiding properties of metamaterials, scientists are in pursuit of a cloaking mechanism leading to 'invisibility' [47, 48, 49].

1.7 Types of Split Ring Resonators

The SRRs are fabricated in different shapes and orientations in order to tap maximum energy from the interacting magnetic field. The first self consistent and quasi analytical modeling of negative μ materials is done using Edge-Coupled Split Ring Resonators (ECSRRs) [2] and Broadside-Coupled Split Ring Resonators (BCSRRs) [50].

Other commonly used structures are Wire SRR [51], Spiral SRR [52, 53], Triangular SRR [54] which along with their variants are schematically

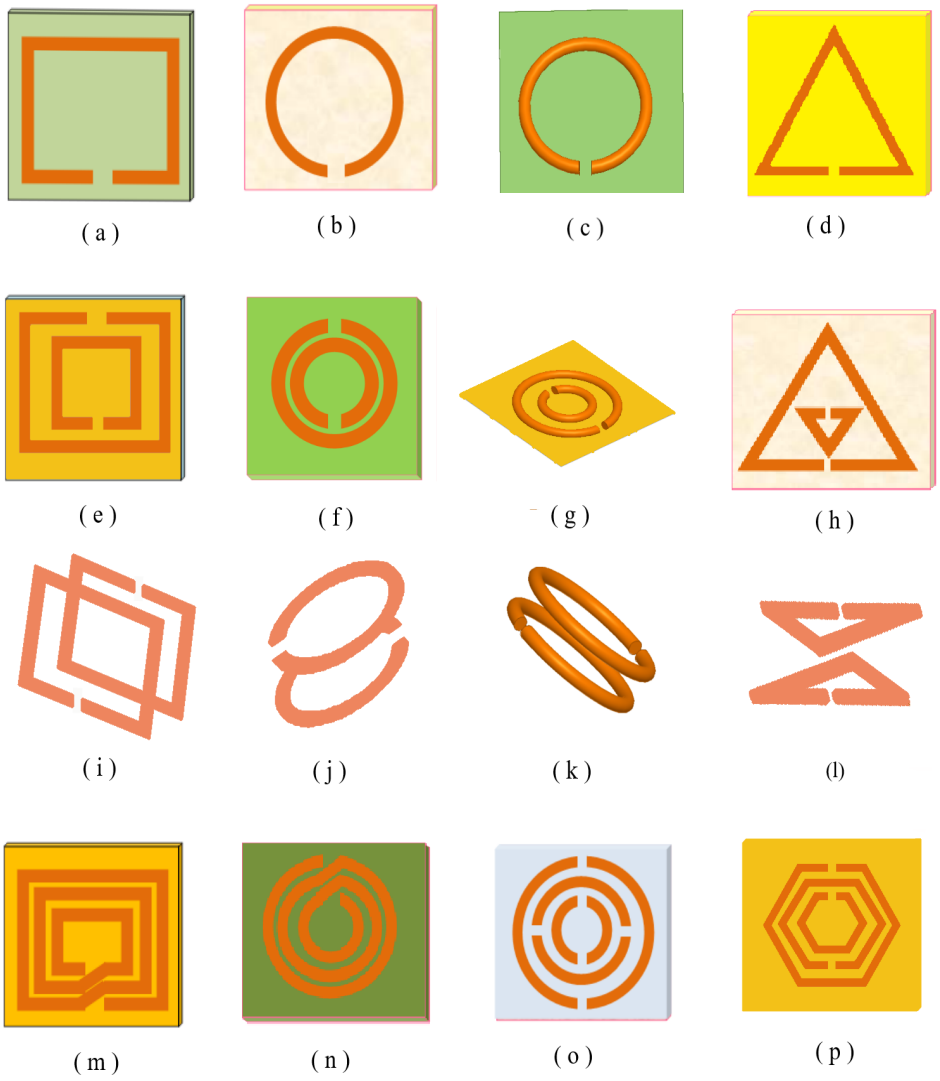

Figure 1.5: Schematic representations of the basic types of split ring resonators - Single split ring resonators: (a) square (b) circular (c) wire (d) triangular; ECSRR: (e) square (f) circular (g) wire (h) triangular; BCSRR: (i) square (j) circular (k) wire (l) triangular; Spirals: (m) square (n) circular; (o) multi-split circular; (p) hexagonal.

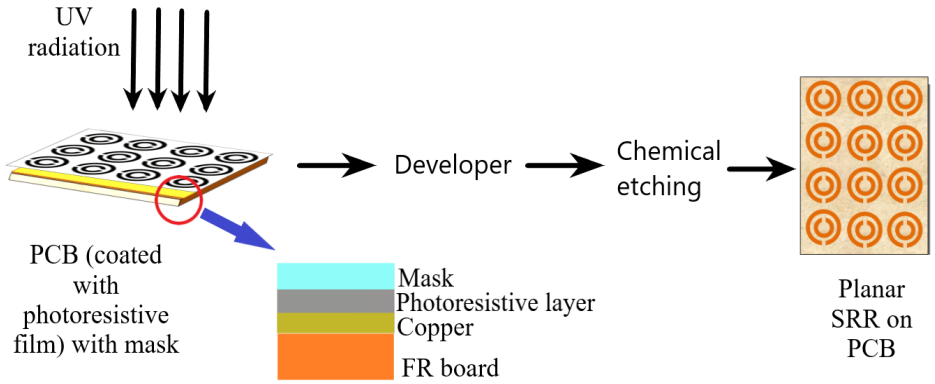

Figure 1.6: Schematic representation of the photo-chemical etching process.

represented in Fig. 1.5. Flexible SRR is another addition to this category with specific applications [55].

1.8 Materials and methods used for the fabrication of SRR structures

This section briefly describes different materials and methods used for fabrication of microwave metamaterials.

As already discussed, electromagnetic parameters depend upon the conductivity/electron density of the medium. The metals like gold, silver and copper having high conductivity are mainly used for the realization of SRRs with an approximation of zero damping (resistive) losses in LC circuit resulting in a narrow resonance curve with high quality factor (Q factor) [56, 57].

In order to fabricate microwave passive devices using SRRs different methods and techniques are adopted out of which the planar photo-chemical etching is the most prevalent one [4, 58]. Here SRRs are printed on low loss dielectric substrates such a Fire Resistant (FR) Printed Circuit Board (PCB)

by following the steps as shown in Fig. 1.6.

Another more precise method is the circuit printing technology using computer assisted milling method, used for bulk production of resonators on printed circuit boards. It does not provide much flexibility in the selection of substrates which highlight the importance of photo-chemical etching.

1.9 Magnetic and electric resonances

In the presence of an EM field, the SRR can show electric and magnetic responses which will result in corresponding resonance effects. The electric resonance of SRR can be explained by considering the equivalent electrical length of SRR in the direction of electric field component of EM field as per Drude-Lorentz model (Section 1.4.1). On the other hand, the effect of magnetic component perpendicular to the plane of SRR induces magnetic resonances in the structure [2].

The electrical field created by the magnetic response and magnetic field created by the electrical response will interact with each other and will result in a bi-anisotropic coupling effect [59]. An Edge-Coupled Split Ring Resonator (ECSRR) with two concentric rings shows bi-anisotropic effects leading to the appearance of clear electric and magnetic resonant absorptions at different frequencies as depicted in Fig. 1.7 [60, 61, 62].

In order to reduce the bi-anisotropic effects, the ring structures are modified to Broadside-Coupled Split Ring Resonator (BCSRR) or to Spiral resonators wherein the electric resonance effects are reduced considerably. At the same time for a Closed Ring Resonator (CRR), where there is no split, the magnetic resonance effect is negligibly small in comparison with its electrical counterpart [63, 59, 64, 65].

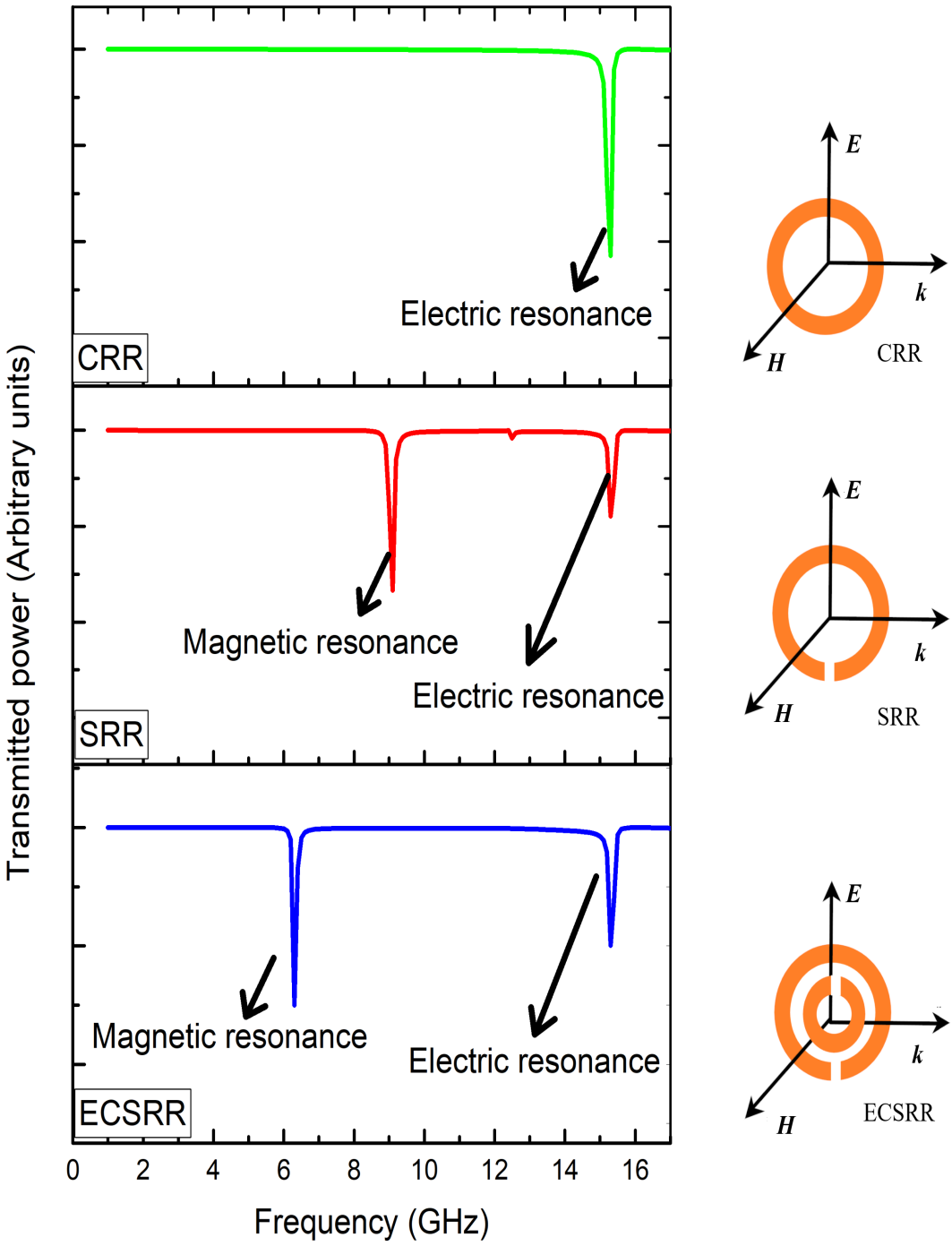

Figure 1.7: Observance of electric and magnetic resonance in CRR, single ring SRR and ECSRR.

1.9.1 Magnetic resonances in Split Ring Resonators

Split ring resonator act as a LC oscillator circuit and its magnetic resonance frequency is given by

$$f = \frac{1}{2\pi\sqrt{LC}} \tag{1.9.1}$$

where L and C are its intrinsic inductance and capacitance respectively as mentioned earlier.

Various empirical relations are proposed by different research groups for L and C [29]. L is formulated in terms of self inductance and mutual inductance terms. Different empirical formulas are suggested for C wherein the effect of split and gap capacitance only are considered [18]. A more accurate approach by considering the capacitance from both planar surfaces of the SRR structure was formulated by Chakyar *et al.* [66]. Since intrinsic L and C values strongly depend on the structural parameters of SRR, resonant frequency variations were observed in different variants of SRR structures.

1.9.2 Factors affecting the resonance

The important factors which affects resonance frequency of SRR [63, 67] are discussed below .

1. Effect of split width (s): Increase in the split width increases the resonance frequency of the SRR structure, since the split region behaves as a parallel plate capacitor. As the split width s (Fig. 1.3) increases, the capacitive effects due to splits will decrease, which in turn increases the resonance frequency of the structure.

2. Effect of gap distance (d): The major contribution to the capacitance of SRR is from the capacitance between the rings of SRR. So, any slight

change in the distance between the rings will cause noticeable variation in resonance frequency due to the resulting variation in mutual inductance.

3. Effect of ring width (w): The effect of ring width can be determined by approximating the SRR as a parallel plate capacitor. When the ring width - which is the measure of area - increases, there will be a corresponding increase in the capacitance and the resonant frequency will decrease accordingly.

Dielectric properties of the substrate on which SRR is fabricated will also affect the effective capacitance and hence the resonance frequency of the structure [50, 67]. Other environmental factors like temperature [68] and humidity will also influence it.

1.10 Aim of the study

Everything is new and exciting in metamaterial world. In this work a novel Split Ring Resonator (SRR) metamaterial structure using the conducting polymer Polyaniline (PANI) is introduced. Polyaniline is usually available in powder form which need to be made into a sheet form to fabricate it into an SRR. This requirement is fulfilled using a Polytetrafluoroethylene (PTFE) matrix.

The thesis focus mainly on the fabrication and characterization of these metamaterial resonator structures made using PANI-PTFE material. The magnetic resonances are verified by comparing the transmission curves of CRR with SRR and its variants. The effect of the variation of geometrical parameter are studied and compared with the conventional metallic SRRs. The role of capacitive coupling is studied using Broadside-Coupled SRRs (BCSRRs) made using these polymers and its results are compared with the

metallic BCSRR counterparts. The results are also verified using simulation studies.

The resistive behaviour of the polymer resonators are analyzed using the resonance curves of resistive thin film metallic resonators. The other key factor which is studied is the humidity dependent microwave responses of these structures. The application of this material as absorbers and sensors is also studied.

1.11 Scope of the study

The study intends to introduce the conducting polymers into the world of metamaterials so that the specific properties as well as the resonance frequency tunability of these materials are utilized to widen the scope of the metamaterial based applications.

1.12 Organization of thesis

This thesis is divided into 5 chapters. A chart representing the thesis organization is shown in Fig. 1.8.

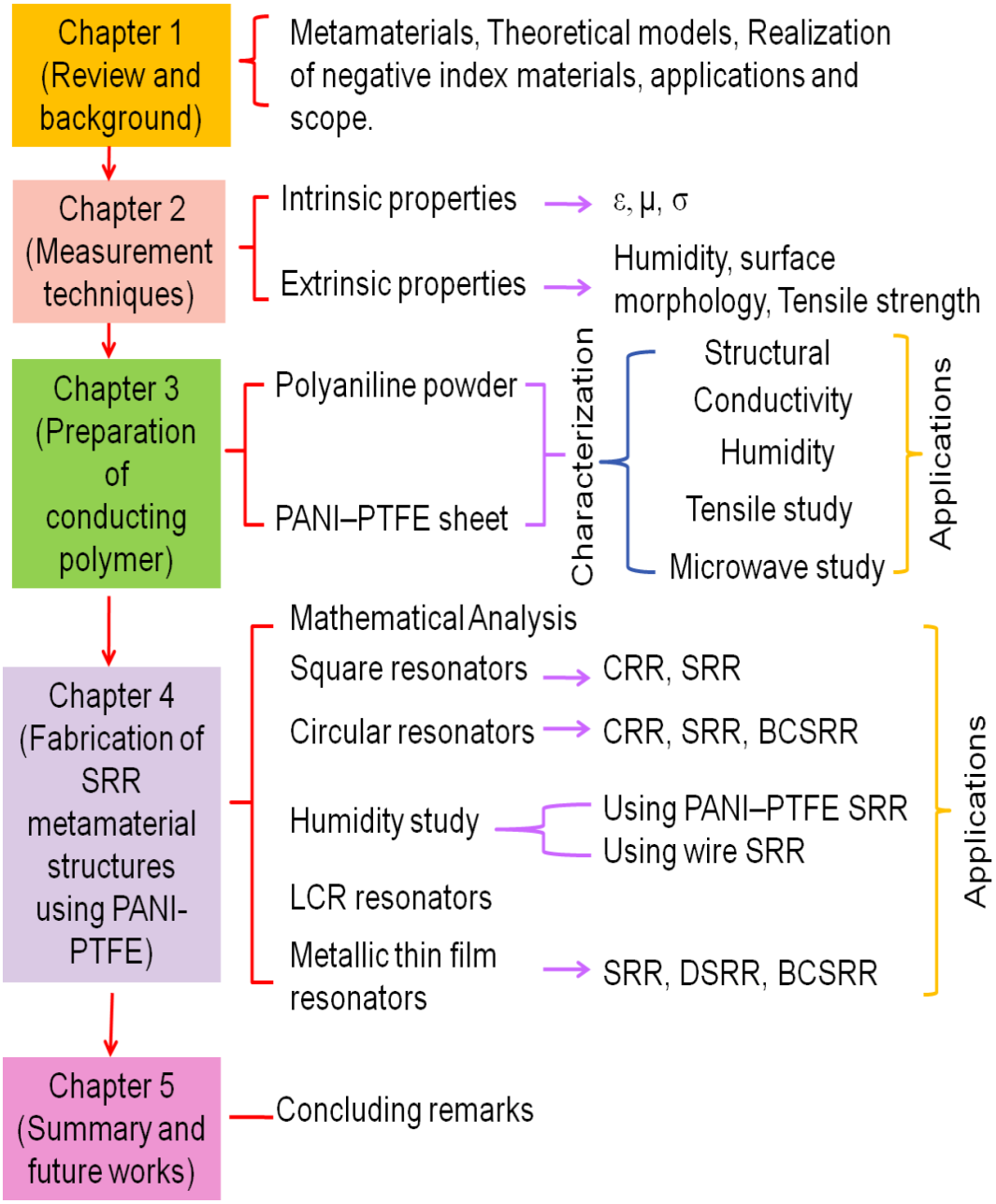

Figure 1.8: Chart representing the organization of the thesis.

CHAPTER 2

MEASUREMENT TECHNIQUES

This chapter summarizes different experimental techniques and setups used for the characterization of the conducting polymer samples, developed for the study. It also describes the methods employed for the measurement of resonant properties of SRR fabricated for the study. Most of the instruments are of conventional type and some of them are improvised for the study. The basic theory behind the measurement techniques and the simulation methods used are also discussed in brief.

This chapter focus on the measurement techniques employed for the characterization of different samples used for the study. The methods used to study the resonance properties of different types of SRRs are also detailed.

2.1 Structural and morphological characterization

2.1.1 X-Ray diffractometer

The atomic planes of the crystal cause the reflected beams of X-ray to interfere with one another as they leave the crystal. This phenomenon is called X-ray diffraction. This is based on Bragg's diffraction law,

$$n\lambda = 2dsin\theta \tag{2.1.1}$$

where λ is the wavelength of the incident beam, d is the distance between atomic layers in the crystal, and n is an integer. X-Ray diffractometer (XRD) gives the direct evidence for the periodic atomic structure of crystals [7]. The samples were analyzed using XRD equipped with CuK_α ($\lambda = 1.54$ A^0). They are scanned at a rate of 2^0 per minute and the angle 2θ ranges from 5^0 to 80^0. XRD pattern taken for PANI powder and PANI-PTFE sheet to analyze the extent of crystalline nature of the samples.

2.1.2 Scanning Electron Microscope

The surface morphology of the samples were investigated using Scanning Electron Microscope (SEM), JOEL-JSM-6390LA. This is a high resolution easy-to-operate SEM which employs a field emission gun as the electron source producing radio-frequency (RF) energy and employing modern computer facilities for the results. SEM image of the experimental sample of PANI-PTFE sheet was taken to check the surface morphology.

2.2 Conductivity: Four-probe method

To analyze variation of conductivity with temperature of samples, conductivity - temperature study was carried out using standard four-probe method. The oven used can increase the temperature of the sample up to 200^0C and the digital voltmeter used can measure the voltage up to 100 mV. The experimental set up employs a constant current generator of 100 mA. The basic equation used for the study is

$$\sigma = \sigma_0 f(w/s) \tag{2.2.1}$$

$$\sigma_0 = \frac{I}{2Vs\pi} \tag{2.2.2}$$

where σ is the conductivity, V is the voltage drop across the probes, I is the corresponding current and $f(w/s)$ is a function which depends upon the thickness of the sample (w) and the separation between the adjacent probes (s). Since w/s is very small, the function $f(w/s)$ can be approximated to $(2s/w)log_e2$. PANI-PTFE sheet samples of different thicknesses were analyzed using this method.

2.3 Humidity: Atomizer-circulating fan setup

For analyzing the humidity dependent properties a rectangular humidity chamber was constructed using Perspex sheet and the humidity was regulated using an atomizer-circulating fan setup. The relative humidity of the chamber can be varied between 30% to 90%. The possible changes in the *d.c.* conductivity in relation to various humidity conditions were measured by keeping the PANI-PTFE sheet sample inside a humidity chamber setup as shown in Fig. 2.1.

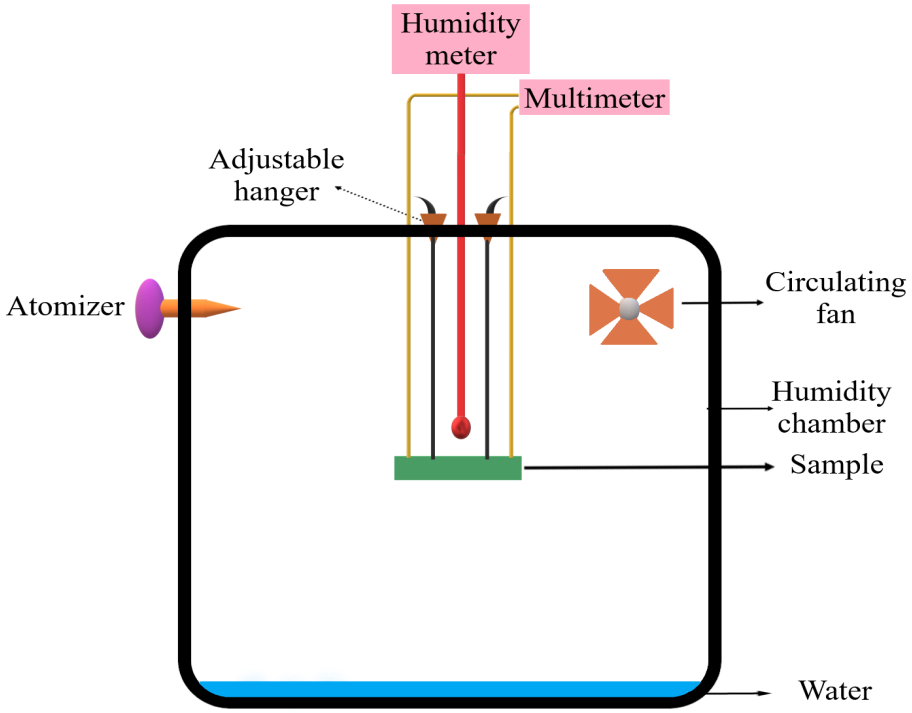

Figure 2.1: Pictorial representation of atomizer-circulating fan setup for measuring the effect of varying the humidity of the sample.

2.4 Mechanical strength: Young's modulus

In order to measure the mechanical strength of the material the Young's modulus of the prepared PANI-PTFE sheet samples with specific width and length were evaluated using the conventional load-extension technique. The elongation of sample is measured for loads up to 100 gms. The measurements are done for loading and unloading. The basic equation employed for the experiment is

$$Y = \frac{mgl}{Ae} \tag{2.4.1}$$

where Y is the Young's modulus of the material, m is the load, g is the acceleration due to gravity, A is the cross sectional area and e is the elongation.

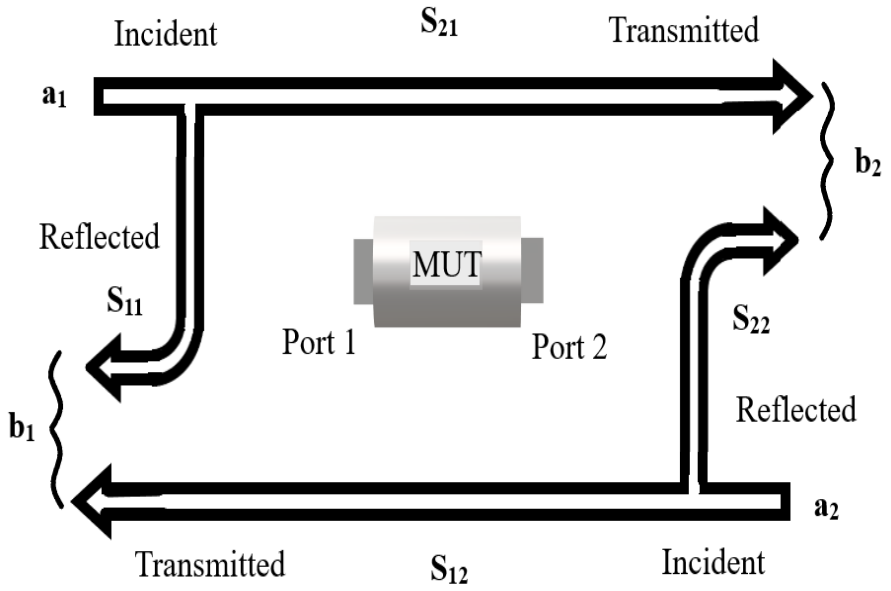

Figure 2.2: Schematic diagram showing the measurement of S-parameters of a 2-port device.

2.5 Microwave characterization studies: Vector Network Analyzer

Microwave response of a material in terms of scattering parameter (S-parameters) [69] can be studied by using a Vector Network Analyzer (VNA). S-parameters do not require any mechanical connection of undesirable loads to the material under test (MUT) and describes how MUT modifies the signal. A two-port device has four S-parameters as shown in Fig.2.2.

These S-parameters are measured using Network Analyzer which automatically switches the internal source and receivers to make both forward and reverse measurements. When the signal comes from port 1, the measurement is said to be in the forward direction and when the signal is from port

Figure 2.3: Photograph of Vector Network Analyzer used for transmission and reflection measurements.

2, the measurement will be in the reverse direction. S_{11} and S_{22} reflection coefficients are used to analyze the reflection component from the MUT. S_{21} and S_{12} transmission coefficients are used to measure the loss or gain through a MUT over a specified frequency range. The matrix equation presenting the S-parameters is

$$\begin{bmatrix} b_1 \\ b_2 \end{bmatrix} = \begin{bmatrix} S_{11} & S_{12} \\ S_{21} & S_{22} \end{bmatrix} \begin{bmatrix} a_1 \\ a_2 \end{bmatrix} \tag{2.5.1}$$

where a_1, b_1, a_2 and b_2 are the components of transmitted and reflected power from port 1 and port 2 respectively (Fig.2.2). Here in this study RF Vector Network Analyzer N9923A of Agilent Keysight (Fig.2.3) is used.

2.5.1 Dielectric parameters

As already mentioned in Chapter 1, microwave properties of any material can be characterized by the measurement of their dielectric properties. The measure of energy stored inside the material in an applied electromagnetic field is indicated by the dielectric constant. Since dielectric parameters are intrinsic properties of every material, its accurate measurement helps improved quality control in research and development. A knowledge of this helps in the design of absorbers, sensors, EM circuits etc. Understanding the dielectric parameters of materials is also important to numerous industrial applications. Out of many methods available for the determination of dielectric constant the prominent ones are, Coaxial Probe Method, Transmission Line Method, Free space Method and the Resonant Cavity Perturbation method [70]. Here the Resonant Cavity Perturbation method, which is one of the most popular methods, is discussed in detail.

2.5.2 Cavity Perturbation method

Slotted cavity resonators for measuring the complex relative permittivity ε, and the complex relative permeability μ are formed by cutting a non-radiating narrow section on the top side of the rectangular copper waveguide with both ends covered by a pair of copper plates with provision for iris coupling as shown in Fig. 2.4.

The narrow slot on the top of the wave guide has negligible effect on changing the field configuration inside the cavity [71, 72, 73, 74]. The insertion of a small sample into the bounded cavity will result in a field distribution inside the resonator given by

$$\mathbf{E}^{'} = (\mathbf{E_0} + \mathbf{E_1})e^{j(\omega+\delta\omega)t} \tag{2.5.2}$$

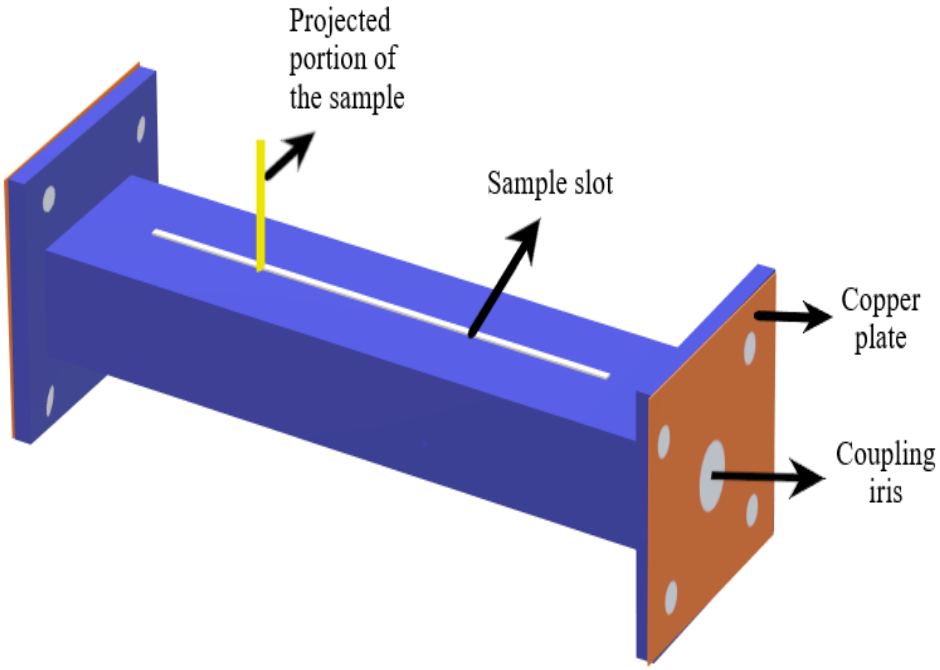

Figure 2.4: Labeled schematic representation of slotted cavity section with sample.

$$\mathbf{H}' = (\mathbf{H_0} + \mathbf{H_1})e^{j(\omega+\delta\omega)t} \tag{2.5.3}$$

where $\mathbf{E_0}$ and $\mathbf{H_0}$ are the unperturbed fields and $\mathbf{E_1}$ and $\mathbf{H_1}$ are the additional fields caused due to perturbation effects corresponding to a change in resonant frequency ($\delta\omega$). The above equations (Eqns. 2.5.2 and 2.5.3) are solved using perturbation theory with the stipulations that $\delta\omega << \omega$ and $\mathbf{E_1}$ and $\mathbf{H_1}$ are small compared to $\mathbf{E_0}$ and $\mathbf{H_0}$ except in the neighbourhood of sample as proposed by Waldron [74] and the resultant relative change in the resonant frequency is given by

$$\frac{\delta\omega}{\omega} = \frac{\int\int\int_{V_s}[(\mathbf{E_1}.\mathbf{D_0} - \mathbf{E_0}.\mathbf{D_1}) - (\mathbf{H_1}.\mathbf{B_0} - \mathbf{H_0}.\mathbf{B_1})]dV}{\int\int\int_{V_0}(\mathbf{E_0}.\mathbf{D_0} - \mathbf{H_0}.\mathbf{B_0})} \tag{2.5.4}$$

Here V_0 is the volume of the cavity and V_s is the volume of the sample, $\mathbf{B_0} = \mu_0\mathbf{H_0}$, $\mathbf{B_1} = \mu_0\mathbf{H_1}$, $\mathbf{D_0} = \varepsilon_0\mathbf{E_0}$ and $\mathbf{D_1} = \varepsilon_0\mathbf{E_1}$.

$\frac{\delta\omega}{\omega}$ is a complex quantity which is related to the changes in the resonance frequency $\delta\Omega$ and the quality factor Q of the cavity through the relation

$$\frac{\delta\omega}{\omega} = \frac{\delta\Omega}{\omega} + \frac{j}{2}[\frac{1}{Q_s} - \frac{1}{Q_0}] \tag{2.5.5}$$

where Q_s and Q_0 are the quality factors of the loaded cavity and unloaded cavity respectively. Quality factor Q is given by

$$Q = \frac{f}{\triangle f} \tag{2.5.6}$$

where f is the resonant frequency and $\triangle f$ is the frequency shift corresponding to 3 dB bandwidth and

$$\frac{\delta\Omega}{\omega} = \frac{f_s - f_0}{f_s} \tag{2.5.7}$$

where f_s and f_0 are the resonance frequencies with and without sample in the cavity respectively. Nature of response curve with and without sample is represented in Fig. 2.5.

Equations 2.5.4 can be further simplified for material with complex permittivity $\varepsilon_r = \varepsilon_r^{'} - j\varepsilon_r^{''}$ and complex permeability $\mu_r = \mu_r^{'} - j\mu_r^{''}$, as

$$-\frac{\delta\omega}{\omega} = \frac{(\varepsilon_r - 1)\int_{V_s}\mathbf{E_1}.\mathbf{E_0}dV + (\mu_r - 1)\int_{V_s}\mathbf{H_1}.\mathbf{H_0}dV}{\int_{V_0}\mathbf{E_1}.\mathbf{E_0} + \int_{V_0}\mathbf{H_1}.\mathbf{H_0}dV} \tag{2.5.8}$$

From the above equations the parameters like permittivity [75, 76, 77, 78] and permeability [79] of the dielectric sample can be obtained by using the following expressions

$$\varepsilon_r^{'} = 1 + \frac{f_0 - f_s}{2f_s}(\frac{V_c}{V_s}) \tag{2.5.9}$$

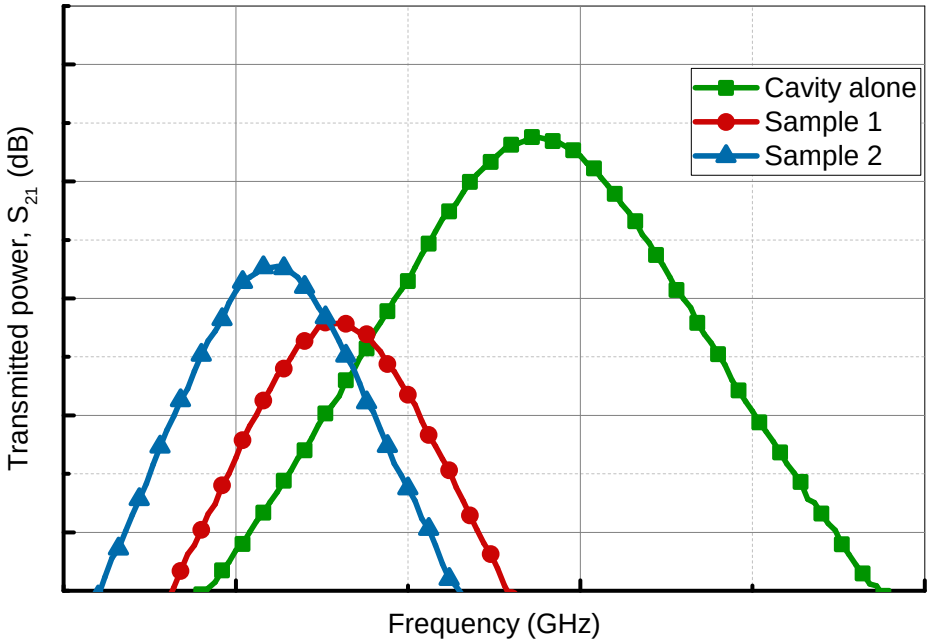

Figure 2.5: Response curve of slotted cavity with and without sample.

$$\varepsilon_r^{''} = \frac{V_c}{4V_s}\left(\frac{Q_0 - Q_s}{Q_0 Q_s}\right) \tag{2.5.10}$$

$$\mu_r^{'} = 1 + \frac{1}{C}\frac{V_c}{V_s}\frac{f_0 - f_s}{f_0} \tag{2.5.11}$$

$$\mu_r^{''} = \frac{1}{2C}\frac{V_c}{V_s}\frac{Q_0 - Q_s}{Q_s Q_0} \tag{2.5.12}$$

where $\varepsilon_r^{'}$ and $\varepsilon_r^{''}$ are the real and the imaginary parts of the complex permittivity of the material respectively and $\mu_r^{'}$ and $\mu_r^{''}$ are the real part and the imaginary part of the permeability respectively with $C = \frac{\int_{V_s} \mathbf{H_1}.\mathbf{H_0} dV}{\int_{V_c} |\mathbf{H_0}|^2 dV}$.

Other dielectric parameters that can also be evaluated by Cavity Perturbation method [77] are given by Eqns. 2.5.13 to 2.5.15. The loss factor

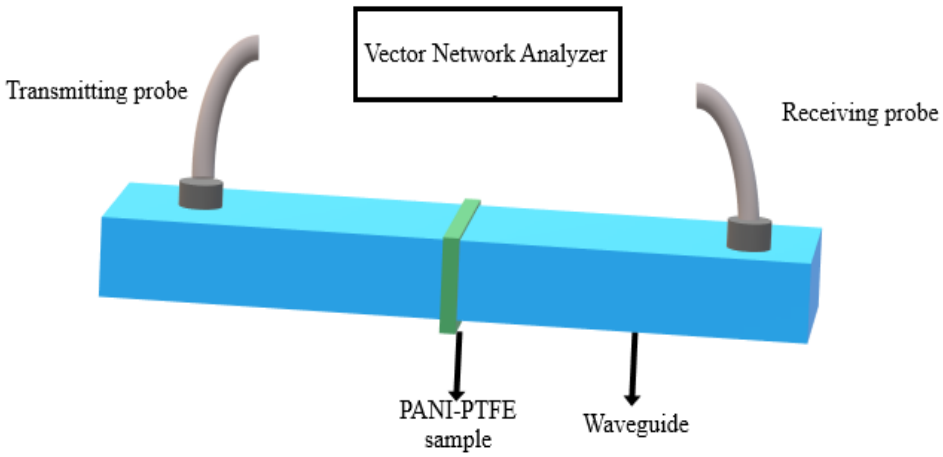

Figure 2.6: Schematic diagram of the waveguide setup for absorption studies.

$tan\delta$ is given by

$$tan\delta = \frac{\varepsilon_r^{''}}{\varepsilon_r^{'}} \tag{2.5.13}$$

The effective conductivity σ due to electric polarization is given as

$$\sigma = 2\pi f \varepsilon_0 \varepsilon_r^{''} \tag{2.5.14}$$

Penetration depth or skin depth δ is the effective distance to which the electromagnetic wave can penetrate into the material and is given as

$$\delta = \frac{1}{\sqrt{\pi \mu f \sigma}} \tag{2.5.15}$$

Thin stripes of PANI-PTFE samples are inserted in the slotted section of the waveguide (Fig. 2.4) connected to the Vector Network Analyzer (VNA) and in terms of the resonance shift observed, the required parameters are calculated.

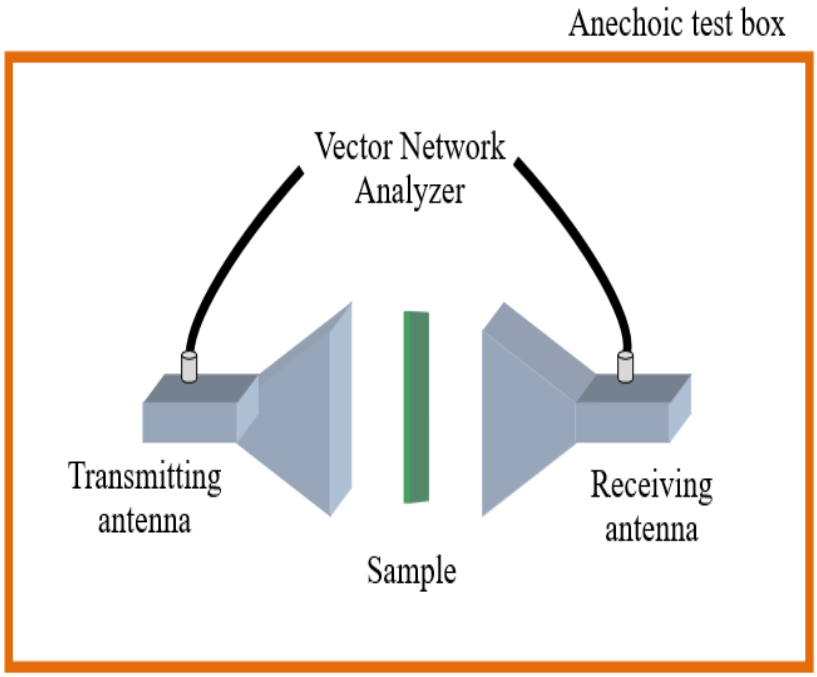

Figure 2.7: Schematic representation of free space measurement setup with sample placed between transmitting and receiving antennas.

2.5.3 Absorption studies

For absorption studies the waveguide method and the free space method.

2.5.3.1 Waveguide method

Here sample is placed between two coaxial rectangular waveguide adapters as shown in Fig. 2.6 and the transmission (S_{21}) and reflection coefficient (S_{11}) curves are obtained for 3-9 GHz. For measurements at different relative humidity (RH) values (30% to 90%) the samples are immediately shifted from the humidity chamber to the waveguide setup.

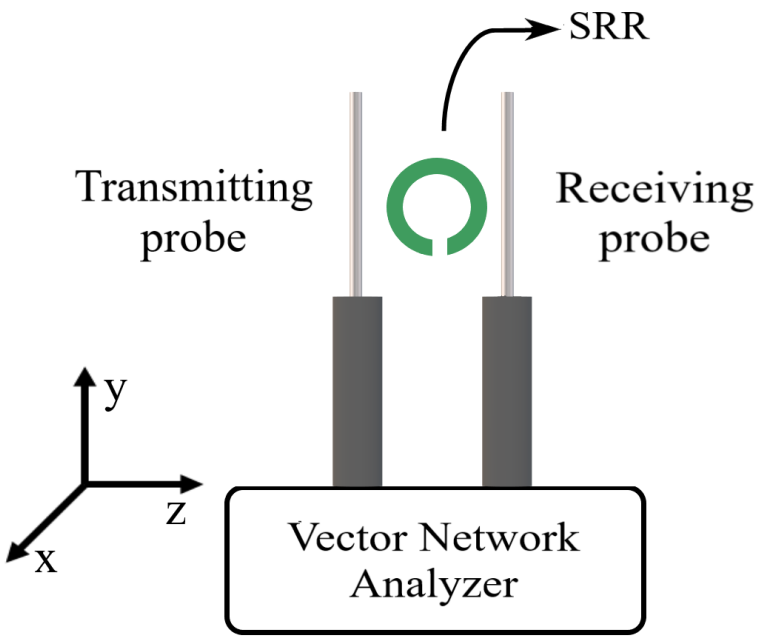

Figure 2.8: Schematic representation of the SRR between monopole antennas connected to the transmitting and receiving probes of a Vector Network Analyzer.

2.5.3.2 Free space method

Microwave absorption characteristics of foam type sample is analyzed using free space method by placing it in between two wide band standard-gain horn antennas connected to the VNA. Schematic diagram of the experimental setup with the sample in between the transmitting and receiving antennas is given in Fig. 2.7.

2.5.4 Resonance measurement using monopole antennas

Resonance absorption of the resonators are analyzed using the transmission spectra (S_{21}) obtained by arranging the proposed experimental SRR structure between two monopole antennas connected to the transmitting and

receiving probes of a VNA as shown in Fig. 2.8 [17, 66]. Here the orientation of ring is such that the electric field **E** is parallel to the slit along y-axis, magnetic field **B** is perpendicular to the plane of the ring in x-axis and propagation **k** is along z-axis. For microwave absorption studies at different relative humidity (RH) values between 30% and 90%, the PANI-PTFE samples were immediately shifted from the humidity chamber to the microwave setup and S_{21} curves were obtained.

For measurements using monopole antennas, errors can be minimized by ensuring the position of the resonator in near field of the antenna. In near field, the resonators should be placed in the plane of the electric field for proper electromagnetic coupling. The position of the resonators is adjusted between the transmitter and receiver antennas for maximum absorption level.

2.6 Simulation

Simulation results are included in the thesis for comparative studies. High Frequency Structure Simulation (HFSS) software employs finite element method (FEM) convergent for EM structures. It is a commercial tool used in antenna designing, complex microwave frequency circuit elements and packaging. This thesis includes simulation results obtained using Ansys HFSS.

For simulation studies samples are placed inside a radiation box with electric excitation parallel to the splits and magnetic excitation perpendicular to the plane of sample.

CHAPTER 3

PREPARATION AND CHARACTERIZATION OF HUMIDITY SENSITIVE CONDUCTING POLYANILINE-POLYTETRAFLUOROETHYLENE POLYMER

Conducting polymers are nowadays widely used in a wide variety of gadgets for specific purposes. This chapter describes the preparation and characterization of Polyaniline based conducting polymer developed with a purposes of introducing it to the world of negative permeability based metamaterials. The microwave characterization studies of this material along with its structural, dielectric, tensile and humidity based conductivity are also discussed in detail. A foam based absorber made using the polymer material, which can be used for wide band EM applications, is also presented[1].

[1]Humidity Sensitive Flexible Microwave Absorbing Sheet Using Polyaniline-Polytetrafluoroethylene Composite, Arabian Journal for Science and Engineering, Springer (2019)

3.1 Conducting polymers

The discovery of polymers/macro molecules and their broad range of properties make them an important component in modern technological advancements. It was in 1976 American physicist Alan J. Heeger, chemist Alan Mac Diarmid and Japanese chemist Hideki Shirakawa together with their research students discovered the conducting polymers which have the capacity to get converted from an insulator state to a conducting state by doping methods [80, 81, 82]. Conducting polymer is an organic polymer with conjugated double bonds which allows the free charge carriers to flow through the long chain. In addition to this, depending on the type of dopant, free charge carriers (holes/electrons) are produced in the material which enhances the conductivity manifolds as a function of doping concentration [83, 84]. Conductive polymer family mainly includes Polyacetylene, Polypyrrole, Polythiophene and Polyaniline [10, 82, 85].

Out of different types of conducting polymers, Polyaniline can be easily prepared with minimum production cost. With suitable doping, Polyaniline have the capability to exhibit new characteristics by switching to different oxidizing states. The high environmental stability along with other tunable properties of Polyaniline makes it an ideal choice to meet the emerging potential applications in areas like alternative energy sources, media for erasable optical information storage and nonlinear optics [81, 86, 87]. This highlights the requirement of further studies for better understanding of its properties and subsequent applications.

3.1.1 Polyaniline

Polyaniline (PANI) is a conducting polymer formed by the polymerization of aniline. The primary structure of Polyaniline consists of benzenoid rings with an imine back bone and quinoid rings with amine back bone as

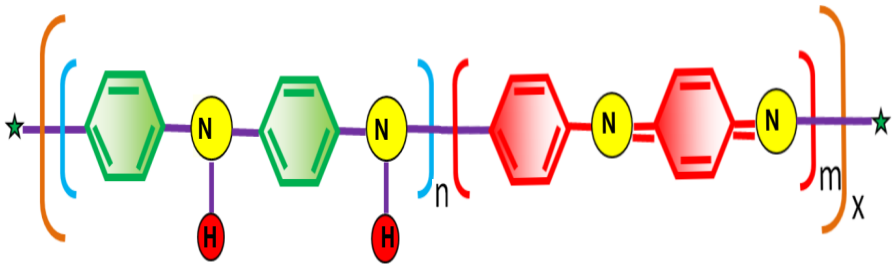

Figure 3.1: Structure of Polyaniline base showing imine (green) and amine (red) backbones.

shown in Fig.3.1. It can exist in various oxidization states characterized by the ratio of imine to amine nitrogen in terms of n and m as discussed below [88]:

1. Leucoemaraldine: It is the fully reduced state of PANI with n=1 and m=0 (Fig.3.1). It is an amorphous material of very poor conductivity, whose colour ranges from pale brown to white. This material is characterized by a high melting point and is insoluble in all solvents.

2. (Per)nigraniline: This is the fully oxidized state of PANI with imine link with n=0 and m=1 (Fig.3.1). It is highly unstable in base and salt forms which quickly decompose to its lower oxidation states on exposure with air. In its base form, nigraniline forms dark blue coloured solutions in acetic acid, formic acid and pyridine, which on heating forms green coloured salts because of its reduction to emeraldine.

3. Emeraldine: The most useful form of Polyaniline is emeraldine. Electrically conducting emeraldine salt is formed from the base by the protonation, which help in de-localization of electrons. Emeraldine consists of equal number of oxidized and reduced repeated units (n=0.5,

m=0.5) which is considered as the half oxidized state of Polyaniline. Emeraldine base is insoluble in water and in some organic compounds.

Among all the oxidation states possessed by PANI, the environmentally stable form is emeraldine salt, which derived much attention due to its easiness to synthesize, easiness to dope by protonic acids and lower cost for the monomer. Properties of Polyaniline are very sensitive to the fabrication condition and preparation technique used. Therefore, the study of its properties with respect to different growing as well as ambient conditions is of much importance. Its properties can be tailored by changing its oxidation states through the addition of dopants or through blending it with other organic, polymeric or inorganic nano-sized semiconducting particles [84]. The nano composites of this salt with metals and metallic oxides exhibit a combination of characteristics like electro-chemical, catalytic and optical properties and conductivity [89, 90, 91]. So conducting polymer nano composites possess the advantages of both low dimensional systems (nano structure filler) and organic conductors (conducting polymer). It was reported that the nano particles themselves could act as conductive junctions between the PANI chains which can lead to an increase of the electrical conductivity of the composites [92, 93]. The electrical conductivity of such composites might also depend upon the molecular structure of the conductive polymer matrix (i.e., crystallinity). Since silver exhibits the highest electrical and thermal conductivity among all the metals, combination of PANI with silver could yield functional materials having enhanced electrical properties [93, 94].

3.1.2 Conduction mechanism

The precise tunability in conductivity offered by Polyaniline makes it an ideal candidate in applications which require high conductivity as a demanding factor. In acid doped PANI, the inter and intra chain conduction

mechanism provided by the available π electrons and charged ions will considerably enhance the conductivity [95]. The charge defects like polaron, bipolaron and soliton introduced in PANI [11, 10] by the partial oxidation/reduction enhances charge transportation and will contribute to the effective conductivity. The band, orbital, molecular and quantum theories are some of the existing conceptual models put forward for the description of conduction mechanism in polymers. Out of these, the quantum mechanical interpretation is the most popular one and is detailed here [96].

3.1.2.1 Quantum interpretation

For an isolated system, according to quantum theory :

- particles occupy quantized energy levels.
- de-excitation of particles from higher energy to lower energy levels will result in a radiation corresponding to a narrow line spectrum.

But in the case of chemically bonded systems, the interaction of each atom with their neighbouring ones within their region of influence will result in broadening of energy levels to form energy bands (valence and conduction bands). This will result in the observance of wide band spectrum on de-excitation to ground states.

For metals with high conductivity the valence and conduction bands will overlap whereas in dielectrics the band gap is very large. Conducting polymers have a narrow band separation which can be further reduced by doping, to resemble metals.

On doping the present oxidized and reduced electrons will associate themselves with the corresponding radical ions resulting in the formation of spin half polarons of charge e. Polaron will occupy an intermediate energy level between the conduction and valence bands. With increase in doping

levels, polaron-polaron interaction occurs forming spinless bi-polaron at a different localized state [11, 10]. On further increase in doping, polaron-bi-polaron interaction result in energy level overlapping thereby easing the electron flow.

The explanation of conduction mechanism in polymers is not limited to these quasi static particles. For highly disordered structure of polymers with crystalline and amorphous regions, other mechanisms like tunneling effect, hopping of charges and space charges contribute to the conductivity. A brief description of each of this mechanism is given below:

- Tunneling current: The electron wave associated with the transporting electron can tunnel through the energy barrier without exploiting much energy. The schematic representation of tunneling process is shown in Fig. 3.2(a). The magnitude of the tunneling current depends upon the applied fields and also on factors like temperature, dielectric constant and the effective mass of the tunneling electron.

- Hopping of charges: Hopping of charges occur between the localized energy levels (Fig. 3.2(b)) by the to-and-fro movement of charges across the potential barrier due to thermal agitations.

- Space charges: The aggregation of charges at the interface (dielectric-conductor) due to mismatch in the transmittance and acceptance of charges across a barrier under the influence of an electric field results in space charge limited conduction (SCLC). Figure 3.2(c) shows a pictorial representation of charge transit between two layers.

These mechanisms are relevant in the presence of electric and thermal potentials which correspond to a frequency dependent conductivity. The two contributions, $\sigma_{ac}(\omega)$ and $\sigma_{dc}(\omega)$ from the frequency dependent *a.c.* and

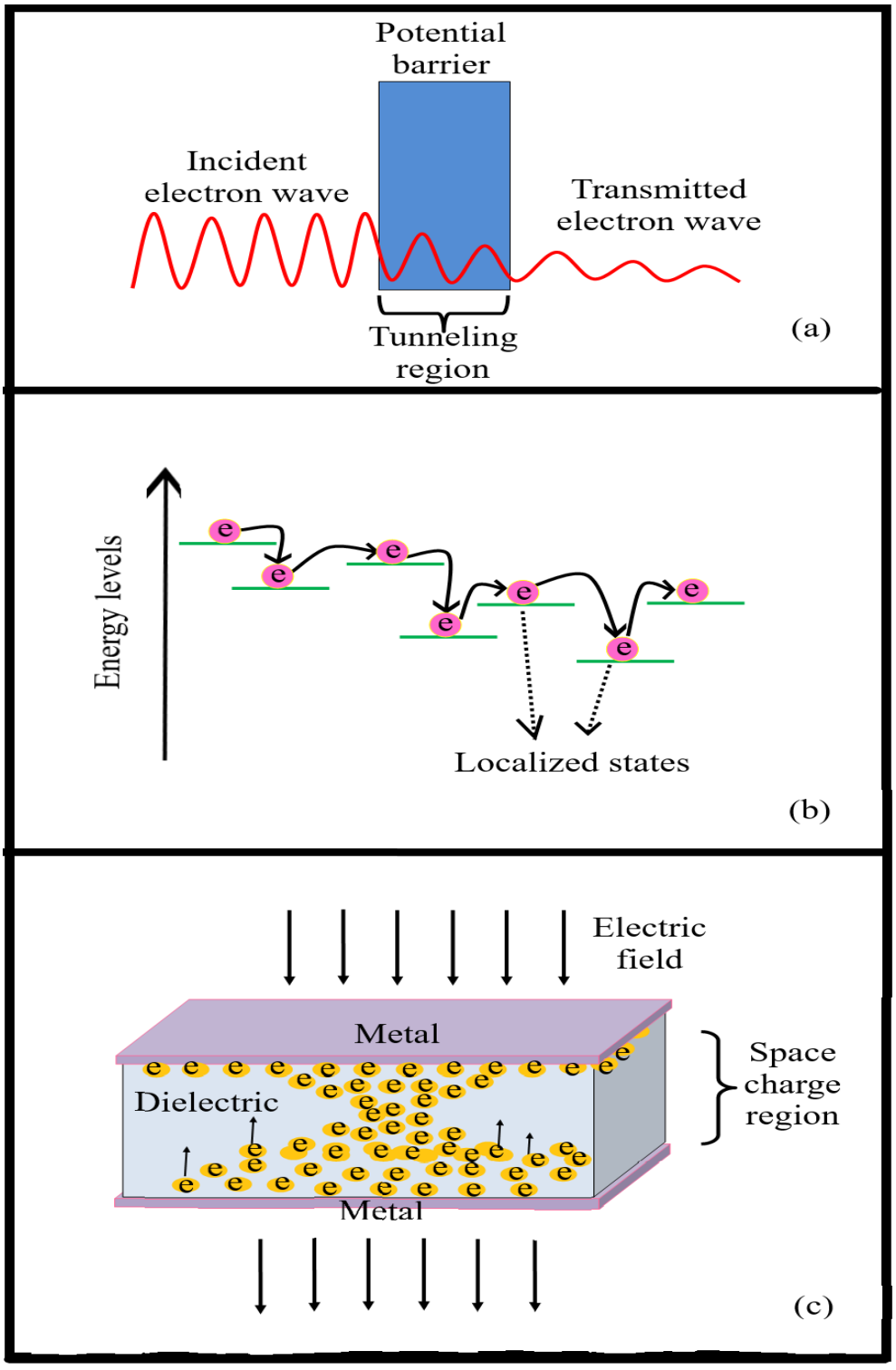

Figure 3.2: Schematic representation of (a) tunneling effect, (b) hopping of charges and (c) space charge conduction.

d.c. currents respectively constitute the net current in the system [97]. The method of preparation and the corresponding variations of physical parameters highly influence the precedence of different conduction mechanisms existing in a particular polymer type. For most of the polymers and their composites it has been experimentally verified that $\sigma_{ac}(\omega)$ increases with frequency. This can be substantiated using pair approximation technique. The conductivity of pure Polyaniline in emeraldine base form is in good agreement with above theories at low temperatures.

3.1.3 Conductivity based applications of PANI

Due to the ease of production and cost effectiveness Polyaniline is used for a variety of applications, of which a few in relation with conductivity is listed below:

1. Electromagnetic interference shielding: Organic or inorganic inclusions or combinations alter the EM absorption characteristics of PANI. These properties are highly dependent on the conductivity and can be varied by the type of dopants used and their concentration [98].

2. Sensor applications: The electrical conductivity of Polyaniline will vary when it is exposed to acidic or basic vapors like HCl, ammonia and CO_2, which make it suitable for usage in various sensors [99].

3.2 Polyaniline-Polytetrafluoroethylene preparation

Polyaniline is in a powdered form and in order to use it for metamaterial based applications it has to be made into a composite form of Polyaniline-Polytetrafluoroethylene (PANI-PTFE) which will have features like durability, malleability and ductility. Materials used for the preparation of PANI-PTFE in a sheet form are presented below.

1. Aniline used as the monomer in the synthesis is of analytical reagent (AR) grade supplied by E.Merck (P) Ltd. with an assay of 99%.

2. Ammonium peroxydisulphate (APS), the oxidant, used for the reaction is of AR grade having an assay of 98% and is from Sigma-Aldrich.

3. Hydrochloric acid (HCl) is ACS reagent of 37% assay supplied by E.Merck (P) Ltd.

4. Acetone and tetrahydroforen (THF) are used to eliminate other oligomers.

5. Polytetrafluoroethylene (PTFE) solution with 60% in de-mineralized water is used as dispersal matrix and is from Sigma-Aldrich.

6. Isopropyl alcohol (IPA) with molecular weight 60.1 is used as binder between PANI and PTFE.

7. Polyurethane foam of 15 mm thickness is used as absorber matrix.

3.2.1 Why PTFE ?

Polytetrafluoroethylene (PTFE) is a linear synthetic polymer with fluorine atoms surrounding the carbon chain. It has a poly-crystalline structure with hexagonal lattice of high degree of order. The lower inter chain force between carbon and fluorine makes the individual molecules to slide easily on each other. This low coefficient of friction existing between the layers can be utilized to make thin sheets. PTFE is a hydrophobic and chemically inert polymer which can form the matrix for several systems [100]. It has high flexural strength so that the matrix can easily bend and flex without losing its integrity. It is an ideal matrix having enough void space to deposit PANI powder within.

Figure 3.3: Photograph of prepared chlorine doped Polyaniline powder.

3.2.2 Preparation of Polyaniline

As discussed earlier there are two ways by which Polyaniline can be doped, one is through acid treatment which is a non-redox doping process, and the other is by oxidation of leucoemeraldine to emeraldine which is a redox process. Here the oxidation by proton doping where radical cations are formed at the nitrogen atoms is followed and the created charge carriers are responsible for the electronic conduction.

Conducting Polyaniline is prepared by chemical oxidation method with chlorine as dopant. The samples are initially prepared in powder form and is made into a rigid form by binding with PTFE thereby acquiring the mechanical properties of it.

Protonated chlorine doped Polyaniline was prepared by the standard chemical oxidation method [95, 101, 102]. Polyaniline in powder form was synthesized at room temperature from aniline in the presence of

1 molar ammonium peroxydisulphate (APS) as oxidant, and 1 molar HCl as dopant in the ratio 1:6:12 and polymerization continued for five hours. The green solution obtained is kept overnight and filtered. The filtrate was then washed with acetone, THF and diluted HCl solutions to remove the un-reacted aniline and is air-dried to get Polyaniline powder (Fig. 3.3 & Fig. 3.4).

3.2.3 Polyaniline-Polytetrafluoroethylene sheet

In order to prepare Polyaniline based microwave absorber sheet the conducting polymer powder was used as filler in PTFE matrix [103]. The light weight PTFE adhesive was chosen as matrix to provide flexibility and to enhance the conductivity of PANI due to the closer arrangement of constituent particles. For this the Polyaniline powder (in gm) was dispersed in de-mineralized water (in ml) in the ratio 1:10 in a ultrasonicator. 7 wt.% of Polytetrafluoroethylene in aqueous solution was added to the above mixture and stirred for one hour using a magnetic stirrer and the suspension was filtered. The filtrate was air dried at room temperature and ground to fine powder using a mortar. By adding a few drops of isopropyl alcohol (IPA), it was made into dough which was rolled into PANI-PTFE hybrid flexible sheets.

The complete steps involved in the synthesis are pictorially represented in Fig. 3.4. During the synthesis of sheet it was observed that the alteration of the wt.% of the PTFE in the solution reduces the feasibility of transforming the composite into sheet form. Two such sheets of thickness 0.4 mm and 0.9 mm were prepared by the above procedure. Figure 3.5 shows the photograph of PANI-PTFE hybrid sheet of thickness 0.9 mm and 0.4 mm.

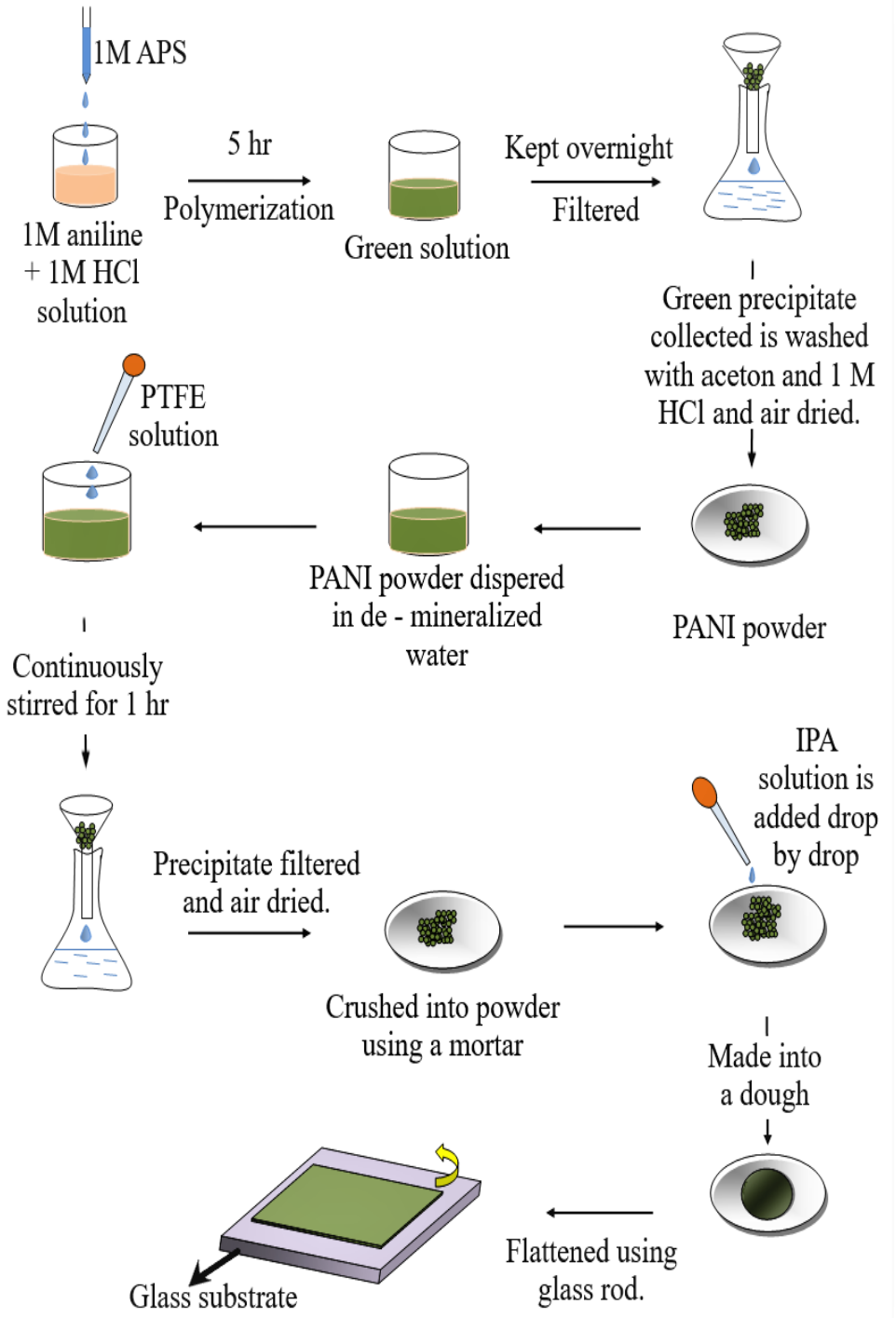

Figure 3.4: Schematic representation of different steps involved in the synthesis of PANI-PTFE sheet.

(a) (b)

Figure 3.5: Photograph of Polyaniline-Polytetrafluoroethylene (PANI-PTFE) hybrid sheet of (a) thickness 0.9 mm and (b) thickness 0.4 mm.

3.3 Results

3.3.1 Structural analysis

The Polyaniline in PTFE matrix may result in the formation of PANI clusters inside the matrix which can reduce the inter-molecular distance and hence can increase the conductivity. PANI is expected to fill the hexagonal structure of PTFE similar to honey in the honeycomb of bees. SEM images of hybrid sheet were taken to show macro porous structure with clusters of PANI-PTFE granules. Figure 3.6 depicts the images obtained for a sample of thickness 0.9 mm. The cylinder shaped inclusions seen scattered in Fig. 3.6(c) are the unglued molecules of PTFE.

The XRD pattern of Polyaniline powder shows the amorphous nature [104, 105, 106] while PTFE shows neither a fully amorphous nor a fully crystalline structure [107, 108, 109]. Figure 3.7 and 3.8 show the XRD pattern

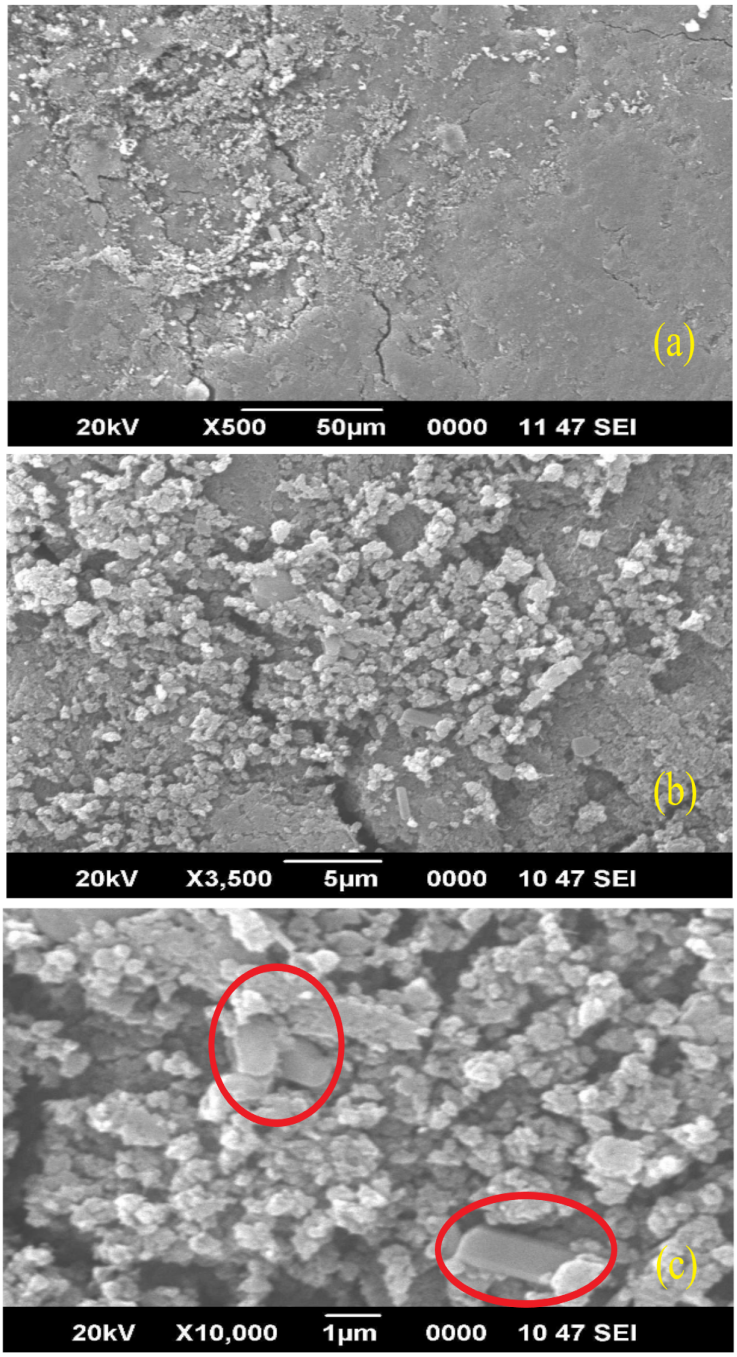

Figure 3.6: SEM images of PANI-PTFE hybrid sheet of thickness 0.9 mm at different resolutions, where unglued PTFE granules are shown within elliptical rings (5(c)).

of PANI powder and PANI-PTFE sheet respectively. As is quite obvious, the amorphous nature of PANI powder is evident from Fig. 3.7. The spectrum of PANI-PTFE shows a poly-crystalline structure due to the presence of peaks marked as 'a' at angles (2θ) 18.869^0, 32.396^0, 37.835^0 and 42.108^0 with spacing 4.70055 A^0, 2.76133 A^0, 2.37595 A^0 and 2.14420 A^0 respectively which is due to the presence of PTFE [107, 108]. The broad peak marked as 'b' at an angle 26.5^0 in the spectrum is due to the PANI [104, 105]. The binding process of PANI with PTFE also resulted in other peaks marked as 'c' at angles 12.401^0, 21.509^0 and 49.914^0 with spacing 7.13174 A^0, 4.12805 A^0 and 1.82563 A^0 respectively depicting the enhanced crystalline nature.

3.3.2 Conductivity and humidity

Researches have already verified that for protonic acid doping in Polyaniline using chlorine ions (Cl^-) show greater carrier mobility resulting in higher conductivity. In the presence of a humid environment, the Polyaniline becomes more conducting than a dry sample. The conductivity of a completely dry sample is observed to be around five times less than the humid sample. The positive effect of humidity on the conductivity of Polyaniline is due to the increase in the charge transfer along the Polyaniline chain. It may be also due to an electrolytic movement of ions in the humid polymer [110].

It has been observed that with the increase in crystallinity due to the addition of PTFE, the conductivity is also increased, because of the structure becoming more organized. In fact, it is known that the inter chain electron mobility in a given polymer is significantly enhanced for a more ordered solid state structure and hence the crystalline domains, the size of crystal grain and the degree of crystallinity dramatically affect the conductivity. It was also observed that electrical conductivity of Polyaniline increases with decrease in reaction temperature but it does not depend on the temperature

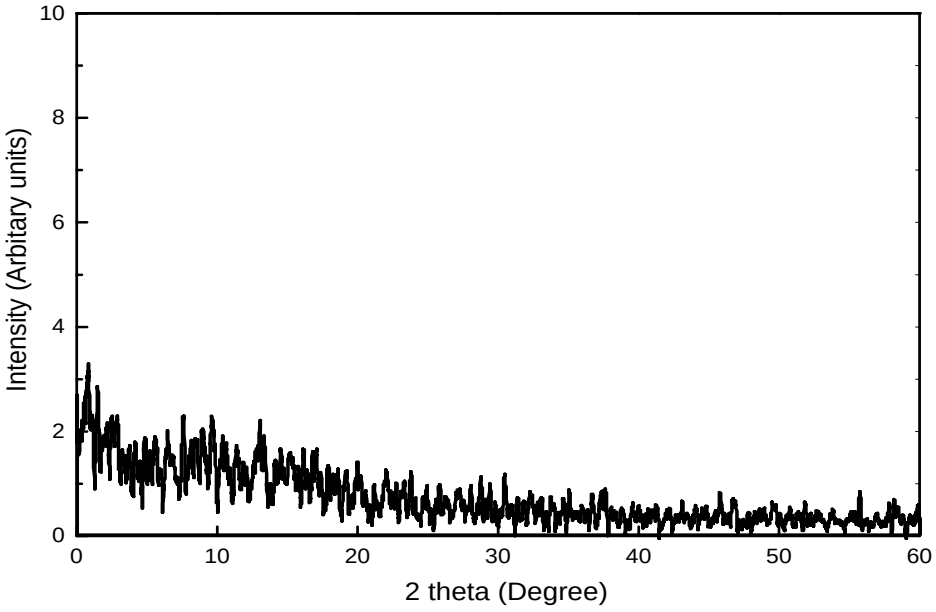

Figure 3.7: X-ray diffraction pattern of PANI powder.

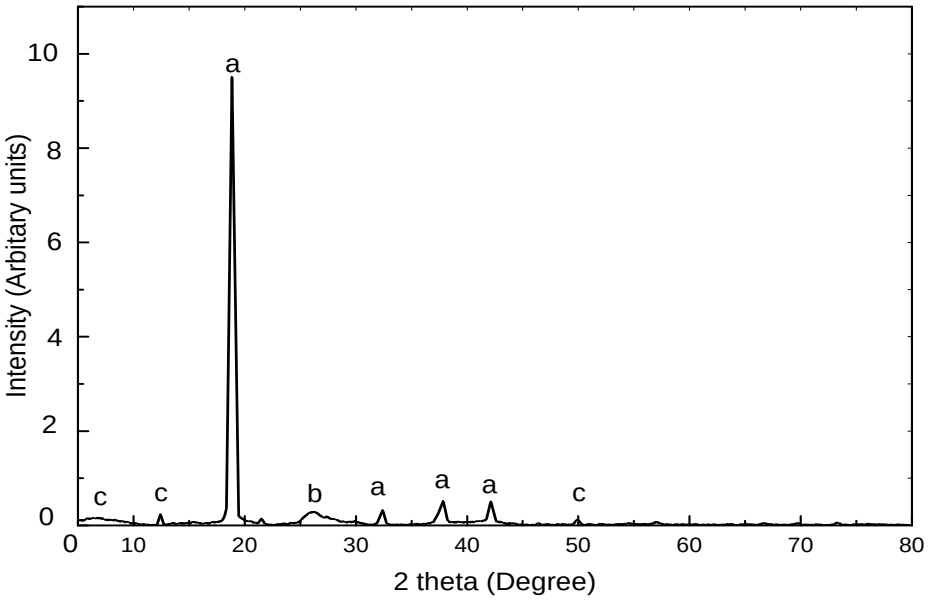

Figure 3.8: X-ray diffraction pattern of PANI-PTFE hybrid sheet.

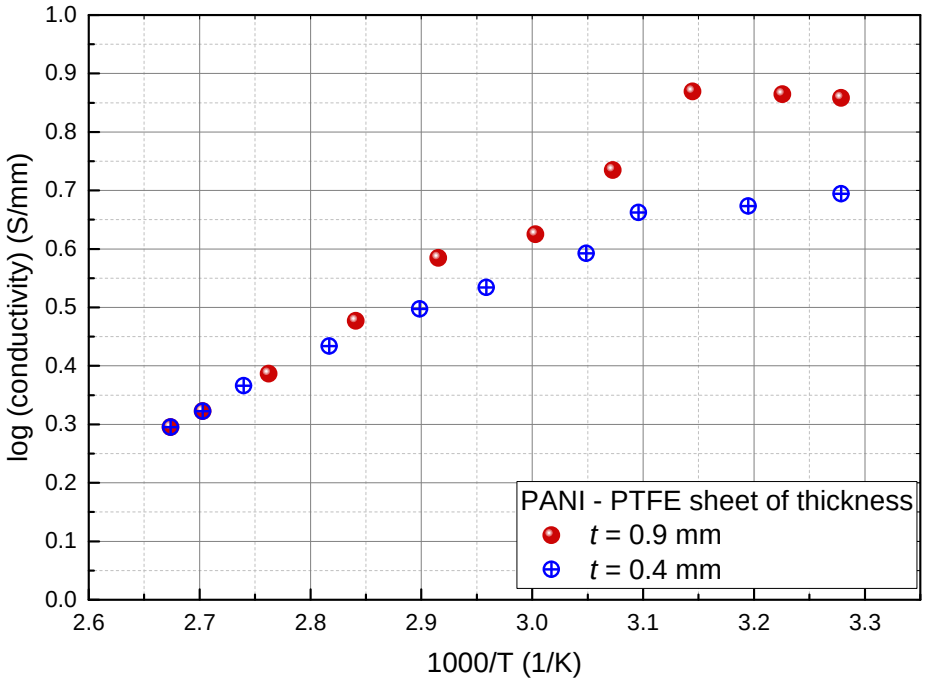

Figure 3.9: Conductivity-temperature curve of PANI-PTFE sheet of 0.9 mm and 0.4 mm thickness measured using four-probe setup at 30% RH.

of surroundings.

Conductivity property of the prepared sheets was analyzed using four-probe method and variation of conductivity with temperature for the two sheets of thickness (t = 0.4 mm and t = 0.9 mm) at a relative humidity of 30% is given in Fig. 3.9. The graph shows relatively steady conductance around room temperature (305 K) for both samples and shows gradual decrease in conductivity with increase in temperature, which clearly indicates the conducting behaviour of the PANI-PTFE sheets. However, the thick sheet (t = 0.9 mm) shows higher conductivity at low temperatures compared to thin sheet (t = 0.4 mm) as expected.

The conductivity dependence on humidity in terms of voltage drop

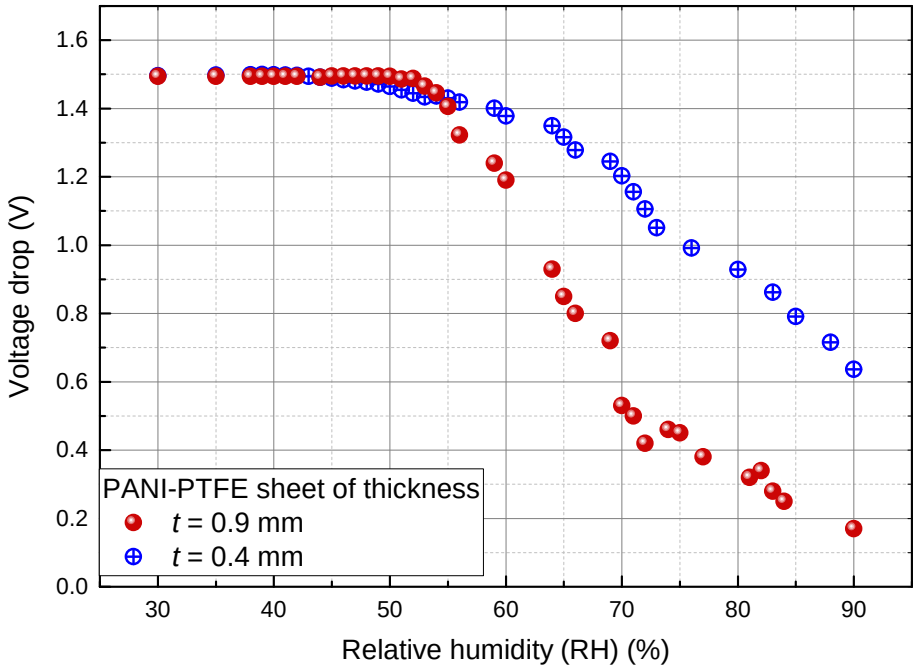

Figure 3.10: Humidity response on the voltage drop measured between two points spaced 1 cm apart for the PANI-PTFE hybrid sheet of 0.9 mm and 0.4 mm thickness at 30^0C.

was measured for both sheets and is depicted in Fig. 3.10. It is quite evident from the graph that as relative humidity increases beyond 50% RH, the conductivity of both sheets show marked enhancement. From the figure it is clear that for the thick sheet voltage drop is lower than the thin sheet for higher humidity values owing to its lower resistance.

The stability of prepared sample is analyzed from the V-I curve plotted at different time intervals after the preparation of sheet. From the plot in Fig. 3.11 we can see that voltage drop is minimum (small resistance) immediately after the preparation and is progressively increasing with drying. The humidity content is relatively high just after the preparation resulting in high conductivity. The dried sheet shows low conductivity which can be

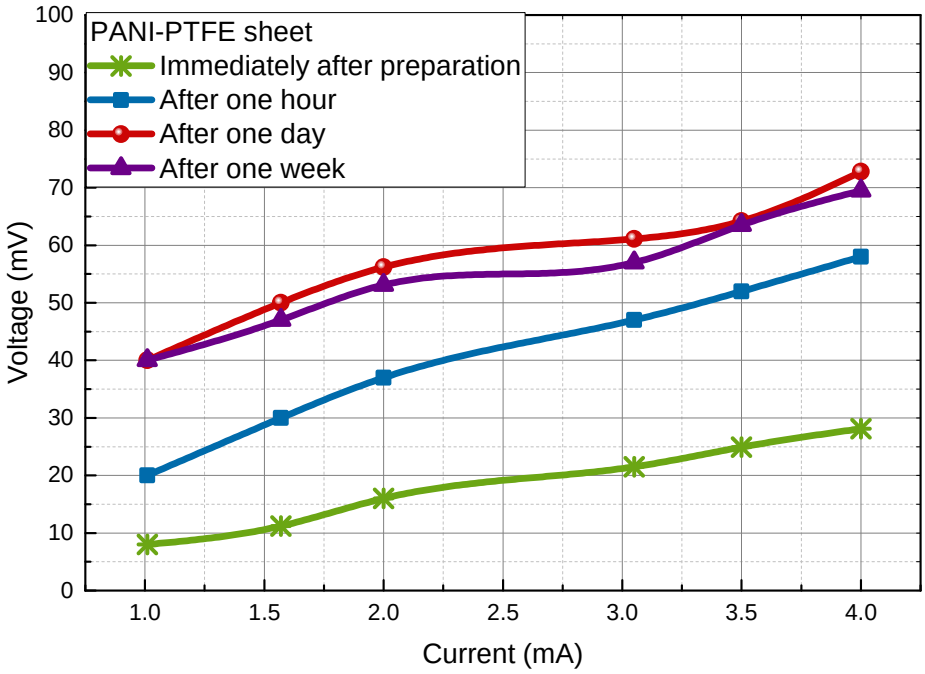

Figure 3.11: Conductivity study at different stages of drying of the PANI-PTFE sheet of thickness $t = 0.4$ mm.

again transformed to a highly conducting one by the process of moisturizing.

3.3.3 Young's modulus

For analyzing the flexibility of the newly formed PANI-PTFE sheet the elasticity in terms of Young's modulus Y was calculated from its load-extension graph. Figure 3.12 and 3.13 show the load-extension graph of two PANI-PTFE hybrid sheets having different dimensions. It is seen that the thick sheet shows less elasticity which may be due to the interplay of more viscous drag between the layers. The average value of the Young's modulus (loading-unloading) was found to be around 4.5 GN/m^2. This value is in the range of a typical nylon fiber which makes our hybrid sheet flexible as well

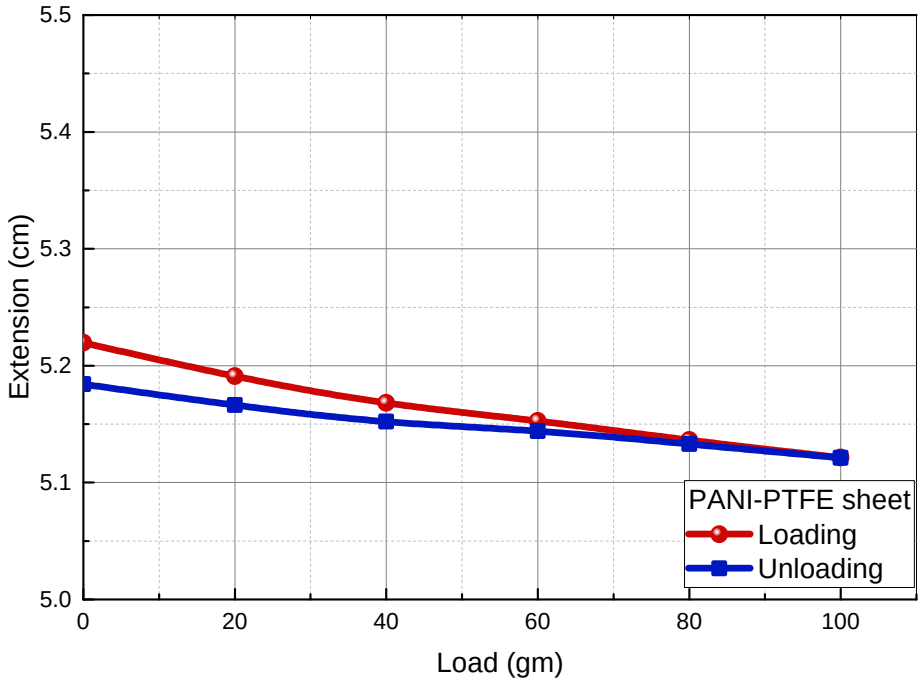

Figure 3.12: Load-extension graph for PANI-PTFE hybrid sheet of dimension 6.8 cm x 1 cm x 0.09 cm.

as a durable one for different applications.

3.3.4 Microwave characterization

The microwave absorption characteristics of the PANI-PTFE hybrid sheet was analyzed at room temperature and room humidity by evaluating its permittivity from the reflection and the transmission coefficients which were obtained by the waveguide method [78]. Measurements were taken for Polyaniline in powder form also. The absorption power level was normalized to 0 dB before taking measurements. For powdered sample this procedure was done by keeping low loss polyvinylchloride (PVC) sample holders as shown in Fig. 3.14 with a filling space of thickness 3 mm inside the rectangular waveguide. The same procedure was repeated for powdered sample

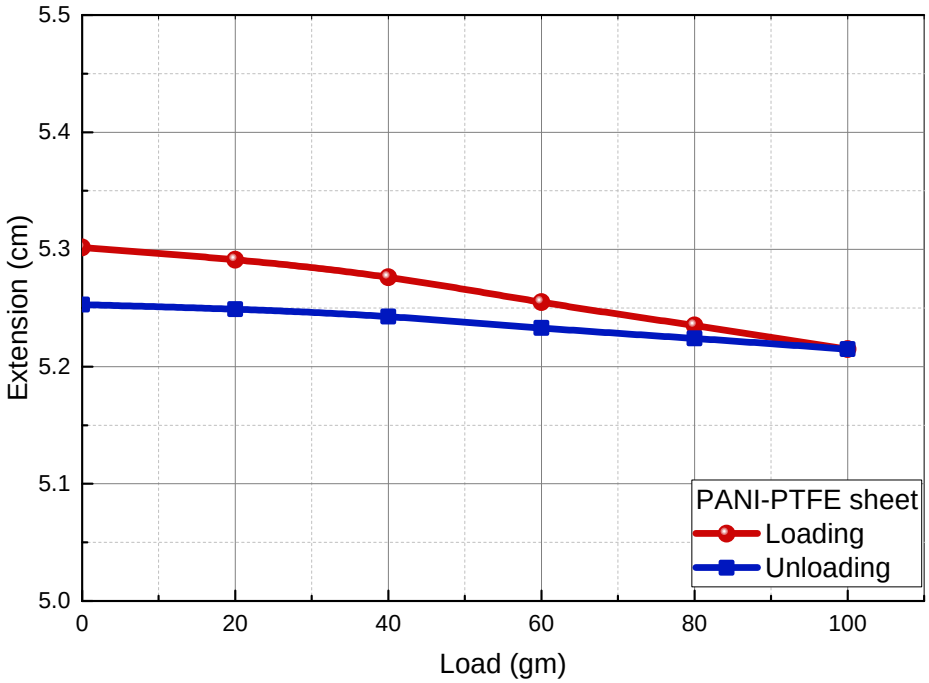

Figure 3.13: Load-extension graph for PANI-PTFE hybrid sheet of dimension 6.8 cm x 2.6 cm x 0.09 cm.

with filling space of 5 mm also.

In the case of PANI-PTFE hybrid sheet, two samples of thickness 0.4 mm and 0.9 mm were used. In both cases, the sample was placed inside the waveguide covering the entire cross section with the plane of absorber perpendicular to the propagation direction. Figure 3.15 gives the photograph of experimental setup, along with the positioning of the PANI-PTFE sheet sample inside the waveguide.

The transmission (S_{21}) and reflection (S_{11}) coefficients (Fig. 3.16 and 3.17) of the powder samples corresponding to a humidity of 60% RH were measured for 3-9 GHz frequencies using suitable waveguide sections connected to a Vector Network Analyzer (VNA) after normalizing the experimental setup with the sample holder.

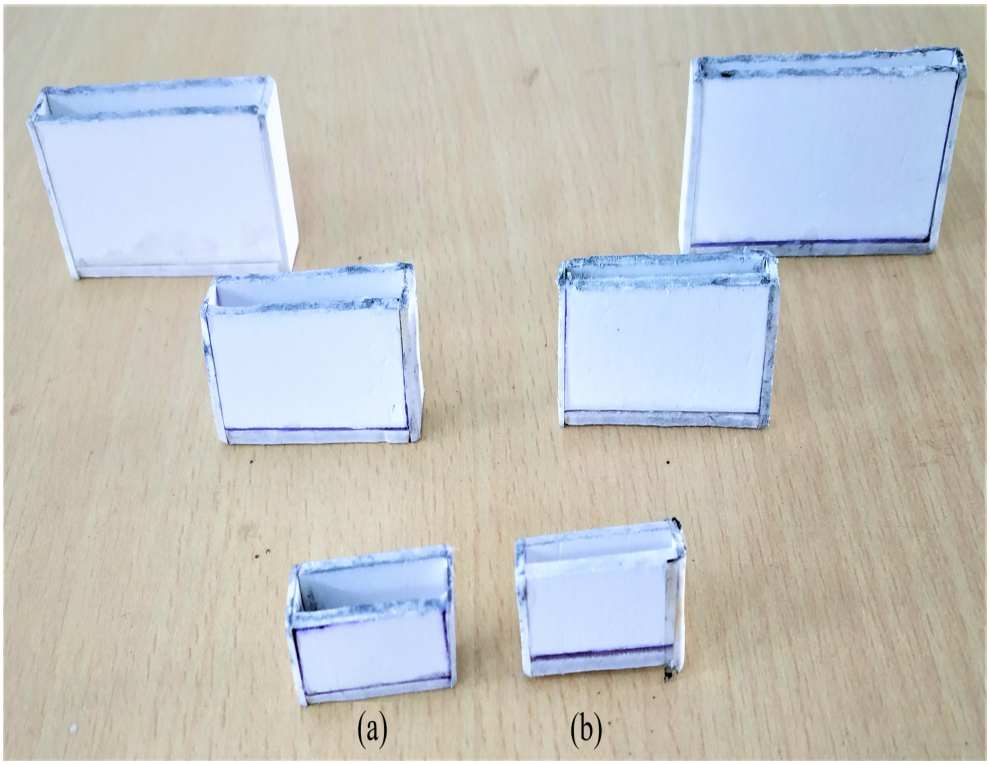

Figure 3.14: Sample holders with filling space of thickness (a) 5 mm and (b) 3 mm for X, C and S microwave frequency bands.

The real and imaginary parts of the permittivity were calculated from the hybrid parameters using Nicholson-Ross Algorithm [111, 112, 113, 114, 115, 116, 117, 118] with the help of the equations:

$$\frac{\mu_r}{\varepsilon_r} = \left(\frac{1+\Gamma}{1-\Gamma}\right)^2 \tag{3.3.1}$$

and

$$\mu_r \varepsilon_r = -[\frac{c}{\omega d} ln(\frac{1}{P})]^2 \tag{3.3.2}$$

where d is the thickness of the sample, ω is the angular frequency, P is the propagation factor, Γ is the reflection coefficient, and c is the velocity of light. Since Polyaniline is a conducting non-magnetic material its effective permeability (μ_r) is assumed to be 1. The real and imaginary values of

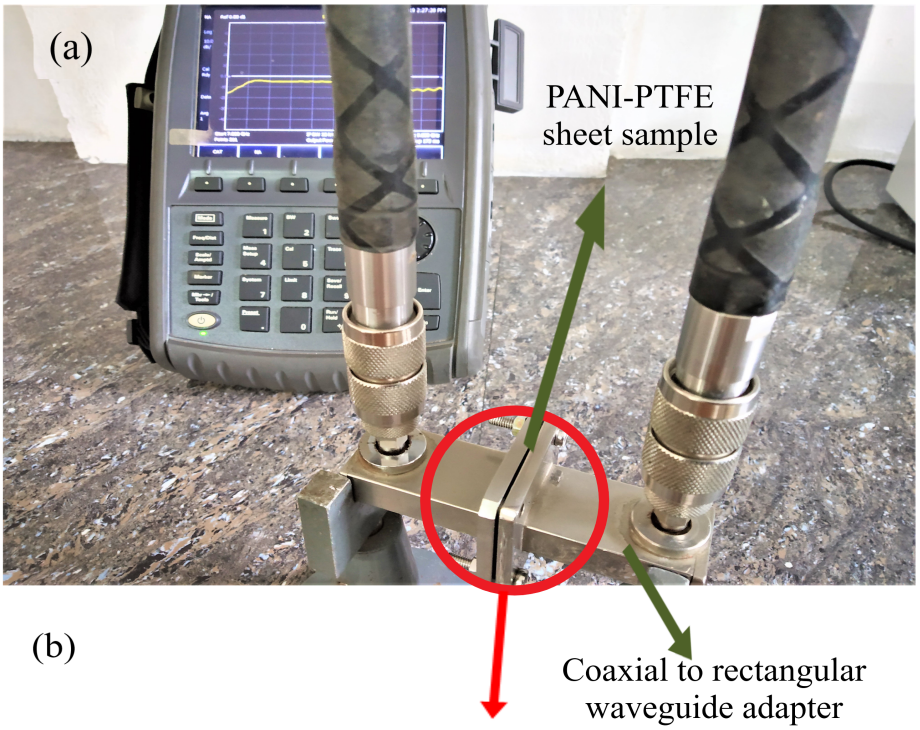

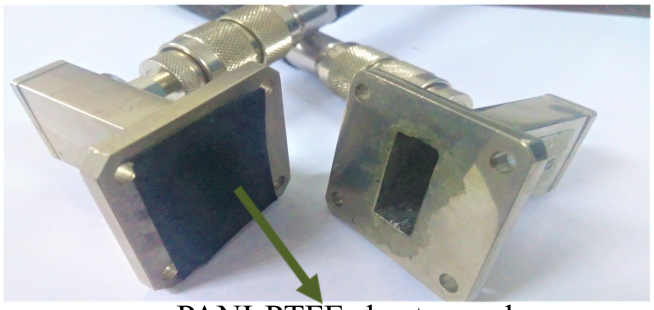

Figure 3.15: Photographs of (a) experimental setup used for measuring the transmission (S_{21}) and reflection (S_{11}) coefficients and (b) positioning of PANI-PTFE sheet sample inside the waveguide.

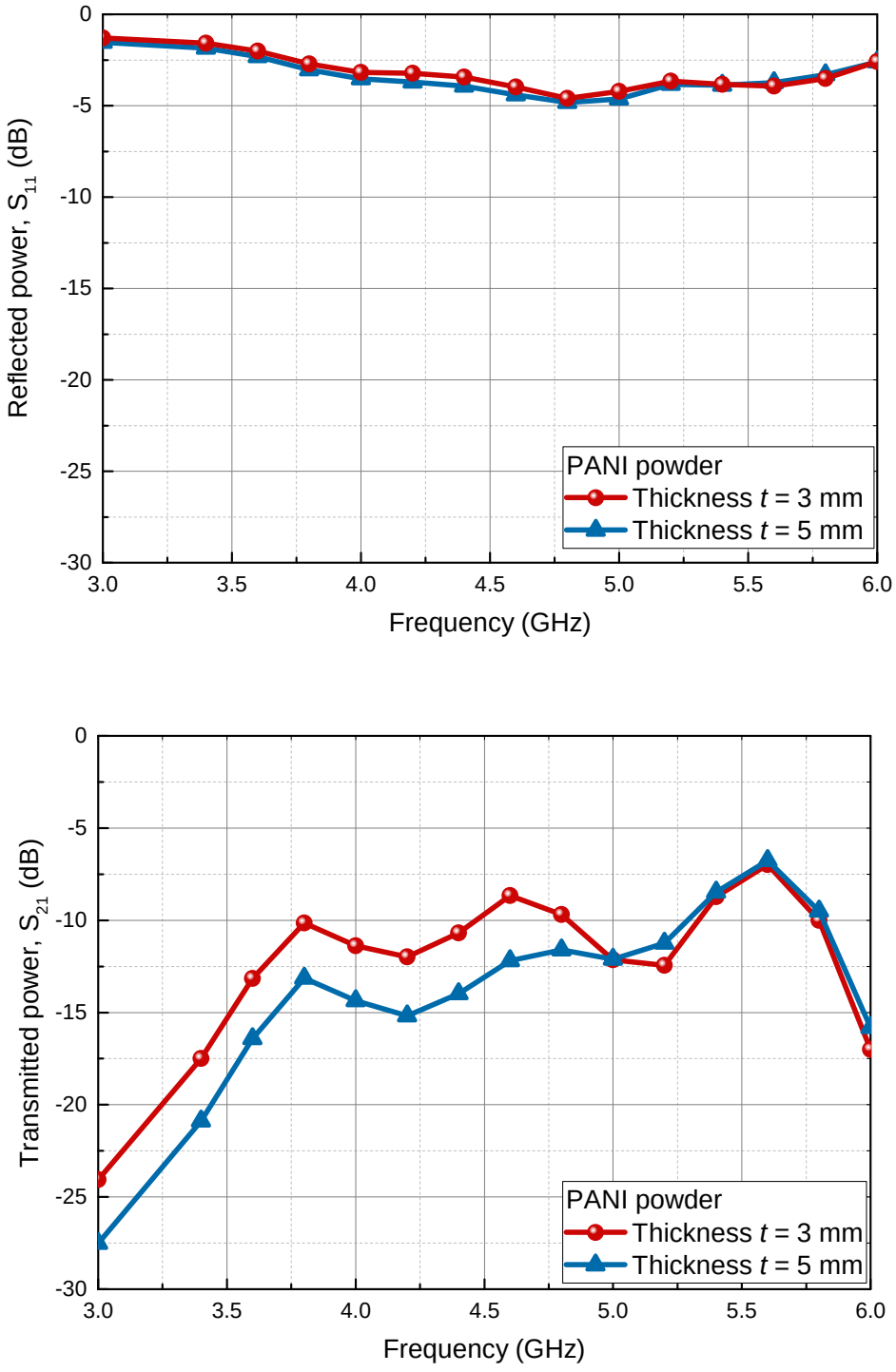

Figure 3.16: Reflection (S_{11}) and transmission coefficients (S_{21}) of PANI powder (60% RH) in rectangular containers of two thicknesses t = 3 mm and 5 mm in 3-6 GHz frequency range.

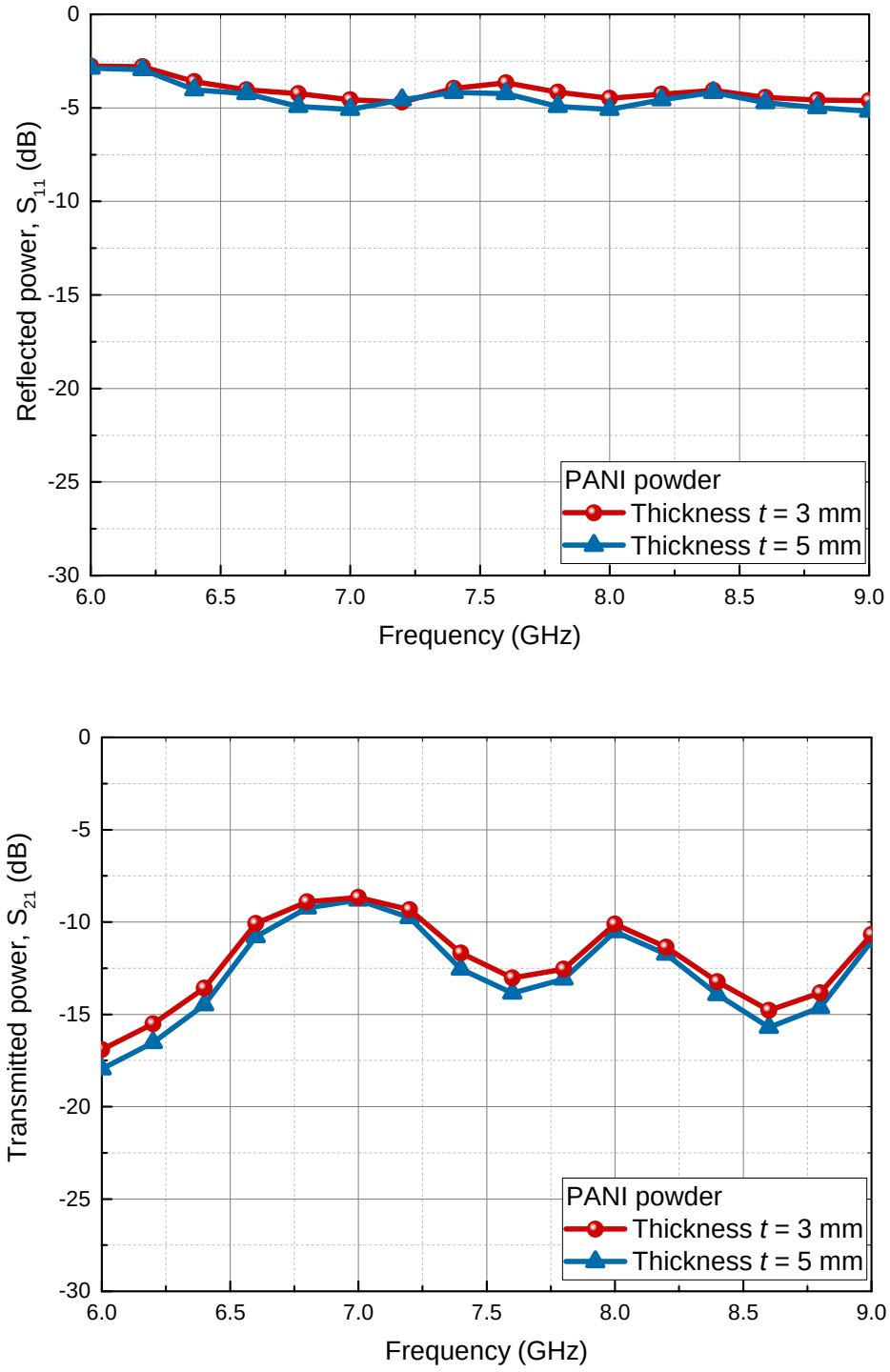

Figure 3.17: Reflection (S_{11}) and transmission coefficients (S_{21}) of PANI powder (60% RH) in rectangular containers of two thicknesses t = 3 mm and 5 mm in 6-9 GHz frequency range.

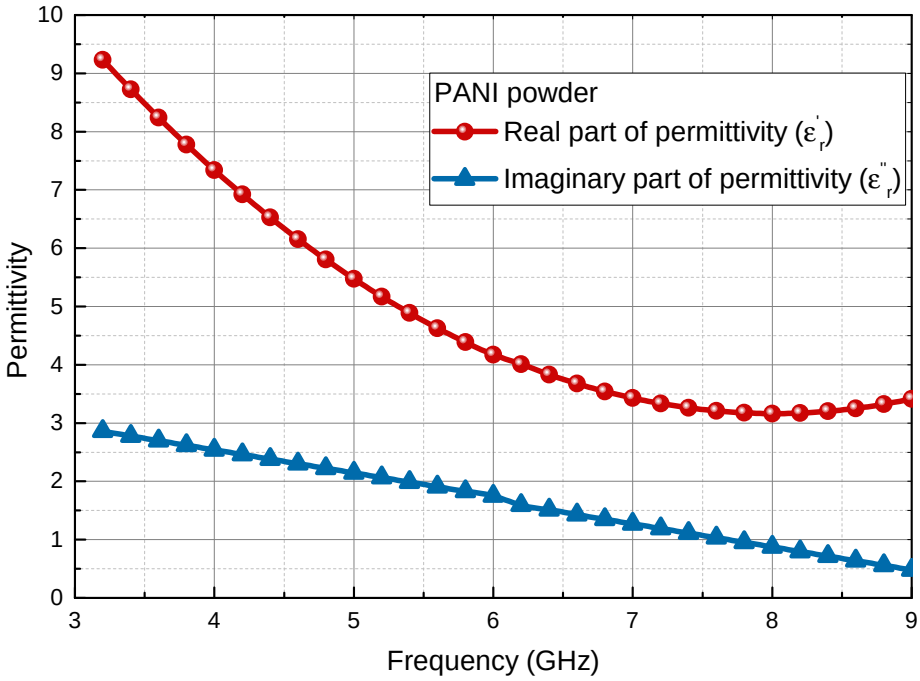

Figure 3.18: Real (ε_r') and imaginary (ε_r'') parts of permittivity of Polyaniline powder (60% RH) of holder thickness of 3 mm.

permittivity using the above equations are plotted in Fig. 3.18 and 3.19.

The real and imaginary parts of permittivity of the PANI-PTFE sheets of thickness t = 0.4 mm and t= 0.9 mm were evaluated from their transmission and reflection coefficients corresponding to a humidity of 60% RH using Nicholson-Ross algorithm (Eqns. 3.3.1 and 3.3.2) and are given in Fig. 3.20 along with that obtained for PANI powder placed inside a holder of 3 mm thickness. Generally, both parts of permittivity show gradual decrease with frequency. It is observed that both the parts of the permittivity differ for the powder and the sheet samples. Also, the effect of the thickness of the sheet is found to be negligible.

The variation for imaginary part of the permittivity between powder

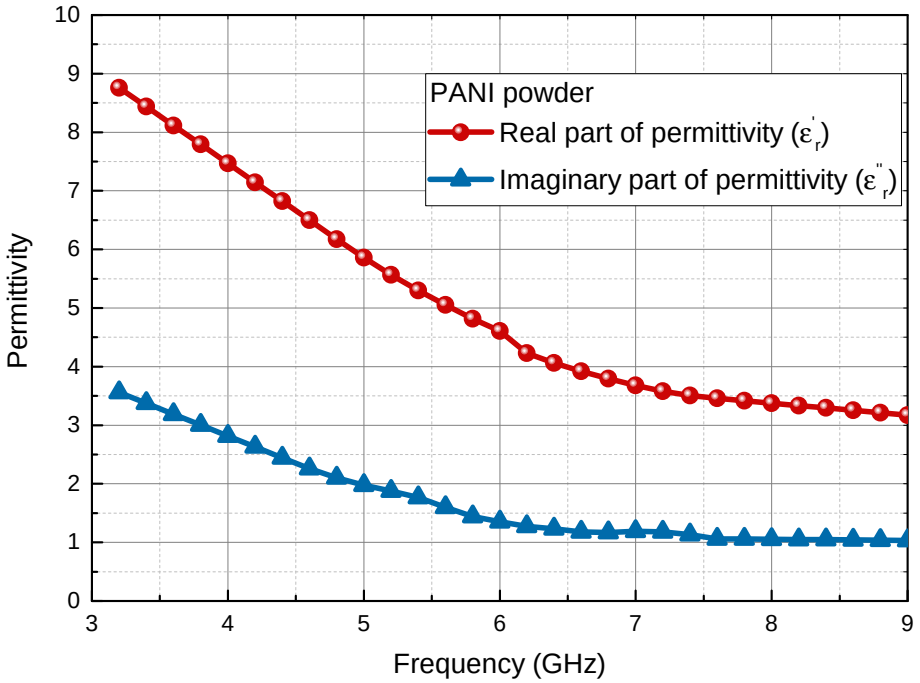

Figure 3.19: Real (ε_r') and imaginary (ε_r'') parts of permittivity of Polyaniline powder (60% RH) of holder thickness of 5 mm.

and sheet form is noticeably high in the lower and higher frequency region whereas for the real part, this deviation is observed in the intermediate frequencies. This markable variation in the imaginary part of permittivity is indicative of the ability of prepared sheets to show more conductivity for these frequencies, which may enhance its microwave absorption properties.

The permittivity values were also verified for the PANI-PTFE hybrid sheet ($t = 0.9$ mm) using cavity perturbation method for selected frequencies. The setup used for the measurements is shown in Fig. 3.21. The results obtained by the algorithm using graphs are compared with the values obtained from the experimental results in Table 3.1

The microwave absorption studies of the PANI-PTFE hybrid sheets

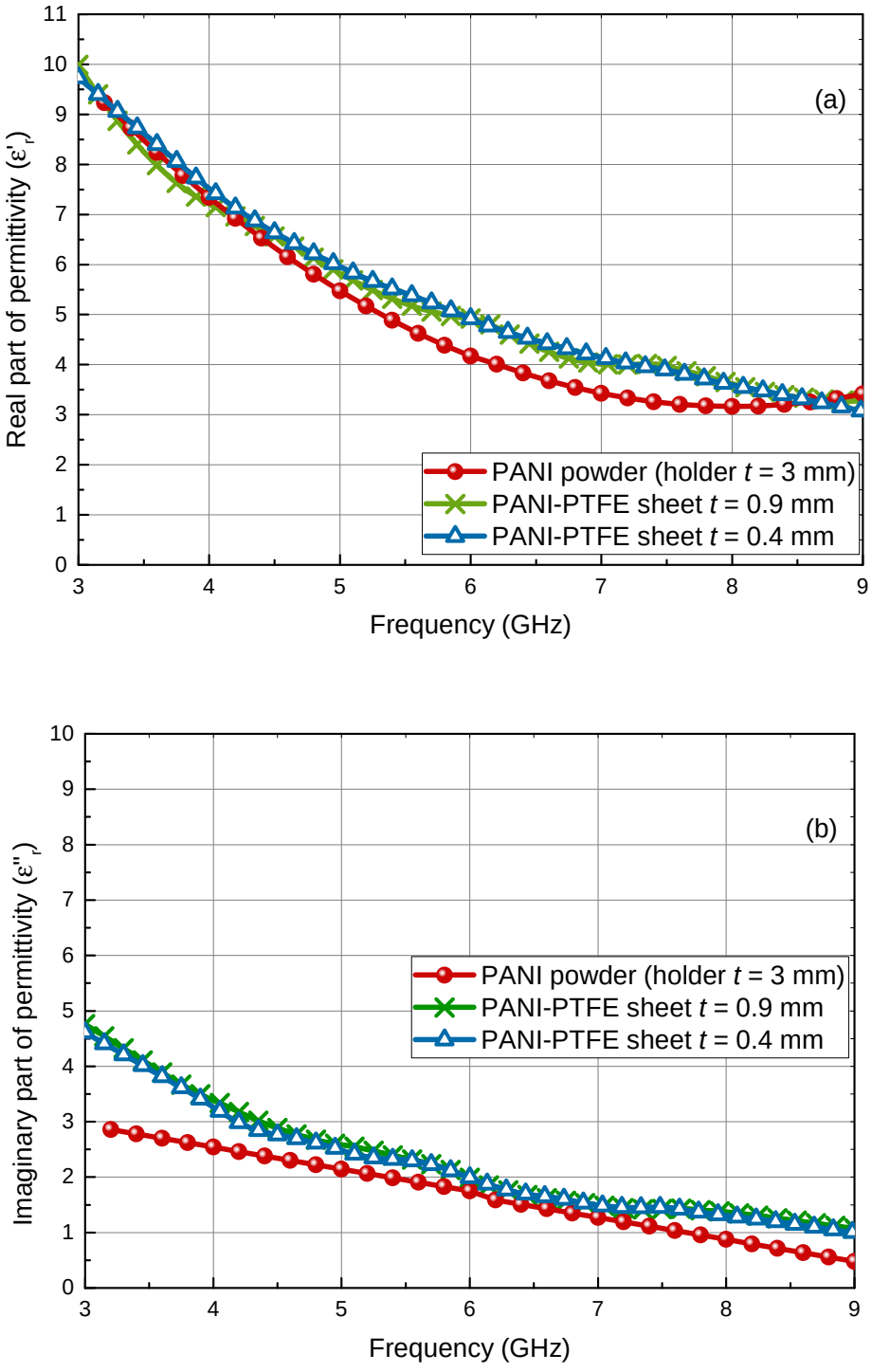

Figure 3.20: (a) Real (ε_r') and (b) imaginary (ε_r'') parts of permittivity of PANI-PTFE hybrid sheets along with that of PANI powder in the containers of thickness t = 3 mm.

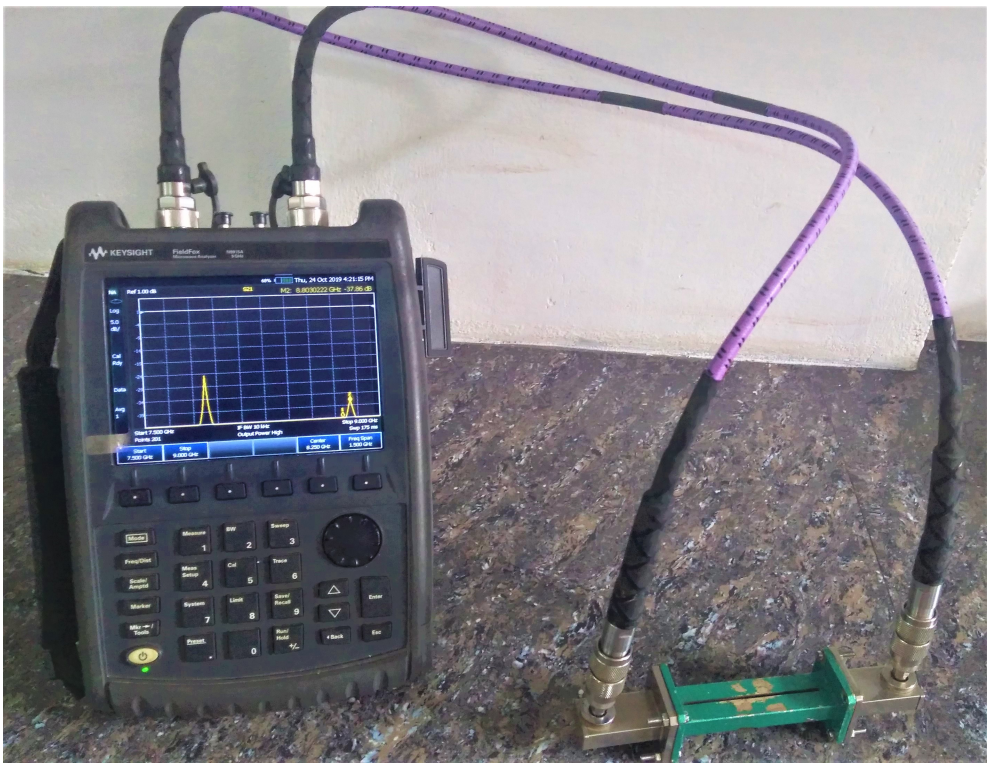

Figure 3.21: Measurement arrangement for Cavity Perturbation method.

of thickness $t = 0.4$ mm and $t = 0.9$ mm were conducted for dry and wet forms by measuring its reflection and transmission coefficients for frequency range 3-9 GHz. The dry sheet is at room humidity of 30% RH and wet one is at high humidity level of 90% RH. Fig. 3.22 gives S_{11} and S_{21} obtained for thickness $t = 0.4$ mm whereas Fig. 3.23 shows the results for $t = 0.9$ mm. It is evident from 3.22 and 3.23 that S_{11} values show a slight decrease in reflection with increase in frequency. Both wet and dry sheets irrespective of thickness show the same results indicating that reflection mainly depends on the surface smoothness and not on the thickness and the moisture condition of the sheet.

From the values of S_{21} the following inferences can be drawn. As the frequency increases the average absorption level decreases, but not in a linear

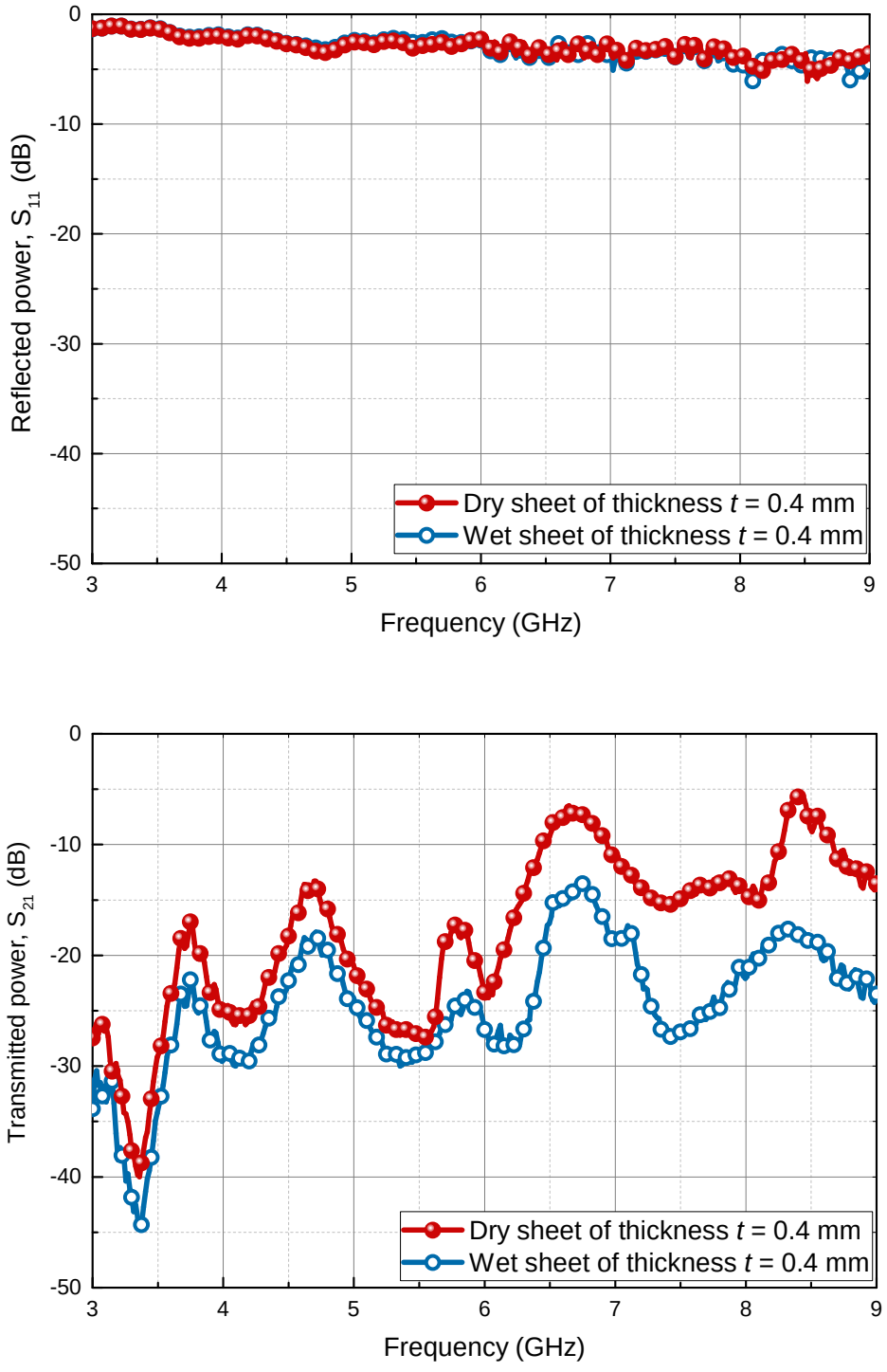

Figure 3.22: Reflection (S_{11}) and transmission coefficients (S_{21}) of PANI-PTFE hybrid sheets of thickness 0.4 mm at different humid conditions in 3-9 GHz frequency range.

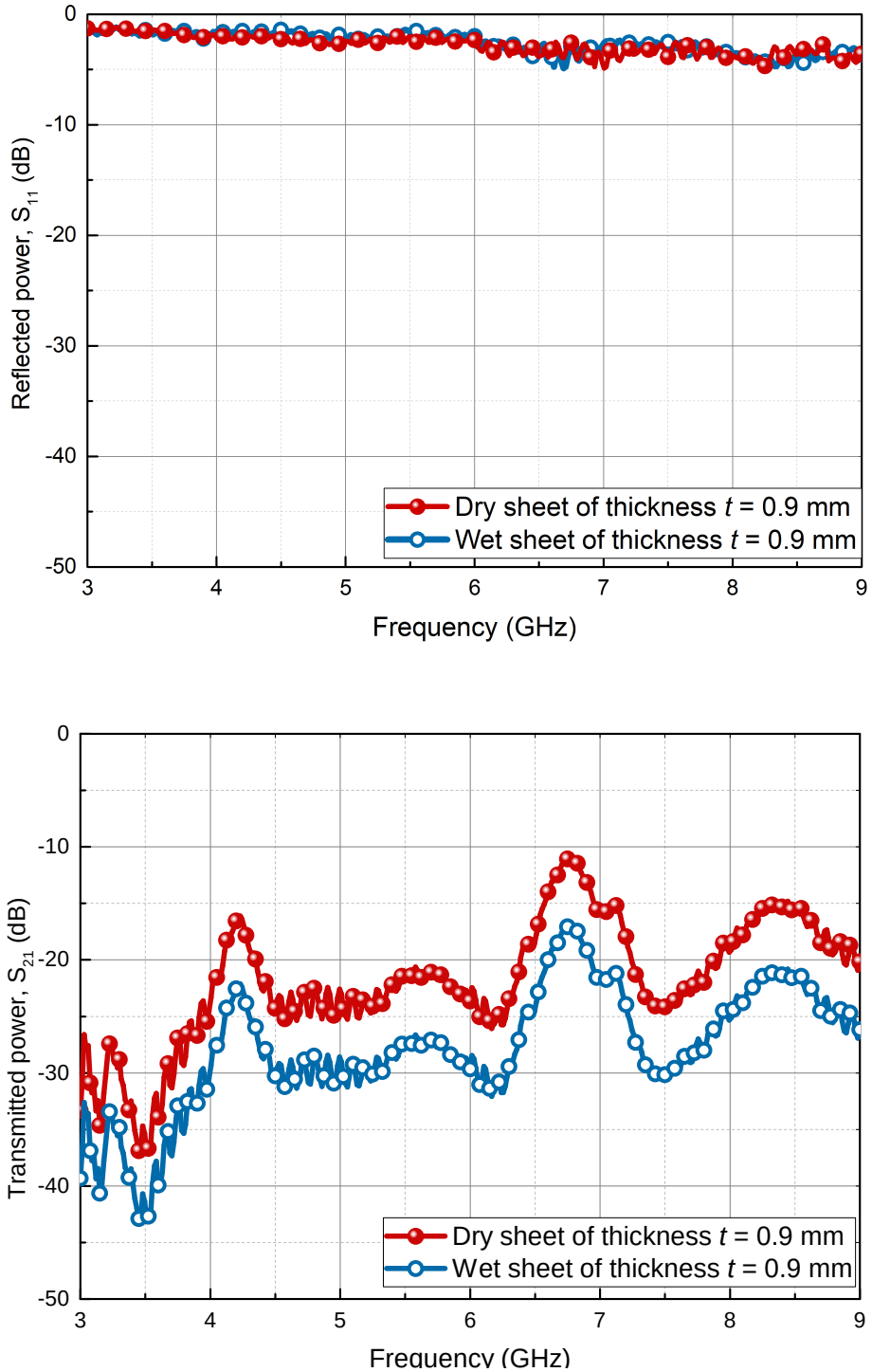

Figure 3.23: Reflection (S_{11}) and transmission (S_{21}) coefficients of PANI-PTFE hybrid sheets of thickness 0.9 mm at different humid conditions in 3-9 GHz frequency range.

Table 3.1: Permittivity values obtained by graphical method and Cavity Perturbation method.

Parameters	Frequency at 7.869 GHz		Frequency at 8.784 GHz	
	Cavity method	From graph	Cavity method	From graph
Real part of permittivity (ε_r')	3.449	3.718	3.2125	3.3243
Imaginary part of permittivity (ε_r'')	1.4007	1.4587	1.2357	1.2686

manner. The absorption level is observed to be dependent on thickness of the sheet more prominently on the upper half of the experimental frequency band. In both cases, an enhanced absorption for the wet sheets is observed which clearly indicate the higher microwave absorption property of the humid sheet. For the thin sheet ($t = 0.4$ mm) the difference between the absorption levels of the wet and dry sheets is on an average around 3 dB at lower frequency region (3-6 GHz) whereas at higher frequency region (6-9 GHz) it is around 12 dB. But in the case of thick sheets this difference is around 6 dB irrespective of the frequency.

The potentiality of using this PANI-PTFE hybrid polymer sheet as a good choice of microwave absorbing material is quite evident from the above figures. Increase in thickness and humidity of the PANI-PTFE sheets result to a good extent in the enhancement of microwave absorption which may be useful in various electromagnetic absorbing and shielding applications. The possibility of metallic inclusions during preparation of PANI-PTFE sheets can be explored for further enhancement of absorption levels.

3.4 PANI as a microwave absorber

By proper adjustment of permittivity ε and permeability μ and by using various trigonometric shapes for the absorbing medium the EM ab-

sorption level can be tailored. Most commonly used absorbents are carbonyl ions [119, 120] and ferrites [121, 122, 123] in different variants like sheet and foam [124, 125]. Cost effective microwave absorbers that uses agricultural wastes and rice husk in pyramidal and sheet forms respectively are also reported [126, 127]. Some of the commonly used absorbents are barium titanate ($BaTiO_3$) [128, 129, 130] strontium ferrites [131], erium oxide (Er_2O_3) [132], iron-nickel alloy (NiFe) [133] and silicon carbides [134] in conducting polymer matrix.

3.4.1 Sheet absorber

The humid PANI-PTFE sheet showing large absorption dip at 3-9 GHz can be utilized in making of thin sheet microwave absorbers. The humidity dependent absorption property can be used in the synthesis of frequency tunable absorbers for ISM (Industrial, Scientific and Medical) applications.

3.4.2 Foam type absorber

Polyurethane and polystyrene are widely used foam type material as microwave absorber in 1-40 GHz region [135, 136]. Carbon with neoprene binders are used now-a-days to prepare microwave absorber foams for anechoic chambers [137, 138, 139].

In order to use newly formulated PANI-PTFE material as a novel microwave absorber in applications like anechoic chamber, the absorption characteristics of PANI-PTFE impregnated inside the polyurethane foam of thickness 15 mm is examined. The photograph of the experimental setup showing the absorber foam arranged between a transmitting horn and receiving horn inside an anechoic test box is given in the Fig. 3.24. The transmission coefficients obtained for dry (30% RH) and humid (90% RH) foam samples using the free space method is presented in Fig. 3.25. A no-

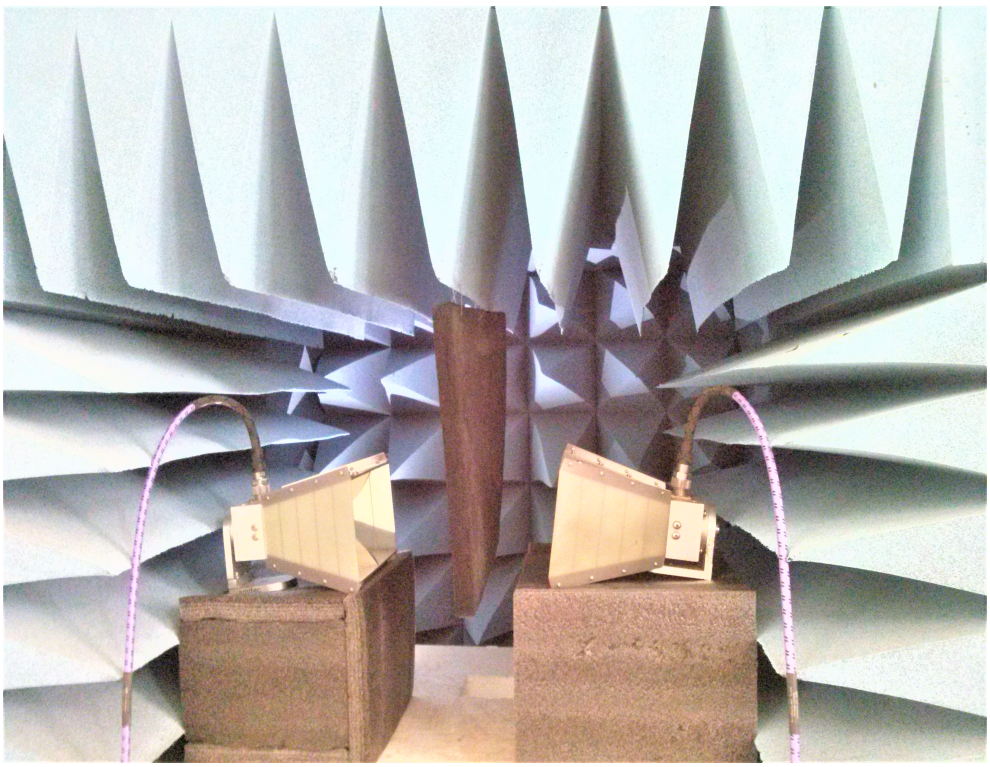

Figure 3.24: Free space measurement setup used for the measurement of transmitted power through a foam type PANI-PTFE absorber.

ticeable increase in absorption level of around 5 dB for the wet foam in the entire frequency range is observed.

In comparison with the properties of already proposed absorbers [119, 120, 126, 133] the PANI-PTFE absorber shows effective response within the frequency range of 3-9 GHz.

3.5 Relevance of the study

Polyaniline showing good conductivity properties is made available in sheet form so that the possibility of using it in the development of metamaterial related structures may be explored. Owing to the attractive features exhibited by PANI-PTFE hybrid sheet, it may also be used in a variety of fields like microwave absorbers, humidity sensors, biosensors and chemi-

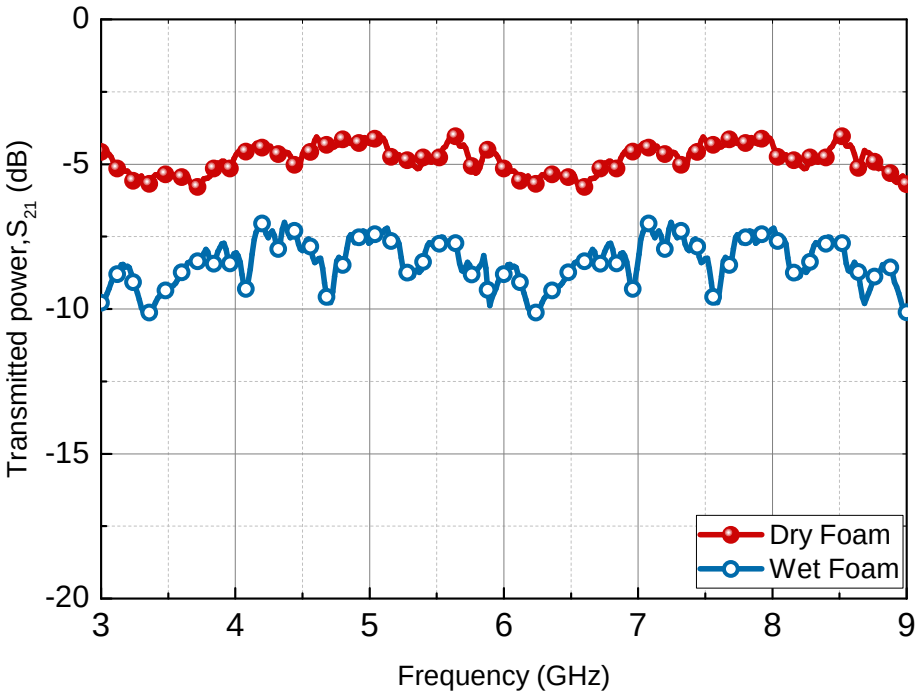

Figure 3.25: Plot of transmission (S_{21}) coefficient of PANI-PTFE embedded foam in dry (30% RH) and humid (90% RH) conditions.

cal sensors [140, 141, 142, 143]. Other potential applications of conducting polymers in the fields of storage devices, super capacitors [144, 145, 146] etc. may also be materialized with added features using the newly developed PANI-PTFE sheet.

3.6 Conclusion

From the investigation of intrinsic and extrinsic properties of the prepared samples the following points can be inferred.

1. From the studies on conductivity and stability of the newly developed PANI-PTFE hybrid sheet, it is observed that this can be used to fabricate metamaterial based structures like SRR, whereby the class of

conducting polymers are introduced into the world of metamaterials.

2. Synthesized Polyaniline-Polytetrafluoroethylene hybrid sheet has a polycrystalline structure and may be used in places where conductivity is a desired parameter.

3. Thin, flexible and lightweight PANI-PTFE sheet has excellent microwave absorption characteristics along with an added property of showing marked variation in absorption level with different humidity content, which makes this sheet an ideal candidate for humidity based microwave sensors and other electromagnetic applications.

4. The studies on mechanical strength and temperature stability of this sheet predict that it is suitable for state-of-the-art microwave technology.

5. This cost effective microwave absorber is also fabricated in thick foam form which makes it suitable for anechoic chamber type applications.

CHAPTER 4

HUMIDITY DEPENDENT RESONANCE PROPERTIES OF METAMATERIAL SRR STRUCTURES USING POLYANILINE-POLYTETRAFLUOROETHYLENE

This chapter presents various metamaterial SRRs made with PANI-PTFE sheet for maximum performance and the study of its humidity dependent resonance behaviour. It includes the simulation studies of PANI-PTFE SRR and its variants for frequency tunability in microwave region. A comparison of resonance behaviour of the SRR made with PANI-PTFE sheet with a metallic SRR is also addressed. The possible explanation for observance of wide band resonance in PANI-PTFE SRR is given in terms of inductive and capacitive reactance[1].

[1]Different portions of this work is presented in International Symposium of Optics at IIT Kanpur, International Conference at CUSAT Kochi and Metamorphose 2019 at Rome. It is also published in IEEE Xplore.

4.1 Introduction

Conducting polymers have emerged as one of the key areas of research in the field of electromagnetic sensors and absorbers during the last decade. There are diverse fields yet to be explored in connection with the electromagnetic behaviour of this state-of-the-art material out of which one of the vibrant areas is that of metamaterials. Metamaterials are artificially structured composites, also called as Left Handed Medium (LHM), having negative values of permittivity and permeability for their constituent structures, a property quite different from that of ordinary materials. Split Ring Resonators (SRR) are negative permeability structures of LHM materials which have widespread applications depending upon the resonance in relation to the dielectric environment of the resonating structure. SRR structures with two concentric conducting rings of different radius arranged co-axially with splits oriented at opposite sides were first proposed by Pendry *et al.* [2].

Split Ring Resonators (SRRs) at microwave frequencies are extensively studied in literature for a wide variety of applications like material characterization, electromagnetic sensors and antennas [39, 147, 148, 149, 150]. Experimental and numerical studies of transmission characteristics of periodic and disordered SRRs with different geometric parameters are reported for novel applications [54, 63]. The studies on SRRs are mainly performed in microwave gigahertz (GHz) and optical terahertz (THz) frequency regimes. Tuning the resonance frequency of SRRs will give an opportunity to design EM devices at desired range of frequencies. The conducting loops of SRRs are two resonators which are magnetically strongly coupled both via magnetic flux and mutual magnetic capacitance between the loops [19, 63]. This system shows strong magnetic resonance as well as an electric resonance obtained at a comparatively high frequency region. Besides the conventional

SRRs with two rings, a single ring with split also shows magnetic response. The purpose of insertion of a ring inside the other is to enhance the resonance absorption by increasing the capacitive contribution due to mutual coupling [18].

4.1.1 SRRs using conducting polymers

The major challenge in the realization of meta related structures using conducting polymers is the availability of a polymer in a sheet form. Having being able to materialize PANI-PTFE conducting sheet, the realization of different forms of meta molecules are possible. Accordingly different types of SRRs are made using PANI-PTFE polymer sheet and their resonance characteristics are analyzed in order to check their suitability as negative permeability material. Both the electrical and magnetic resonances are thoroughly examined and tuned to make sure that they behave in a similar manner as that of their metallic counterpart.

4.2 Role of displacement current in polymer SRR

The resonance in PANI-PTFE conducting polymer depends upon the conduction current as well as the displacement current. It is well known that in ordinary conditions PANI-PTFE exhibits relatively lower conduction current effects compared with metals. As is seen in the last chapter, the humidity percentage critical in determining the total conductivity of PANI-PTFE material. Having been put under the category of dielectrics with conductivity, it is reasonable to consider the displacement current effects also which may lead to overall conductivity related resonance in a PANI-PTFE ring.

The dielectric related displacement current effects in a PANI-PTFE ring when it is exposed to an electromagnetic field are briefed below.

Figure 4.1: Shows the orientation of PANI-PTFE ring in an external EM field.

Consider a PANI-PTFE ring in an external EM field as shown in Fig. 4.1 with the magnetic field vector **H** perpendicular to the plane of ring. Unlike in the case of a metallic ring, in dielectric ring (permittivity ε), the induced emf generates an electric displacement $\mathbf{D} = \varepsilon\mathbf{E}$ inside the ring which in turn contribute a displacement current $\mathbf{I_D}$.

This alternating displacement current will, in turn, produces an alternating magnetic field which results in another electric field in accordance with Maxwell's curl equations. By considering the above effects in a dielectric ring A. B. Shavartsburg *et al.* [151] deduced the following equation for resonant frequency,

$$\Omega = \frac{c}{r}\sqrt{\frac{2(1+\varepsilon k)}{\varepsilon l_1}} \tag{4.2.1}$$

where $l_1 = \ln[8R/r] - 7/4$, c is the velocity of light, $k = s/2\pi R$, R is the outer radius of the ring, r is the inner radius of ring and s is the split spacing.

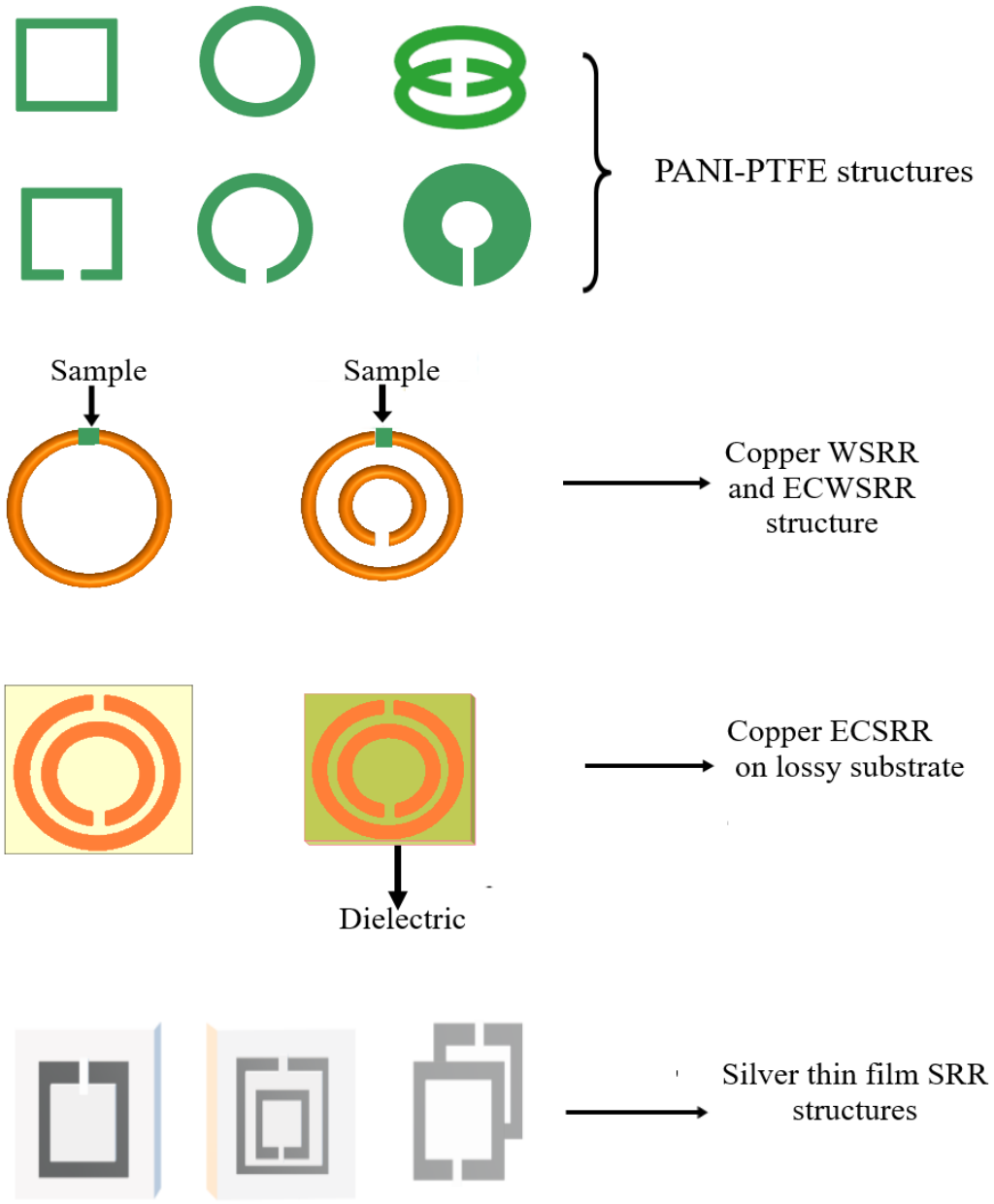

Figure 4.2: Schematic representation of SRRs used for the study.

4.3 PANI-PTFE SRR: Preparation and resonance study

The SRR resonator structures of different geometries are cut out from the conducting PANI-PTFE sheets of thicknesses 1 mm, 1.5 mm and 2 mm, using surgical blades and cylindrical cutters. The Closed Ring Resonator (CRR) and single Split Ring Resonator (SRR) structures are fabricated for electric and magnetic resonance studies in square and circular forms [152]. The resonators with different structural parameters like split width, thickness and radius are also fabricated for understanding the geometry dependent resonance behaviours. The circular BCSRR metamaterial structure is also made using PANI-PTFE rings to study the enhancement in resonant absorption behaviour. Wire single ring SRR and Edge-Coupled Split Ring Resonator (ECSRR) with the split gap filled with small samples of PANI-PTFE are fabricated for humidity related studies.

For theoretical and conceptual understanding of the wide band nature of magnetic resonance observed for PANI-PTFE SRR rings, resonance behaviour of conducting rings with resistive component is studied. For this, conventional SRRs are fabricated with a lossy substrate and the effect of loss factor is examined.

SRRs are also made using silver thin films of thickness less than the skin depth so that the resistive element in the flow of microwave induced current is incorporated. This thin film square SRRs thinner than the skin depth are fabricated on glass substrates by employing RF sputtering technique. Single ring SRRs, ECSRRs and BCSRRs of thickness 350 nm, 550 nm, and 750 nm are also fabricated. The schematic representation of different SRR structures used for the study is shown in Fig. 4.2.

The fabricated CRR and SRR structures are analyzed for their electric and magnetic resonances in 3-9 GHz by arranging them between two

monopole antennas connected to the transmitting and receiving probes of a Vector Network Analyzer (VNA) as shown in Fig. 4.3. Here the orientation of ring is such that electric field **E** is parallel to the slit and magnetic field **B** is perpendicular to plane of the ring (Fig. 4.3). The magneto-electric coupling effects are analyzed for circular BCSRRs by placing it between the monopole antennas (Fig. 4.3). The effect of humidity on the resonance for an SRR structures are studied by placing them in a humidity chamber. SRR based humidity sensor studies are carried out by inserting a strip of PANI-PTFE material in the split gap of a wire SRR kept inside the humidity chamber.

The studies of wide band SRRs having lossy dielectric substrates as well as silver thin film SRRs, ECSRRs and BCSRRs are also carried out using the above system.

4.3.1 Square SRR and CRR

With the purpose to demonstrate the magnetic resonance of PANI-PTFE ring for its proposed inclusion in the metamaterial group, the observance of magnetic resonance in PANI-PTFE is verified in relation to metallic SRR having the same dimension. As demonstrated by the response figures of Chapter 1 (Fig. 1.7), a CRR shows only an electric resonance while a SRR exhibits strong magnetic resonance along with a weak electrical resonance.

The structural parameters of PANI-PTFE square type SRR (single) and CRR rings fabricated for the above purpose are the following: outer length l_{outer} = 10 mm, inner length l_{inner} = 5 mm, thickness t = 1.5 mm and split width s = 0.5 mm. Schematic representation of square SRR and CRR used for the study is shown in Fig. 4.4. Copper SRR and CRR are also fabricated with the same dimensions except for a change in thickness. Thickness, t of copper ring is 18 μm and it is obvious that there is not much effect on the resonance behaviour of copper due to change in thickness

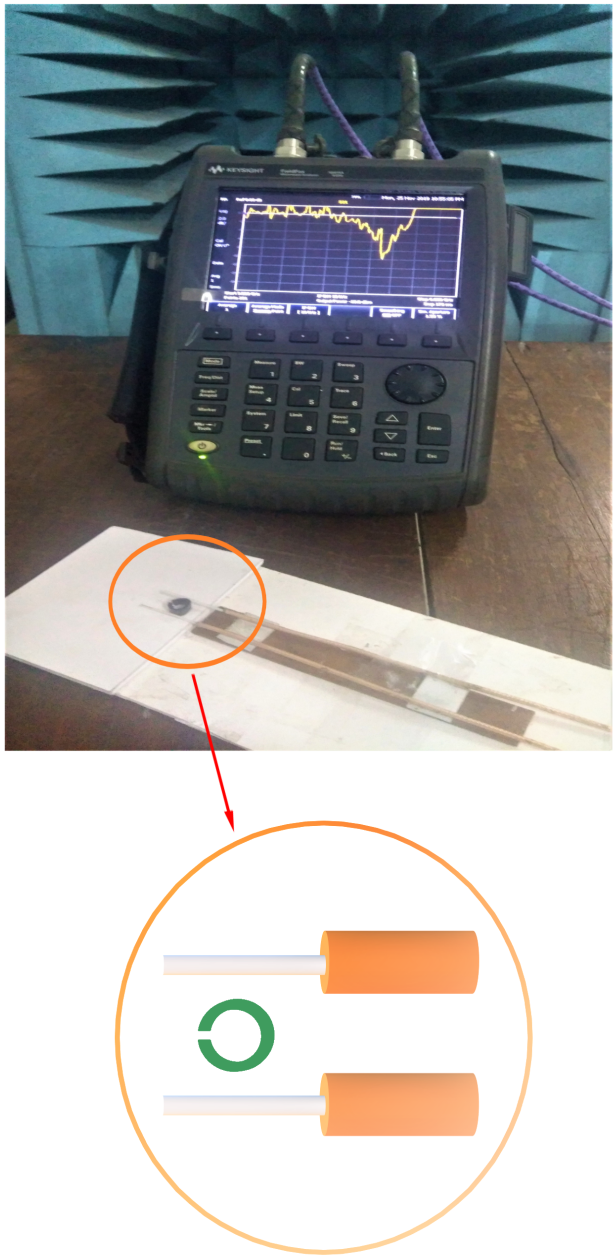

Figure 4.3: Photograph of experimental setup to study the transmission coefficient of PANI-PTFE ring. Inset gives the schematic representation of the ring between transmitting and receiving probes.

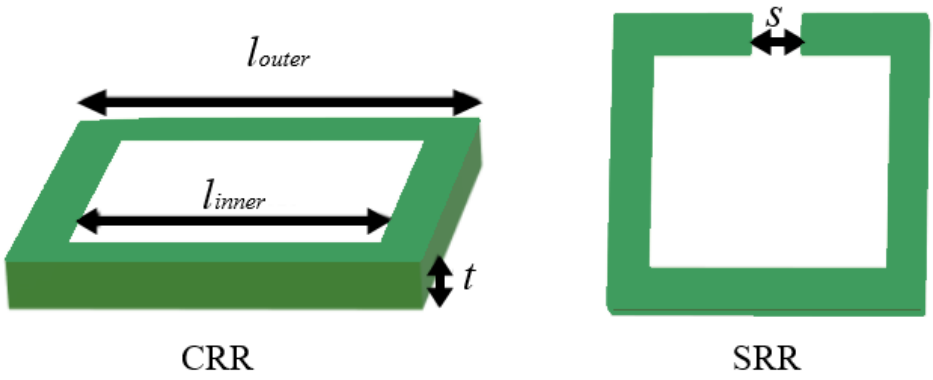

Figure 4.4: Schematic representation showing the structural parameters of square CRR and SRR made using PANI-PTFE material.

and it is because of a high density of charge carriers in materials of high conductivity.

Figure 4.5(a) shows the electrical resonance curves obtained at 6.7 GHz for the CRR made of copper and PANI-PTFE. Fig. 4.5(b) represents the magnetic resonance obtained at 5.5 GHz for the SRRs of both the cases. Their electric resonances appear at a higher frequency with reduced absorption as detailed in the Section 1.9 of Chapter 1.

For further verification, the magnetic resonance in the PANI-PTFE square SRR of above dimensions with thickness $t = 1.5$ mm is simulated using HFSS and its resonance behaviour is found to be in good agreement with the experimental value as plotted in Fig. 4.6.

The analysis of above results clearly verifies the observance of magnetic resonance in PANI-PTFE polymer SRRs. In view of the lower absorption dip around -15 dB (Fig. 4.6) observed for square structures, circular resonators are tried for better results.

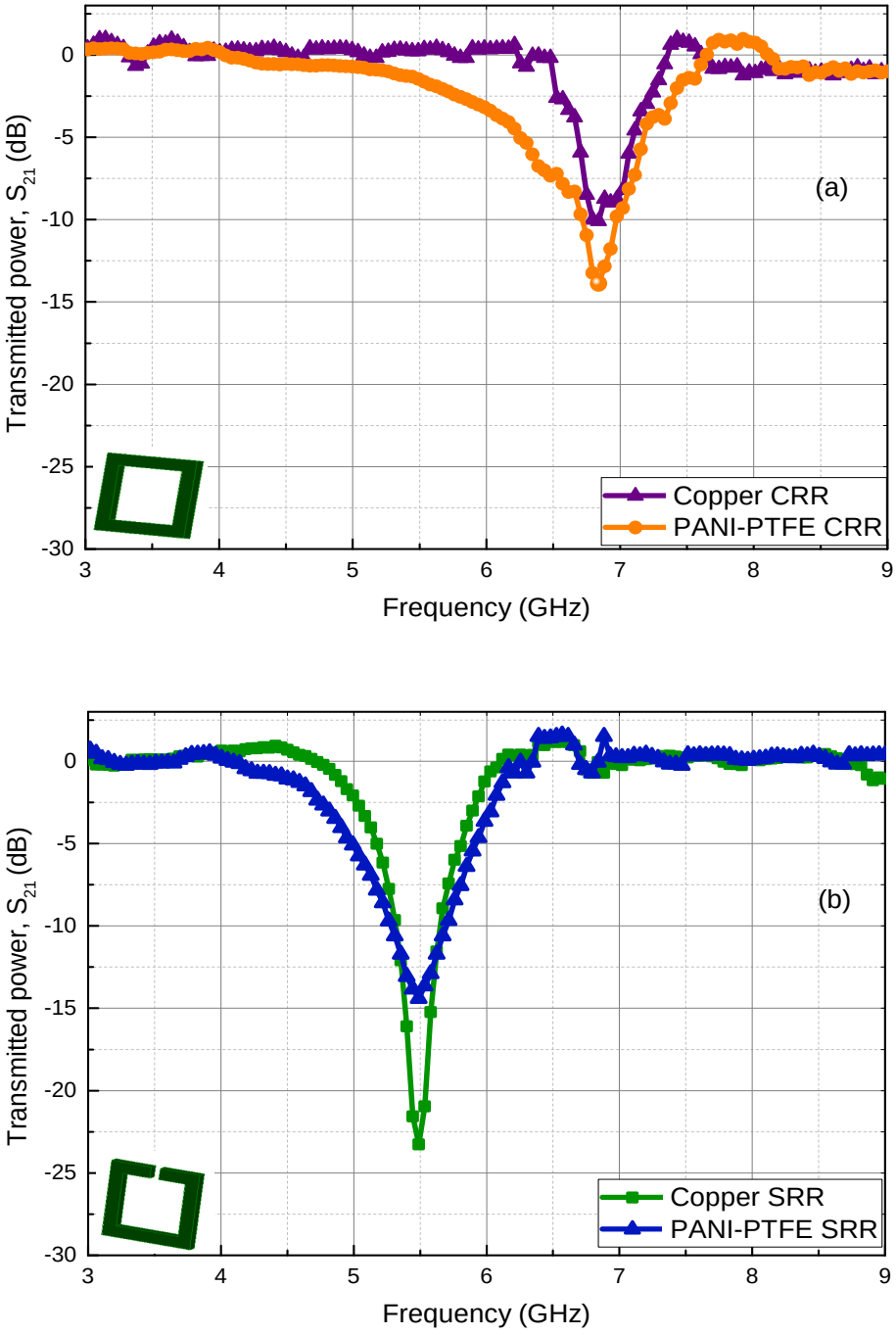

Figure 4.5: (a) Electric resonance observed (experimental) in copper and PANI-PTFE single ring CRR (b) Magnetic resonance observed (experimental) in copper and PANI-PTFE single ring SRR. (Dimensions of the rings are outer length l_{outer} = 10 mm, inner length l_{inner} = 5 mm and split width s = 0.5 mm. The thickness of PANI-PTFE ring is t = 1.5 mm and of copper is t = 18 μm.)

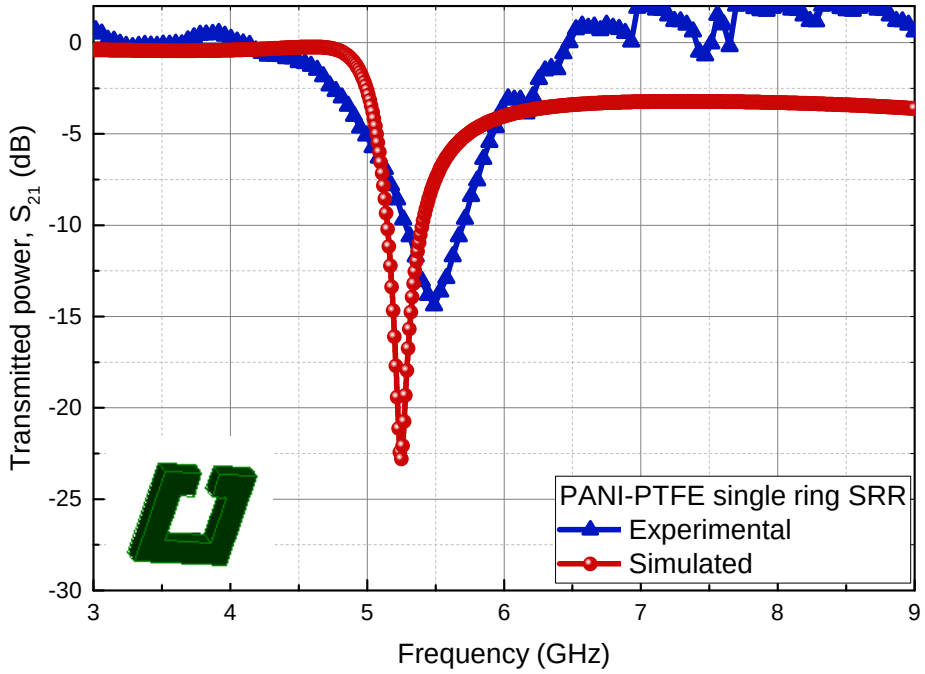

Figure 4.6: Experimental and simulated magnetic resonance curves for PANI-PTFE square ring of outer length l_{outer} = 10 mm, inner length l_{inner} = 5 mm and split width s = 0.5 mm and thickness t = 1.5 mm.

4.3.2 Circular SRR and CRR

To analyze the magnetic resonance and structural parameter dependent changes of resonance frequency, circular SRRs and CRRs using PANI-PTFE are also prepared. Initially CRR and SRR of following dimensions are prepared. For CRR the parameters are inner radius r = 4 mm, ring width w = 1 mm and thickness t = 3 mm. For SRR, while keeping all the structural parameters same, a split width s = 1 mm is made. Figure 4.7 shows the magnetic resonance curves obtained for these resonators along with the simulation results. Simulated result of circular copper ring CRR and SRR with same dimensions are also shown for comparison.

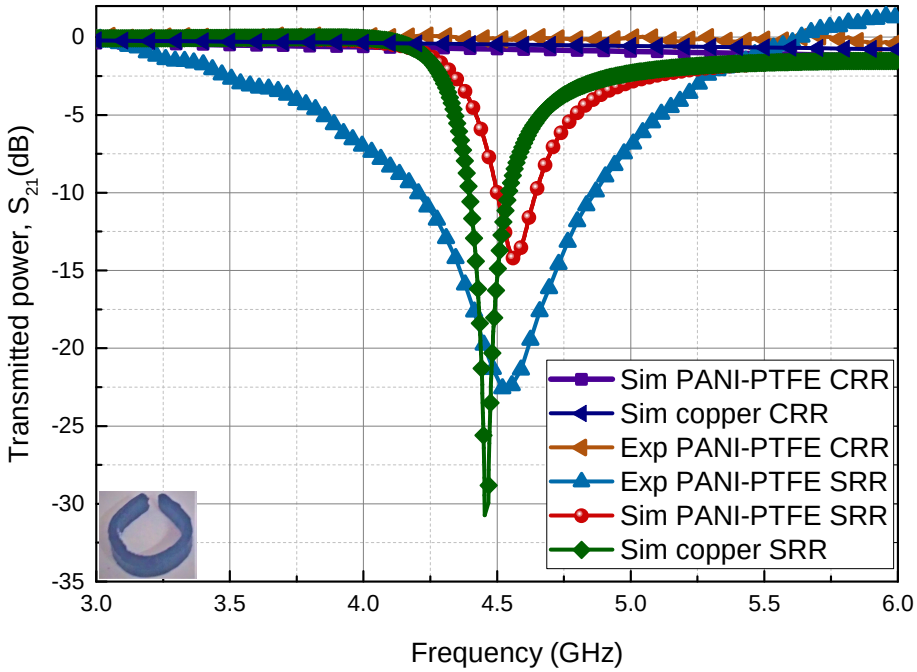

Figure 4.7: Magnetic resonances present in a copper and PANI-PTFE CRR and SRR rings of inner radius r = 4 mm, ring width w = 1 mm, split width s = 1 mm and thickness t = 3 mm. Inset: Photograph of PANI-PTFE single ring SRR used for the study.

The resonant frequency of copper ring is slightly lower than that of PANI-PTFE ring of same dimensions. From the above figure it is observed that resonance band width of PANI-PTFE rings is quite broader than its metallic counterpart. This wide band resonance behaviour of PANI-PTFE ring may be due to the lower conductivity of the material. Absence of magnetic resonance for CRR is also noticed. Almost same resonance frequency of PANI-PTFE ring resonator with that of copper SRR may be due to the significant displacement current contribution from the polymer chain.

The absorption dip of -25 dB is obtained for circular SRRs which is comparably higher when compared to -15 dB in square ring (Fig. 4.6).

Henceforth, further analysis of different characteristics of the newly prepared PANI-PTFE SRRs is based on circular geometry.

As already discussed in Section 1.9.2 of Chapter 1, resonant frequency depends upon the split width, ring width and the radius. Here the effects of the above structural parameter variations on the resonant frequency are experimentally analyzed for the case of PANI-PTFE ring.

From the resonance curves of square (Fig. 4.6) and circular (Fig. 4.7) SRRs the deviation in the experimental and simulated curves are expected from the variation in effective length in terms of current conduction mechanism.

4.3.2.1 Split width and resonance frequency

Schematic representation of CRR and SRR is given in Fig. 4.8(a) and (b). PANI-PTFE single ring SRRs of inner radius $r = 1.5$ mm, ring width $w = 3.5$ mm, thickness $t = 1$ mm and split widths $s = 1$ mm, 0.7 mm, and 0.4 mm respectively are prepared for the study and their corresponding magnetic resonances obtained are shown in Fig. 4.9 along with the simulation results.

For split width of 0.4 mm, 0.7 mm and 1 mm the resonant frequencies obtained are 6.2 GHz, 6.5 GHz and 6.8 GHz respectively, i.e. a difference of 0.3 mm in split width results in a frequency change of 0.3 GHz. For the single ring SRR, the shift in resonance frequency with the split width variation is observed to be a linear one. Figure 4.10 gives the experimental and simulated results and this dependence may be explained in terms of relation between split capacitance and the resonance frequency, a result in the same line as that of the metallic ring [63].

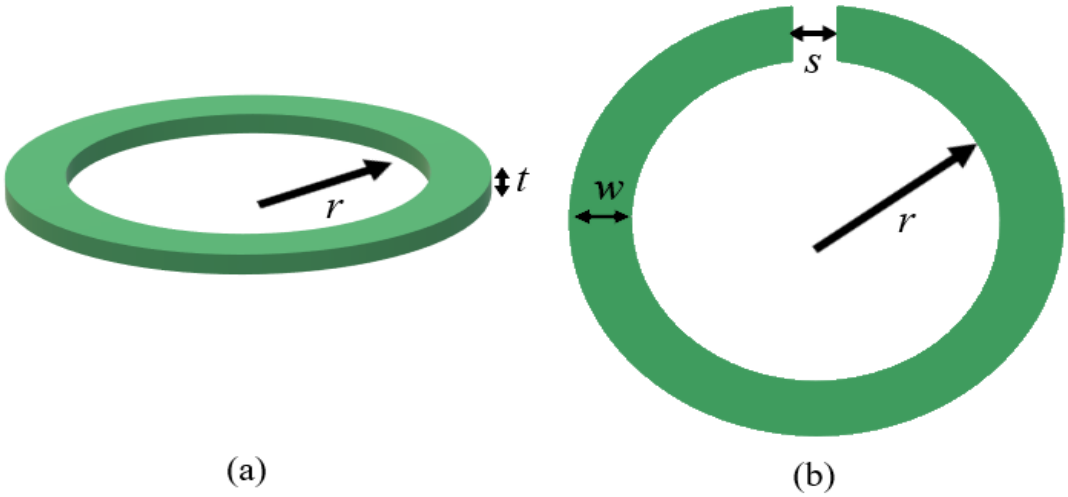

Figure 4.8: Schematic representation of (a) CRR and (b) SRR (r is the inner radius, w is the ring width, t is the thickness and s is the split width).

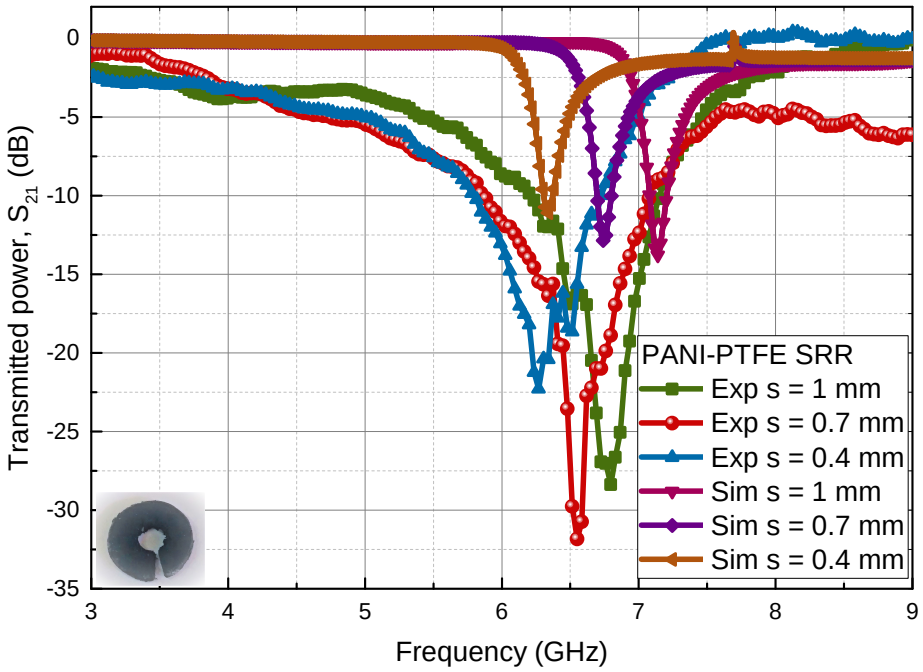

Figure 4.9: Resonance frequency dependence of PANI-PTFE ring of inner radius r = 1.5 mm, ring width w = 3.5 mm, thickness t = 1 mm and split width s = 1 mm, 0.7 mm, and 0.4 mm respectively. Inset: Photograph of PANI-PTFE single ring SRR used for the study.

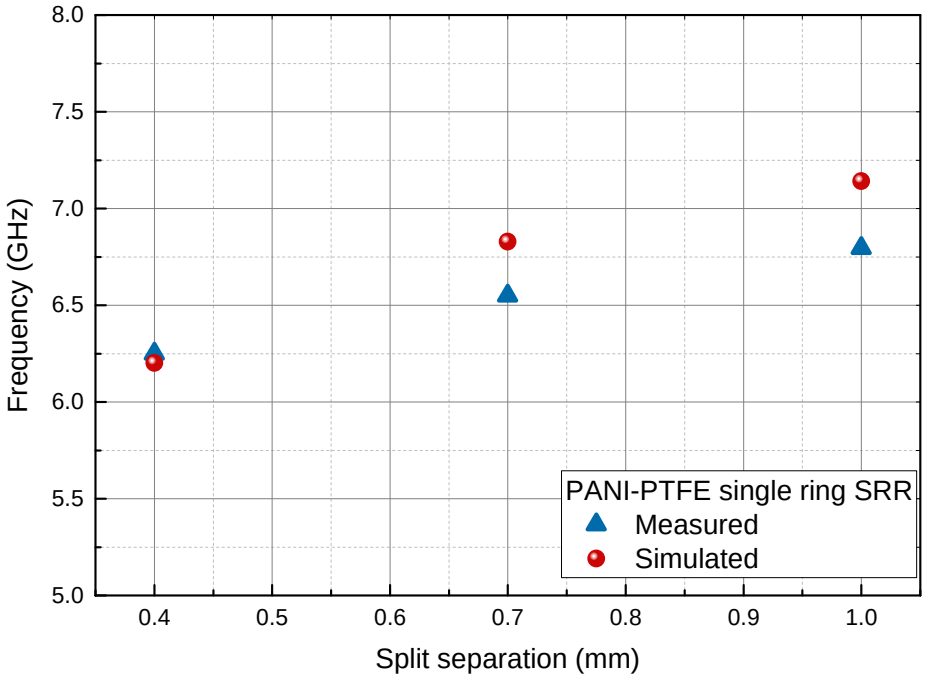

Figure 4.10: Measured and simulated results of split width s versus resonance frequency of PANI-PTFE ring of inner radius r = 1.5 mm, ring width w = 3.5 mm and thickness t = 1 mm.

4.3.2.2 Radius and resonance frequency

For radius variation studies, SRRs of inner radius 5 mm, 4 mm and 3 mm are used. PANI-PTFE SRR of the above radii are made by taking the other parameters of the ring (width w, thickness t and split width s) as 1 mm for all the three cases.

From Fig. 4.11 we can observe that as the radius increases resonant frequency shifts towards lower value, a result similar to that of the metallic ring [67].

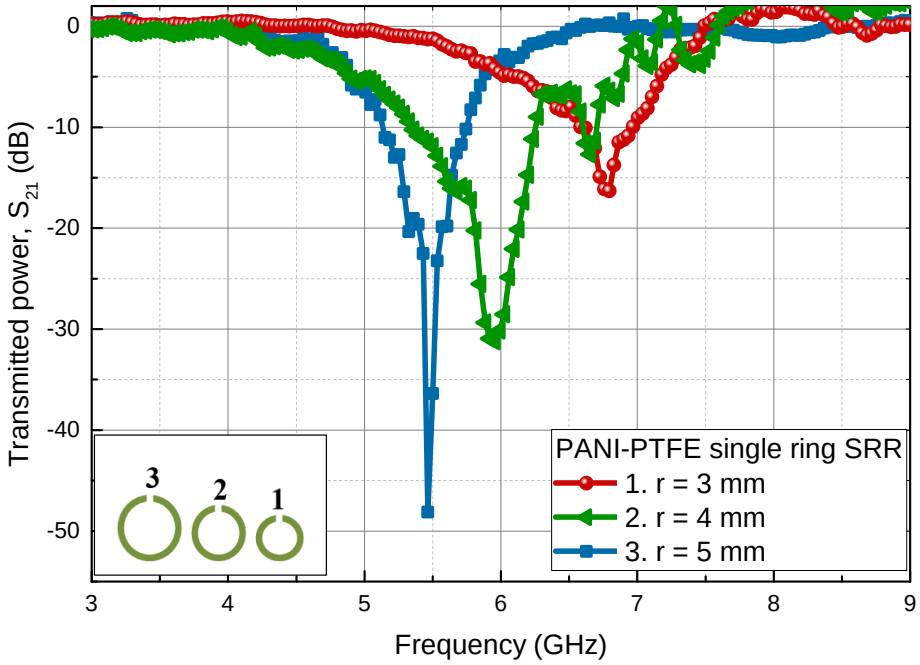

Figure 4.11: Magnetic resonances observed in PANI-PTFE rings of varying inner radius r = 5 mm, 4 mm and 3 mm and constant width w = 1 mm, thickness t = 1 mm and split width s = 1 mm.

4.3.2.3 Thickness and resonance frequency

The next study conducted is on the dependence of resonance frequency on thickness of PANI-PTFE ring. The structural parameters of SRR rings are inner radius $r = 4$ mm, width $w = 1$ mm, split width $s = 1$ mm. Two rings of thicknesses $t = 1$ mm and $t = 2$ mm were used. The magnetic resonance curves obtained are shown in Fig. 4.12.

With increase in thickness, the split capacitive contribution to resonance frequency increases and frequency shifts towards the lower regime. Capacitive term is associated with area of cross section at the split and as it increases capacitance increases resulting in a decrease in resonant frequency.

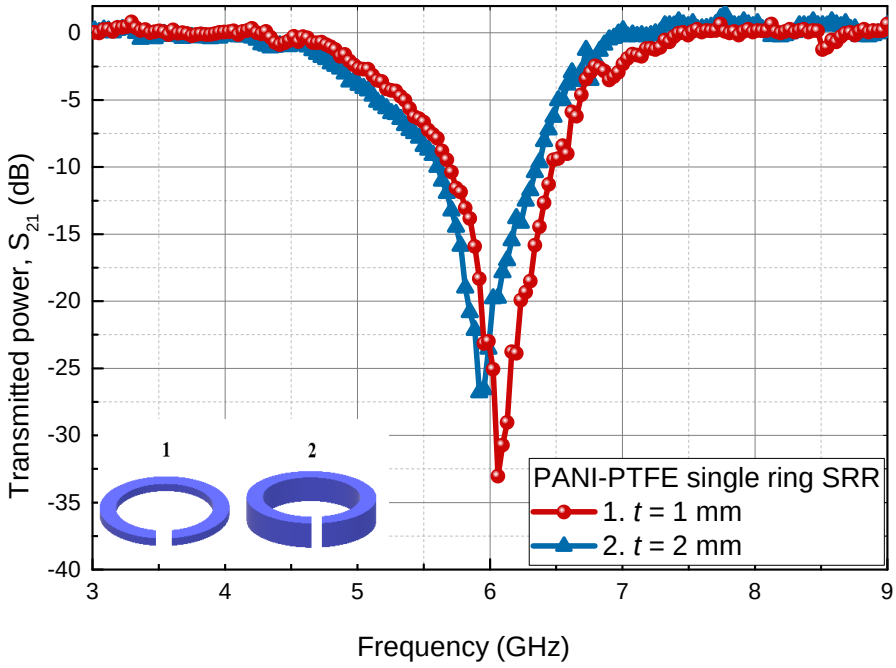

Figure 4.12: Magnetic resonances observed in PANI-PTFE rings of dimensions: inner radius r = 4 mm, width w = 1 mm and split width s = 1 mm for two rings of thicknesses t = 1 mm and t = 2 mm.

A similar trend with thickness is also seen in metallic SRRs [51, 153].

The results obtained from the resonance study of circular PANI-PTFE CRRs and SRRs can be summarized as:

- The magnetic resonance in PANI-PTFE SRR may be explained by the conduction currents as well as the displacement currents.
- Resonance frequency of PANI-PTFE SRR varies with structural factors like radius, split width and thickness as in the case of metallic resonators.
- The resonant behaviour of PANI-PTFE ring shows a wide band characteristics apart from that observed in metallic SRRs.

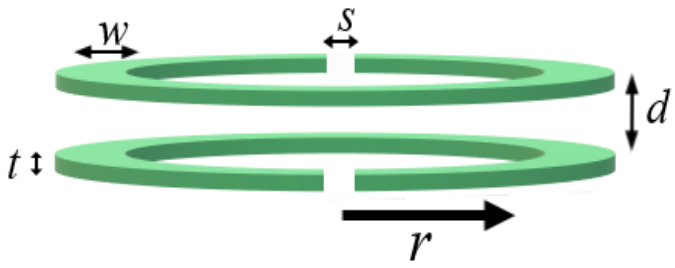

Figure 4.13: Schematic representation of BCSRR (inner radius r, width w, thickness t, split width s and spacing between the rings d) using PANI-PTFE.

Thus this newly prepared PANI-PTFE single ring SRR structure can be used to fabricate wide band negative permeability metamaterial structures.

4.3.3 Broadside-Coupled Split Ring Resonator

Due to the comparatively lower conduction in PANI-PTFE than in metals possibilities are also explored to find out SRR structures which will enhance the mutual coupling between rings. The two possible identified simple structures are ECSRR and BCSRR. Since in ECSRR strong coupling between the rings is limited to neighbouring edge regions, the suitable choice for enhanced performance may be BCSRR in which the entire width area contributes to coupling. Experimental results with test ECSRR are found to substantiate the above argument and accordingly studies are done using BCSRR structures.

PANI-PTFE BCSRRs of dimensions inner radius $r = 4$ mm, width $w = 1$ mm, thickness $t = 3$ mm, split width $s = 2$ mm and spacing between the rings $d = 1$ mm is prepared and the schematic representation is given in Fig. 4.13. The corresponding magnetic resonance curves are given in Fig.

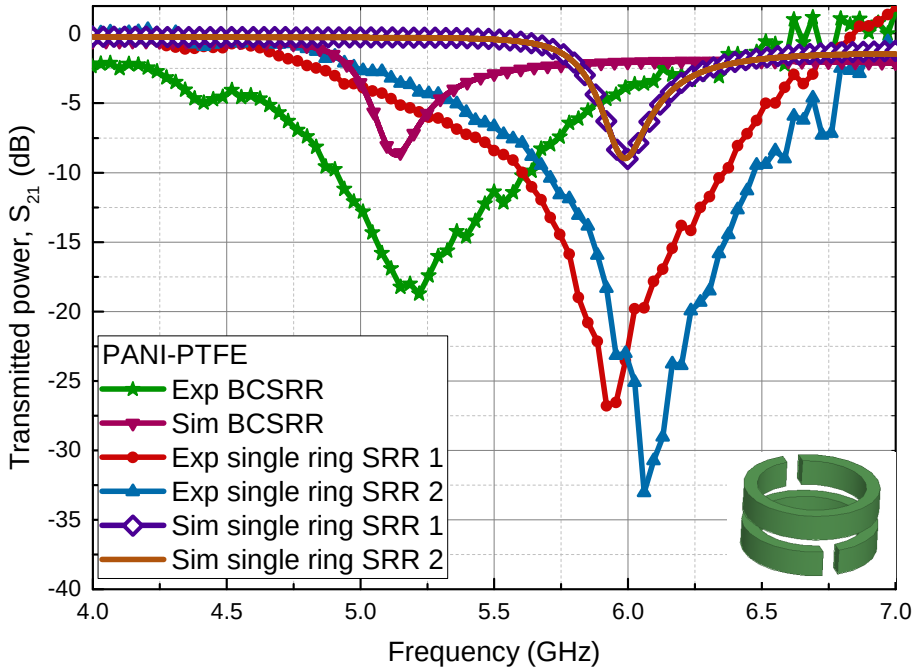

Figure 4.14: Magnetic resonances observed in PANI-PTFE BCSRR of dimensions inner radius r = 4 mm, width w = 1 mm, thickness t = 3 mm, split width s = 2 mm and separation between the rings d = 1 mm.

4.14. The resonance curves of individual rings are also shown for comparison. Deviations in resonance frequency of the two identical single ring SRRs may be due to instrumental and environmental errors in measurement system. Simulation studies are also presented in the figure for comparison.

Similar to metallic BCSRRs the resonance frequency of PANI-PTFE BCSRR is also shifted to a lower frequency due to enhanced capacitive and inductive coupling effects. Table 4.1 gives a comparison of simulated and measured resonance frequency of single ring SRR and BCSRR made using PANI-PTFE.

With the realization of metamaterial BCSRR using PANI-PTFE having behavioural resemblance to metallic BCSRRs an opening for conduct-

Table 4.1: Resonance frequency of PANI-PTFE BCSRR and individual single ring SRRs.

PANI-PTFE	Frequency (GHz)	
	Measured	Simulated
Ring 1	6.06	5.991
Ring 2	5.92	5.991
BCSRR	5.15	5.133

ing polymers to the world of negative permeability structures is obtained. For enhancing the magnetic responses these polymers can also be used with metallic inclusions resulting in better conductivity. Thus the advantage is that tunability and viability of conducting polymers is much beneficial in the fabrication of wide band negative permeability metamaterial structures.

Along with the proposed metamaterial applications, the property of humidity dependent conductivity variations exhibited by PANI-PTFE can be utilized for SRR based humidity sensors.

4.3.4 Humidity dependent SRR sensors using PANI-PTFE

Humidity dependent conductivity of PANI-PTFE sheet is an important parameter that can be utilized for the fabrication of humidity sensing devices. In the following section, different types of humidity dependent SRR structures are presented and they are

1. PANI-PTFE single ring SRR.
2. Metallic wire single ring SRR with PANI-PTFE embedded in split gap.
3. Metallic wire ECSRR with PANI-PTFE embedded in split gap.

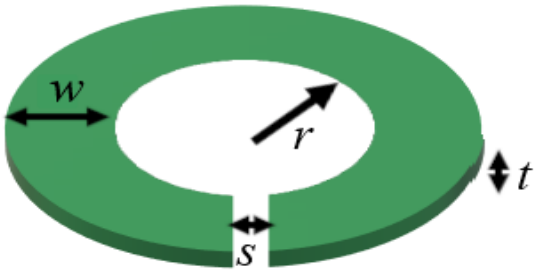

Figure 4.15: Schematic representation of PANI-PTFE SRR sensor ring with inner radius r, width w, thickness t and split width s used for humidity study.

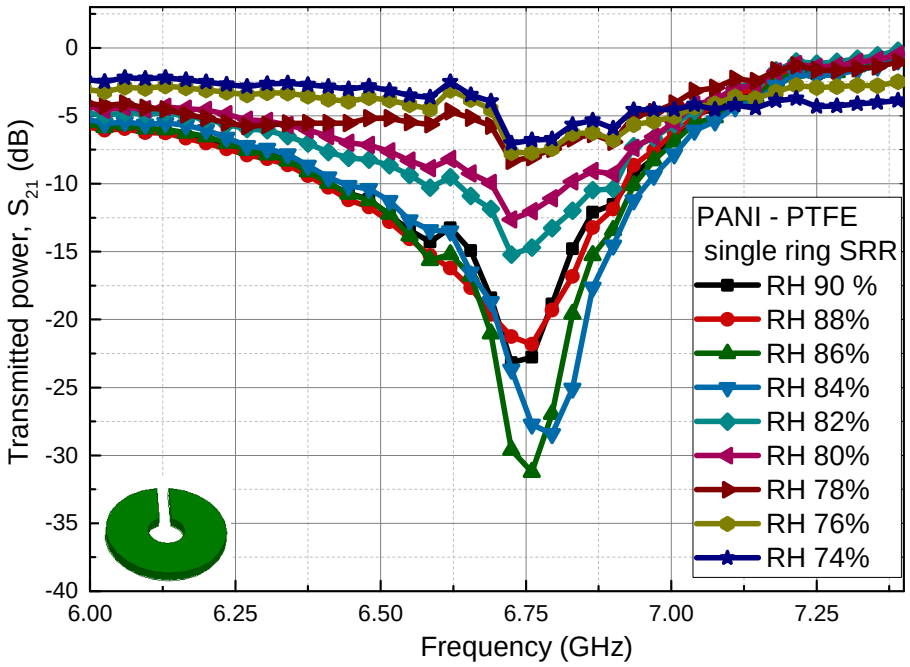

Figure 4.16: Magnetic resonances observed in PANI-PTFE SRR with dimensions inner radius r = 1.5 mm, thickness t = 1 mm, split width s = 1 mm and width w = 3.5 mm for different humidity conditions.

Table 4.2: Resonance absorption of single ring PANI-PTFE SRR with dimensions inner radius r = 1.5 mm, thickness t = 1 mm, split width s = 1 mm and width w = 3.5 mm for different humidity conditions.

Relative humidity (%)	Frequency (GHz)	Power absorption level (dB)
90	6.725	-18.18
88	6.76	-16.82
86	6.76	-26.23
84	6.795	-23.43
82	6.725	-10.23
80	6.725	-7.65
78	6.725	-3.36
76	6.725	- 2.72
74	6.725	-2.04

4.3.4.1 Humidity dependent properties of the PANI-PTFE SRR

Humidity dependence on magnetic response of PANI-PTFE single ring SRR structure is analyzed for different humidity condition. With a purpose for getting more sensitivity for humidity variations, PANI-PTFE ring is fabricated with moderately high width w whereby the sensing material component of rings will be enhanced. A schematic representation of SRR sensor ring with inner radius $r = 1.5$ mm, width $w = 3.5$ mm, thickness $t = 1$ mm and split width $s = 1$ mm is given as Fig. 4.15. Magnetic resonance observed with varying humidity content is plotted as Fig. 4.16. As the humidity increases, it is observed that the resonance absorption level increases due to increase in conductivity.

Power absorption level of PANI-PTFE SRR sensor corresponding to % RH is tabulated in Table. 4.2 along with the observed resonant frequency. Maximum resonance level of -27 dB is observed for 86% RH and it decreases on further increase in humidity. A possible reason may be that in highly humid condition there is a chance for generation of water domains inside

the polymer which act as a lossy region thereby reducing the transmitted power. At lower humidity conditions the resonance dip reduces and this can be attributed to a decrease in conducting current owing to the reduction in hydrous environment.

4.3.4.2 Humidity dependent properties of the PANI-PTFE embedded metallic wire SRR

In order to study the variations in resonance behaviour of humidity dependent SRR structure, another novel humidity sensor is made using metallic wire SRR in which the split gap is filled with PANI-PTFE polymer. Schematic representation of the wire SRR sensor with PANI-PTFE sample is given as Fig. 4.17

To form single ring SRR, copper wire of radius $r^{'} = 0.5$ mm is bend into rings of radius $r = 5$ mm with a split width $s = 1$ mm. The sample PANI-PTFE with 0.5 mm thickness having length and breadth 1 mm each is carefully inserted at the split gap of the wire ring and its resonance characteristics are analyzed in various humid conditions.

Insertion of PANI-PTFE sheet into the gap changes the gap capacitance which is reflected in the expression for resonant frequency f_0 given as

$$f_0 = \frac{1}{2\pi\sqrt{LC}} \tag{4.3.1}$$

where L is the inductance and C is the capacitance.

The major contribution of capacitance is from the split gap and it is given by the relation [51, 154]

$$C_{gap} = \varepsilon[\frac{\pi(r^{'})^2}{s}] \tag{4.3.2}$$

where ε is the permittivity of the gap capacitor, s and $r^{'}$ are the split width and the radius of the ring respectively as depicted in the Fig. 4.17.

The resonance curves obtained for different humidity conditions are plotted in Fig. 4.18 along with that in the absence of PANI-PTFE sample.

In presence of PANI-PTFE sample in the split region, resonance frequency shows a decrease due to increase in C_{gap} in relation to ε (Eqn. 4.3.2).

As humidity of the PANI-PTFE sample increases, its permittivity also increases which in turn causes resonance frequency to reduce further. The possibility of a leakage current in presence of humid sample at split region may not be ruled out, even though the capacitive effect dominates for moderate values of humidity. However for highly humid samples (above 85% RH) the magnetic resonance shows a remarkable change in terms of absorption dips as well as band width, due to the domination of leakage current over capacitive contribution.

When the humidity increases above 90% RH the magnetic resonance vanishes due to increase in conductivity which leads to a short circuiting effect at the split ends and then the WSRR changes to a WCRR. Resonant frequencies for various humidity values along with their power absorption levels for a WSRR are given in Table. 4.3. The power absorption levels for different humidity conditions are plotted in Fig. 4.19.

From the plot it is clear that the maximum magnetic coupling occurs around 65% to 70% RH as in the case observed in humidity study of single ring PANI-PTFE SRR also.

4.3.4.3 Humidity dependent properties of the PANI-PTFE embedded metallic ECWSRR

Humidity dependent resonant property is also examined in the case of the popular metamaterial negative permeability ECWSRR structure hav-

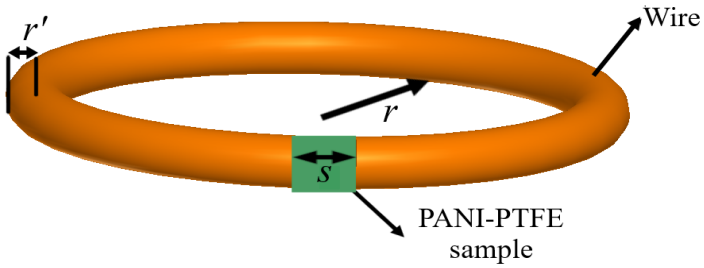

Figure 4.17: Schematic representation of the proposed wire SRR sensor with PANI-PTFE sample inserted at the split region.

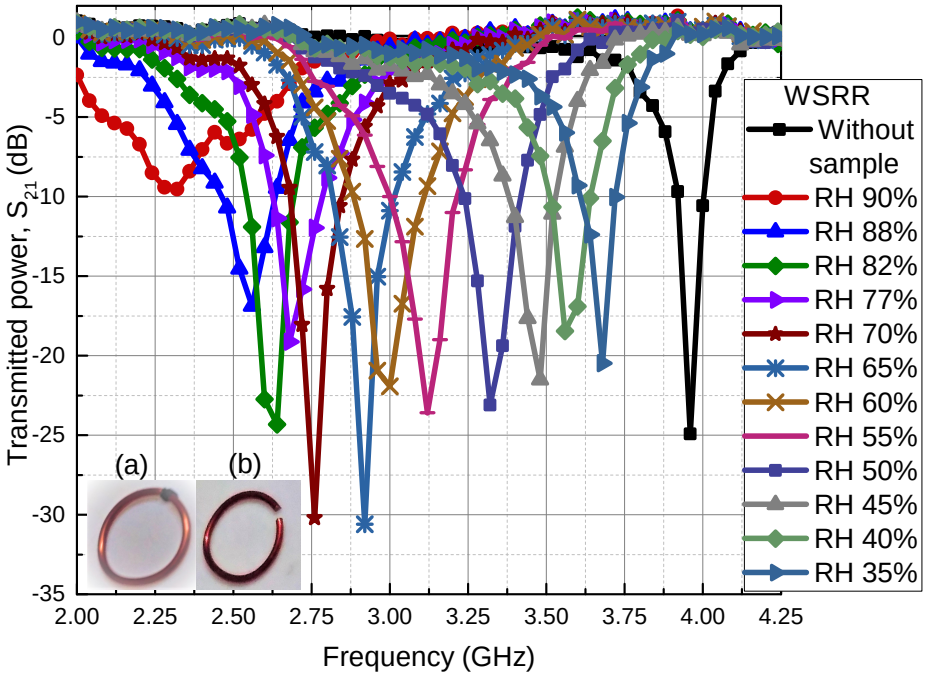

Figure 4.18: Humidity dependent magnetic resonance observed in PANI-PTFE embedded single WSRR sensor (Wire radius $r^{'}$ = 0.5 mm, ring radius r = 5 mm and split width s = 1 mm). Inset: Photograph of the WSRR (a) with and (b) without the PANI-PTFE sample.

Table 4.3: Humidity-resonant frequency table for single ring WSRR (Wire radius $r^{'}$ = 0.5 mm, inner radius r = 5 mm, split width s = 1 mm)

Relative humidity (RH%)	Frequency (GHz)	Power absorption level (dB)
WSRR (No sample)	3.96	-24.91
30	3.72	-20.44
31	3.72	-17.24
32	3.72	-15.91
35	3.68	-20.46
38	3.64	-21.18
40	3.56	-18.44
43	3.56	-23.36
45	3.48	-21.49
48	3.4	-24.59
50	3.32	-23.09
53	3.2	-27.77
55	3.12	-23.58
58	3.04	-21.89
60	3	-21.92
63	2.92	-24.89
65	2.92	-30.60
68	2.84	-23.77
70	2.76	-30.20
75	2.72	-21.11
77	2.68	-19.13
80	2.68	-19.95
82	2.64	-24.30
85	2.6	-26.90
88	2.56	-16.80
90	2.32	-9.50

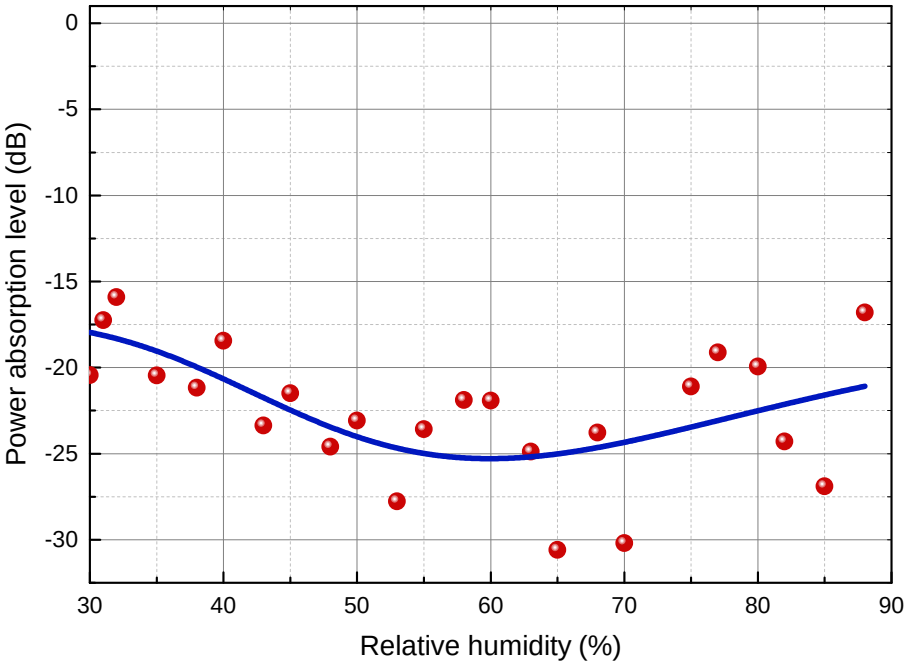

Figure 4.19: Plot of the average values of power absorption levels of PANI-PTFE embedded single ring WSRR (Wire radius $r^{'}$ = 0.5 mm, ring radius r = 5 mm, split width s = 1 mm) at different relative humidity values along with the actual values shown by the bullets.

ing PANI-PTFE sample embedded in the split gap of the outer ring. The structural parameters of the metallic ECWSRR are taken as follows: wire radius $r^{'} = 0.5$ mm, inner ring radius $r = 2$ mm, split width $s = 1$ mm and ring spacing $p = 2$ mm. Schematic representation of PANI-PTFE ECWSRR is given as Fig. 4.20. Resonance frequency obtained in the case of various humidity levels for this resonating structure is given in Fig. 4.21.

Resonant absorption of ECWSRR without PANI-PTFE sample at the split region is found to be around 4.24 GHz as given in the Fig. 4.21. When the PANI-PTFE sample is inserted into the outer ring split gap as shown in the Fig. 4.20, resonance is observed to shift to higher frequency region.

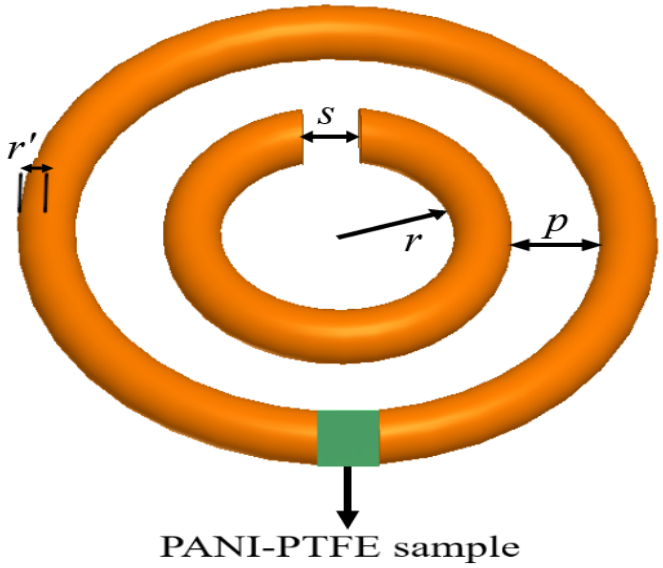

Figure 4.20: Schematic representation of the proposed ECWSRR sensor with PANI-PTFE sample.

Frequency shift may be explained in the following manner. In the case of ECWSRR, total capacitive contribution to resonance is from the split gap capacitance (C_{gap}) and capacitance due to the coupling between the rings ($C_{spacing}$). Normally the values of $C_{spacing}$ is very much higher than C_{gap}.

In present case, though C_{gap} contribution due to outer ring slightly increases by permittivity of sample, the $C_{spacing}$ decreases in a noticeable manner because of non-ignorable leakage current through the PANI-PTFE sample placed at the split region. This will result in decrease in total capacitance of ECWSRR structure, leading to an enhancement in resonant frequency. As humidity content increases, the leakage current dominates further which can be seen by the gradual increase of resonant frequency with humidity as depicted in the Fig. 4.21.

For cases with higher humidity, short circuiting effect as mentioned in the previous case makes the outer ring to act as a CRR resulting in drastic

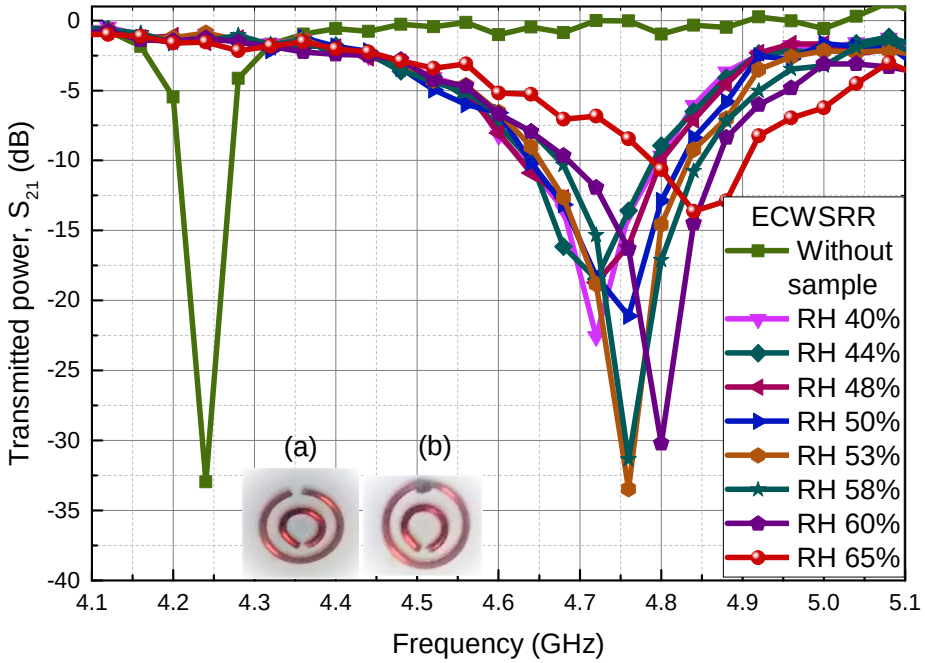

Figure 4.21: Humidity dependent magnetic resonance observed in ECWSRR with a PANI-PTFE sample placed in the split region of the outer ring structure (Wire radius $r^{'}$ = 0.5 mm, inner ring radius r = 2 mm, split width s = 1 mm and ring spacing p = 2 mm). Inset: Photograph of ECWSRR (a) without and (b) with the PANI-PTFE sample.

reduction in magnetic coupling effect reducing the resonance effect. In this stage, even though mutual coupling effects vanish there may be the resonance of inner ring which will be at a much higher frequency (not shown in the Fig. 4.21). Resonant frequencies for various humidity values along with their power absorption levels are given in Table. 4.4.

4.3.5 Band width broadening

The wide band resonance observed for PANI-PTFE ring may have variety of applications in communication technology. In this section reasons behind this behaviour is addressed. Band width of the resonance curve is

Table 4.4: Humidity-resonant frequency table for ECWSRR (Wire radius $r^{'}$ = 0.5 mm, inner ring radius r = 2 mm, split width s = 1 mm and ring spacing p = 2 mm).

Relative humidity (RH%)	Frequency (GHz)	Power absorption level (dB)
ECWSRR (No sample)	4.24	-32.96
40	4.72	-22.58
44	4.72	-18.48
48	4.72	-18.74
50	4.76	-21.12
53	4.76	-33.46
58	4.76	-31.36
60	4.8	-30.22
65	4.84	-13.63

greater for PANI-PTFE ring resonators compared to conventional metallic SRRs. Possible reason for band width broadening is the reduction in Q value due to appearance of resistive part in resonating unit. By considering the case of an LCR resonance circuit this behaviour can be explained.

4.3.5.1 *LC* resonance in presence of a resistive component (*LCR*)

For a series LCR circuit the Q value is given by

$$Q = \frac{1}{R}\sqrt{\frac{L}{C}} \tag{4.3.3}$$

Band width (BW) of resonance curve is inversely proportional to Q value. With increase in R, the Q value decreases and BW increases. For a LCR resonator, the resistance associated with either inductor or the capacitor will also contribute to the inductive or capacitive impedance respectively.

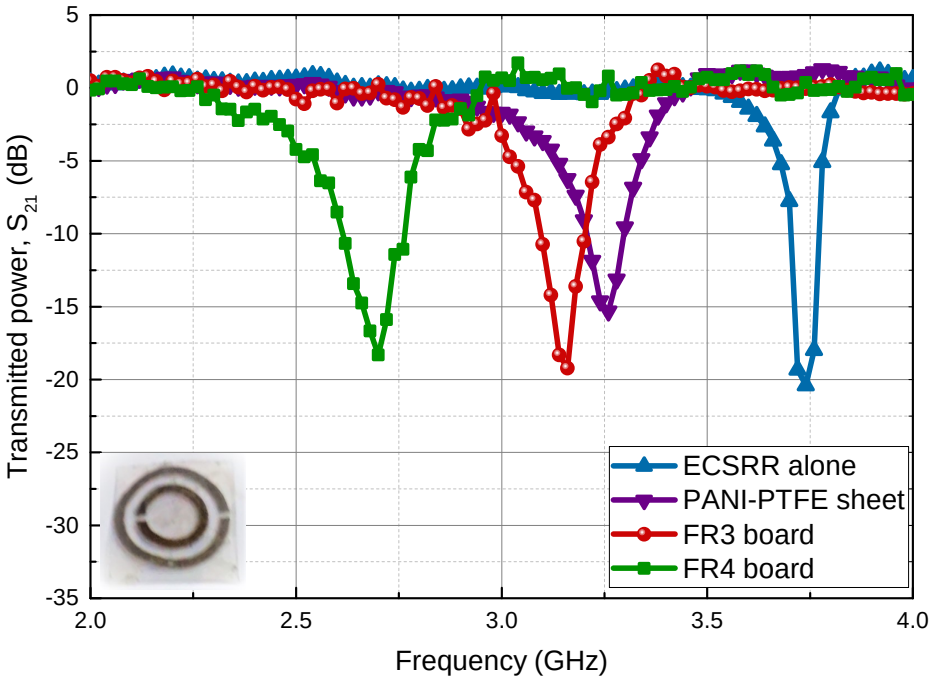

Figure 4.22: Observance of wide band spectrum for copper ECSRR (inner radius r = 2.45 mm, split width s = 0.8 mm, width w = 0.7 mm and spacing between rings p = 0.5 mm, thickness t = 18 μm) in the presence of lossy dielectrics (area = 1 cm^2). Inset: Photograph of ECSRR used for the resonance study.

4.3.5.2 SRR on a lossy dielectric substrate

In order to check the band broadening effects in a metallic SRR in the presence of a lossy dielectric substrate the following procedure is followed. ECSRRs are fabricated using copper sheets of 18 μm thickness with the structural parameters as inner radius r = 2.5 mm, split width s = 0.5 mm, width of the ring w = 1 mm and spacing between the rings p = 0.5 mm.

The required ECSRR pattern is printed on the copper sheet and is subjected to chemical etching after fixing it on polypropylene sheet of negligible thickness (20 μm) for getting the SRR as detailed in [55].

Resonance curve of this ECSRR prepared on thin polypropylene is

Figure 4.23: Schematic representation of SRRs (a) without substrate (b) on a lossy dielectric (PANI-PTFE/FR3 board/FR4 board) substrate.

Table 4.5: Table of resonant frequency, band width and loss tangent of ECSRR with lossy dielectric substrates.

Substrate sample	Resonant frequency	Band width (MHz)		Loss tangent
	(GHz)	3 dB	10 dB	
ECSRR (No substrate)	3.74	48.810	69.405	
ECSRR (PANI-PTFE)	3.26	63.110	204.402	0.006308
ECSRR (FR3 board)	3.16	50.220	120.040	0.003467
ECSRR (FR4 board)	2.68	71.430	176.790	0.013650

shown in Fig. 4.22. Three such SRRs are prepared and pasted on three different lossy substrates of area 1 cm^2 out of which two are Flame Resistant (FR) circuit boards and one is a sheet of PANI-PTFE. The schematic representation of SRRs on lossy substrates is given as Fig. 4.23.

The resonance curves obtained with the lossy substrates are also shown in Fig. 4.22. It is quite evident from the graph that band width has increased due to the effect of resistive element in the presence of lossy dielectric in the resonating structure. Normal shift in resonant frequency due to the effect of permittivity related enhanced capacitance is also clearly seen

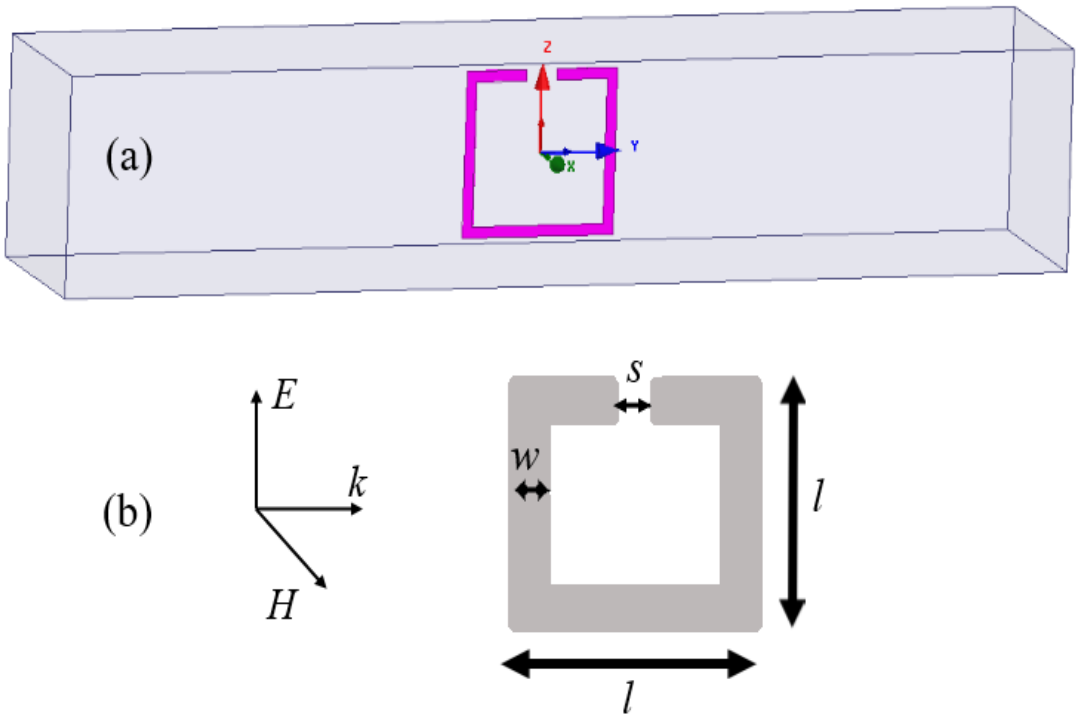

Figure 4.24: (a) The structure of resonator (length l = 10 mm, width w = 2 mm and split width s = 1 mm) used for HFSS shown within the radiation box (x = 20 mm, y = 100 mm and z = 13 mm). (b) Geometrical parameters and orientation of the ring with respect to the applied field.

in the figure. Loss factor, band width (3 dB and 10 dB band width measured with respect to the absorption minimum [150, 155]) and resonance frequency are given in Table 4.5.

4.3.5.3 SRR made of metallic thin films

While for the case of SRR with lossy substrate band width broadening was effected by the introduction of resistive elements in its near field environment. In this case it is achieved by making the resonator itself resistive. For this purpose metallic SRR (single ring square SRR, ECSRR and BCSRR) are made with rings having thickness less than the skin depth and resonance behaviour is studied.

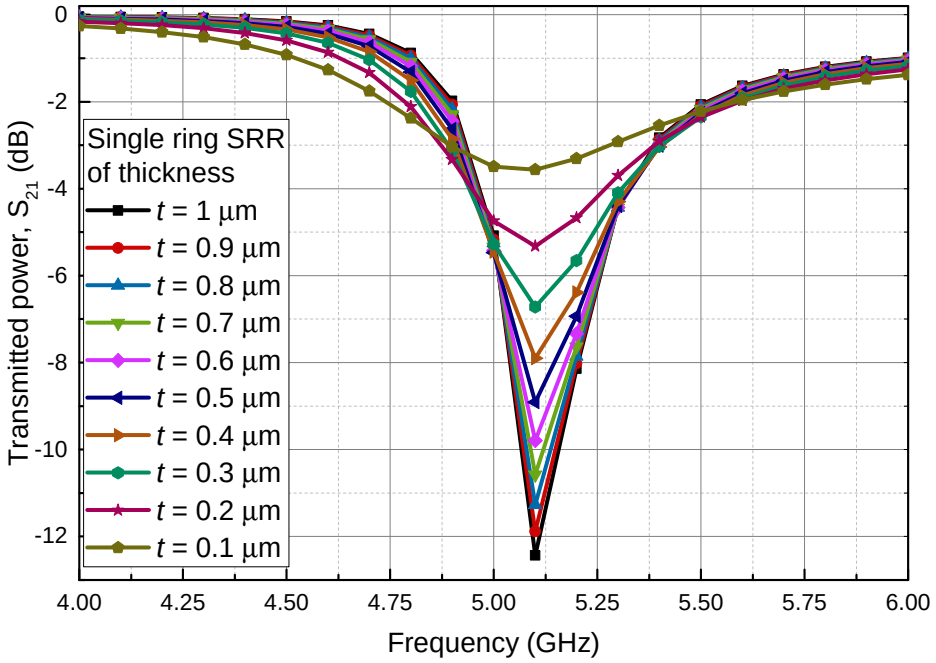

Figure 4.25: Magnetic resonances (simulation curves) of silver square SRRs below skin depth (length l = 10 mm, width w = 2 mm and split width s = 1 mm) for different thickness.

For checking wide band nature of the thin metallic SRR, simulation studies are also carried out using HFSS. For this, a square silver single ring SRR of dimensions length l = 10 mm, width w = 2 mm and split width s = 1 mm is placed inside a radiation box (x = 20 mm, y = 100 mm and z = 13 mm) with electric excitation parallel to the splits and magnetic excitation perpendicular to the plane of SRR. The positioning of resonator is shown in Fig. 4.24(a).

The magnetic resonance obtained for thin silver film SRR for different thicknesses using simulation is shown in Fig. 4.25. From the figure it is clear that band width increases with decrease in thickness t and that the magnetic resonance absorption level decreases as t decreases. Skin depth of silver

metal for the corresponding resonance frequency is around 1 μm and it is evident from the simulation curve that, the band width broadens directly with decrease in t.

For experimental verification of the above results, thin film silver SRRs of different thicknesses are prepared using RF magnetron sputtering technique. The glass substrate is cleaned using traditional cleaning techniques with ultrasonic bath and isopropyl alcohol. Then one side of the oven-dried slide is covered with high temperature resistant kapton tape. Resonator structure is then stenciled on the tape and is then fixed in sample holder of sputtering chamber facing the target. The silver target used is 50 mm diameter and 99.99% pure. Plasma was activated by a 13.56 MHz RF power of 25 W in argon pressure of 3 X 10^{-3} Torr with argon flow of 20 sccm. After coating, the mask (kapton tape) is carefully removed to get the ring resonators on the glass substrate [156]. Schematic representation of the preparation process is shown in Fig. 4.26.

The prepared film is shown in Fig. 4.27. SRR and BCSRR structures of thicknesses 350 nm, 550 nm and 750 nm in square shape are prepared using this technique by varying the sputtering duration. For the BCSRR, rings are fabricated on both sides of glass substrate of thickness 1.3 mm.

The prepared thin film is placed between the monopole transmitter and receiver probes connected to a VNA for resonance measurement.

The resonance absorption spectra of single ring square SRRs of different thickness are presented in Fig.4.28. It is quite evident from the graph that resonance curve is of wide band nature owing to the resistive nature of the resonator due to the lowering of thickness below skin depth, which is around 1 μm at the resonating frequency. A shift in resonant frequency towards higher end is observed as the thickness decreases, which may be due to the fact that the resistive element associated with the inductive part of

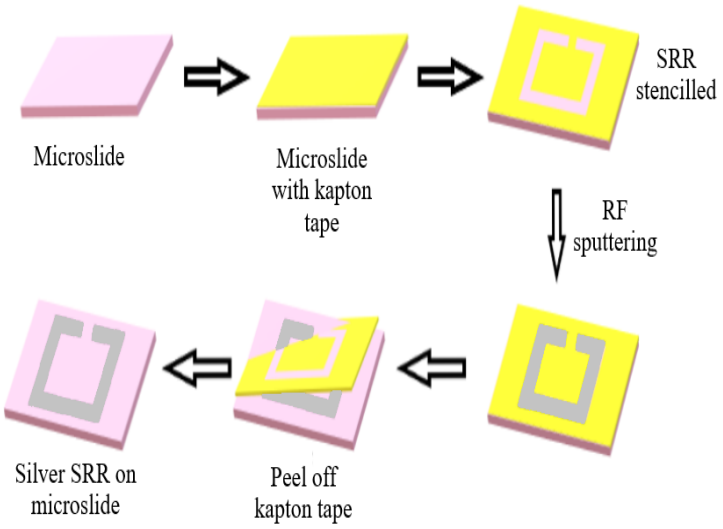

Figure 4.26: Schematic representation of the procedure used for thin film square SRR preparation using RF sputtering technique.

the resonator becoming more prominent.

Having observed the wide band resonance behaviour in a single ring thin film square SRR, the resonance studies are extended to square ECSRR and square BCSRR made using thin film deposition techniques.

For ECSRR, the structural parameters are outer length $l_{outer} = 10$ mm, inner length $l_{inner} = 6$ mm, width $w = 2$ mm, split width $s = 2$ mm and spacing between the rings $p = 2$ mm. In the case of BCSRR, the dimensions are length $l = 10$ mm, width $w = 2$ mm, split width $s = 1$ mm and thickness of the substrate 1.3 mm.

A photograph of the fabricated ECSRR square structure is given in Fig. 4.29. Figure 4.30 gives the resonance graphs obtained for different thickness for ECSRR case. Figure 4.31 depicts the resonance curves obtained for thin film BCSRR for a thickness of 750 nm. As expected both ECSRR and BCSRR show broadening of resonance band. It is worth mentioning that

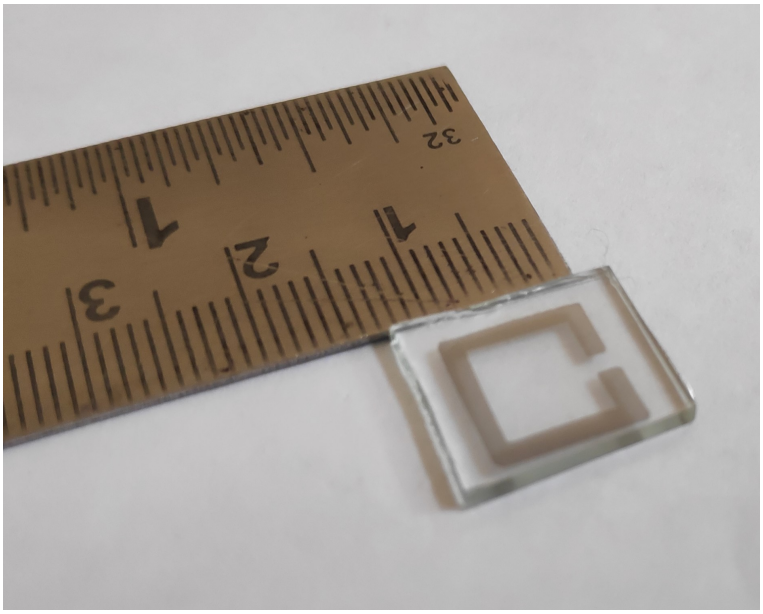

Figure 4.27: Photograph of the silver thin film square SRR of dimensions: length l = 10 mm, width w = 2 mm and split width s = 1 mm prepared using RF sputtering technique.

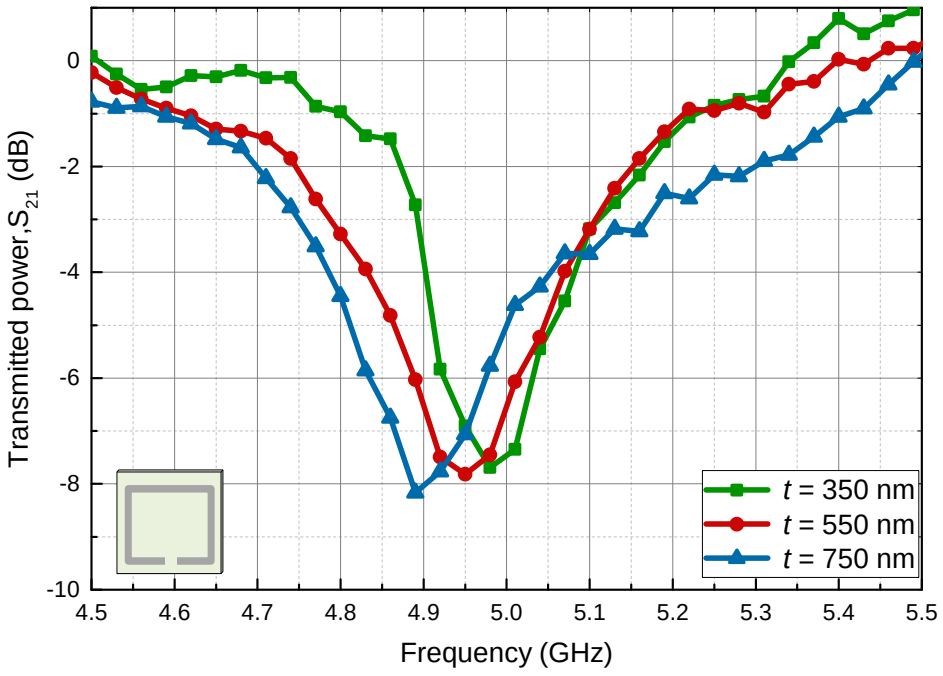

Figure 4.28: Magnetic resonance in single square ring thin film SRRs of different thickness t of 350 nm, 550 nm and 750 nm respectively made on glass substrate with dimensions length l = 10 mm, width w = 2 mm and split width s = 1 mm.

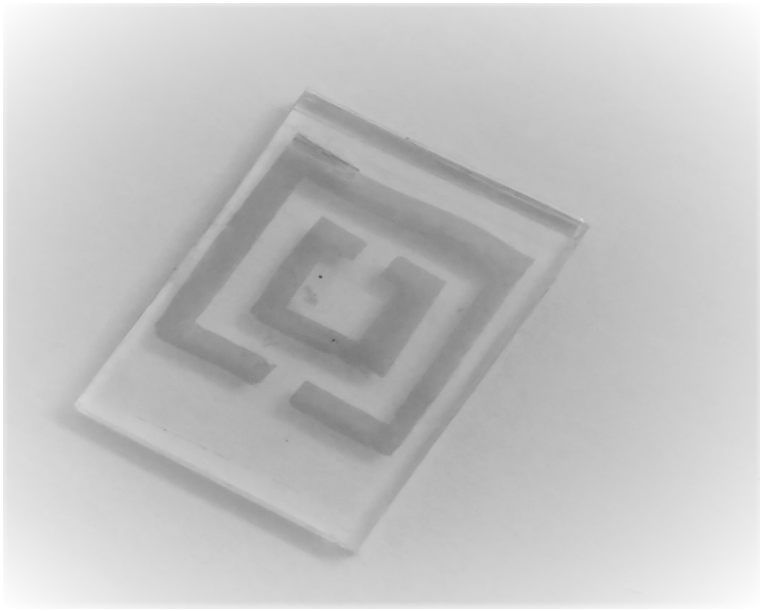

Figure 4.29: Photograph of silver ECSRR (outer length l_{outer} = 10 mm, inner length l_{inner} = 6 mm, width w = 2 mm, split width s = 2 mm and spacing between the rings p = 2 mm).

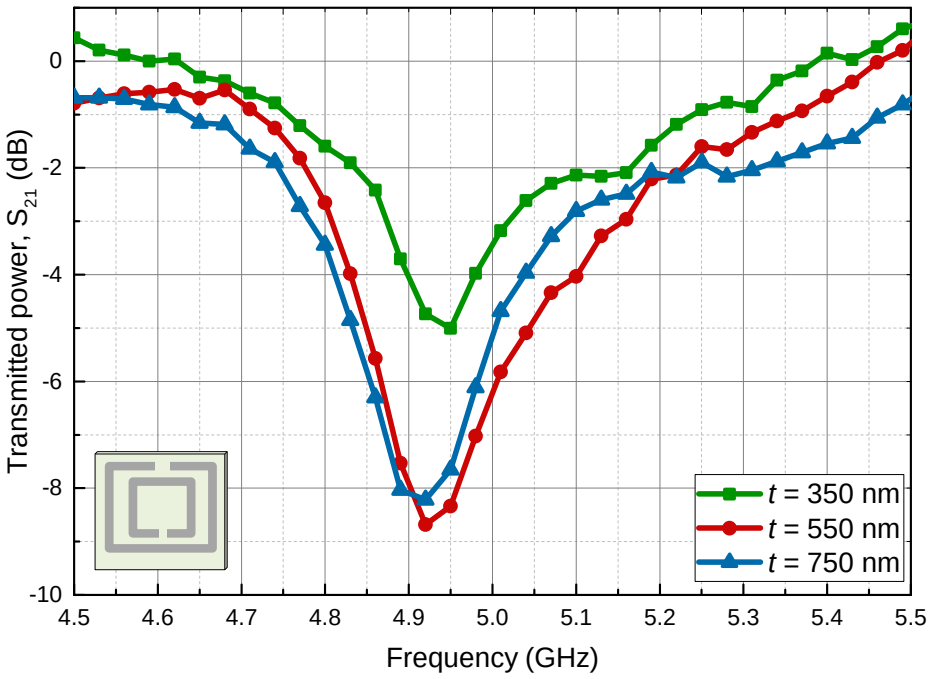

Figure 4.30: Magnetic resonance in silver ECSRRs of different thicknesses t of 350 nm, 550 nm and 750 nm respectively made on glass substrate with dimensions outer length l_{outer} = 10 mm, inner length l_{inner} = 6 mm, width w = 2 mm, split width s = 2 mm and spacing between the rings p = 2 mm.

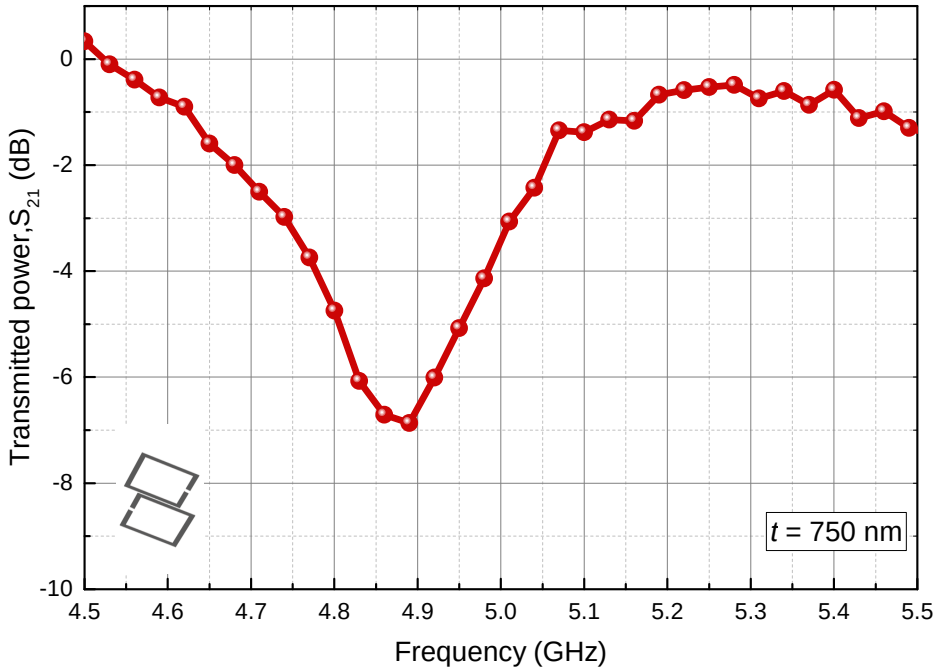

Figure 4.31: Magnetic resonance in silver BCSRRs of thickness 750 nm made on glass substrate with dimensions length l = 10 mm, width w = 2 mm, split width s = 1 mm and thickness of substrate 1.3 mm.

the study of the thin film resonating structures has facilitated the suggestion of a new structure into the realm of metamaterials.

4.4 Conclusion

From the study of the resonating structures fabricated using the humidity dependent conducting PANI-PTFE polymer sheet the following observations can be made.

1. The study of magnetic resonance in Split Ring Resonators (SRRs) made of Polyaniline based conducting polymer is done for the first time and the results are verified using simulation.

2. Magnetic resonance being achieved for a conducting polymer ring, make it possible for the entry of conducting polymers into the world of metamaterials.

3. The humidity sensitive characteristics of the PANI-PTFE material used to make the SRR structures, make them an ideal candidate for the development of humidity related sensors.

4. The wide band resonance properties observed for PANI-PTFE SRR structures compared to its thin metallic counterpart, make them suitable for specific wide band applications.

5. Investigations has led to the emergence of a new class of metamaterial molecule made using thin films on substrates.

CHAPTER 5

SUMMARY AND FUTURE WORKS

Summary and scope of the present study along with possible future works are detailed in this chapter. Existing applications of newly developed humidity sensitive conducting polymer by embedding PANI powder in PTFE matrix in the form of a sheet with novel electrical and mechanical properties are explored in this thesis. Impact of these materials in the state-of-the-art technology and in different research fields owing to the realization of metamaterials showing negative permeability properties using PANI-PTFE is briefly addressed.

The aim of this work is to introduce conducting polymers into the world of metamaterials. This interesting research helped to develop resonating structures showing variable properties using newly developed conducting polymer. The various steps covered for this process along with the possible potentialities may be briefly summarized as follows.

1. At first, Polyaniline synthesized in powder form is made into a thin sheet with the help of PTFE matrix.

2. Newly prepared PANI-PTFE sheet was thoroughly examined for its characteristics such as permittivity, conductivity and tensile strength which led to the conclusion that material is suitable for a good number of applications where conductivity and material strength are desired factors.

3. Another interesting property of the PANI-PTFE sheet is its humidity dependent conductivity which hinted at its potential usage as microwave absorber and a humidity sensor.

4. Having identified as an ideal polymer sample for the realization of metamaterial resonant structures, different types of ring resonators were fabricated to check their suitability in metamaterial based applications.

5. Distinct characteristics observed for newly developed PANI-PTFE SRR structures like that of humidity dependent conductivity and wide band resonance behaviour hint at their potential uses in new areas where conventional metallic SRRs may not be quite suitable.

6. Supporting theoretical analysis of the conducting mechanism in the dielectric type PANI-PTFE polymer and logical argument for the observance of wide band resonance in SRRs made of this material are also detailed.

7. Studies on the wide band resonance behaviour exhibited by PANI-PTFE resonating structures also lead to the invention of thin film metamaterial structure which may result in the introduction of metamaterial into thin film based microelectronic circuits.

The research findings open up interesting possibilities of future works in different fields. New methodology of making polymer into a rigid sheet using a binder matrix can be widely applied for making other powdered polymer samples into usable sheet forms which may show mechanical strength along with other added properties. The humidity dependent conducting property of the foam and sheet type absorber can be extended to the realization of anechoic chambers and tunable absorbers. The entry of PANI-PTFE conducting polymer into the regime of metamaterials in the form of negative permeability structures can be further extended into realization of structures having negative permittivity and negative refractive index. Humidity dependent resonating sensors realized by PANI-PTFE material may be widely used in a variety of gadgets operating on humidity dependent characteristics. Another interesting area which may evolve from the materialization of thin film SRR may be their potential applications in the field of microelectronics in the form of embedded circuitry.

Studies presented in the thesis reveal promising introduction of conducting polymers into the exciting world of metamaterials. The intrinsic characteristics of newly developed conducting polymer material both in the form of a material and in the form of a meta resonator may trigger vibrant research in this fascinating area for the development of manifold gadgets and instruments to cater the device requirement of modern science and technology.

Bibliography

[1] V G Veselago. Electrodynamics of substances with simultaneously negative values of epsilon and mu. *Usp. Fiz. Nauk*, 92:517, 1967.

[2] John B Pendry, Anthony J Holden, David J Robbins, and W J Stewart. Magnetism from conductors and enhanced nonlinear phenomena. *IEEE transactions on microwave theory and techniques*, 47(11):2075–2084, 1999.

[3] David R Smith, Willie J Padilla, D C Vier, Syrus C Nemat-Nasser, and Seldon Schultz. Composite medium with simultaneously negative permeability and permittivity. *Physical review letters*, 84(18):4184, 2000.

[4] Richard A Shelby, David R Smith, and Seldon Schultz. Experimental verification of a negative index of refraction. *science*, 292(5514):77–79, 2001.

[5] John David Jackson. *Classical electrodynamics*, volume 13. John wiley & sons, New York, 1999.

[6] Hung-Chi Chang and George Jaffé. Polarization in electrolytic solutions. part i. theory. *The Journal of Chemical Physics*, 20(7):1071–

1077, 1952.

[7] Charles Kittel and Paul McEuen. *Introduction to solid state physics*, volume 8. Wiley New York, 1996.

[8] Ivan Stepanovich Zheludev. *Physics of Crystalline Dielectrics: Volume 1 Crystallography and Spontaneous Polarization*. Springer Science & Business Media, 2012.

[9] Helmut G Kiess et al. *Conjugated conducting polymers*, volume 102. Springer, 1992.

[10] Chwan K Chiang, C R Fincher Jr, Yung W Park, Alan J Heeger, Hideki Shirakawa, Edwin J Louis, Shek C Gau, and Alan G MacDiarmid. Electrical conductivity in doped polyacetylene. *Physical review letters*, 39(17):1098, 1977.

[11] Alan J Heeger, S Kivelson, J R Schrieffer, and W P Su. Solitons in conducting polymers. *Reviews of Modern Physics*, 60(3):781, 1988.

[12] C K Chiang, Young-Woo Park, A J Heeger, Hideki Shirakawa, E J Louis, and Alan G MacDiarmid. Conducting polymers: Halogen doped polyacetylene. *The Journal of Chemical Physics*, 69(11):5098–5104, 1978.

[13] A N Papathanassiou, I Sakellis, and J Grammatikakis. Universal frequency-dependent ac conductivity of conducting polymer networks. *Applied Physics Letters*, 91(12):122911, 2007.

[14] P Dutta, S Biswas, M Ghosh, S K De, and S Chatterjee. The dc and ac conductivity of polyaniline–polyvinyl alcohol blends. *Synthetic metals*, 122(2):455–461, 2001.

[15] Peter W Milonni. *Fast light, slow light and left-handed light*. CRC Press, 2004.

[16] P Markoš and C M Soukoulis. Absorption losses in periodic arrays of thin metallic wires. *Optics letters*, 28(10):846–848, 2003.

[17] K Aydin and E Ozbay. Identifying magnetic response of split-ring resonators at microwave frequencies. *Opto-Electronics Review*, 14(3):193–199, 2006.

[18] B Sauviac, C R Simovski, and S A Tretyakov. Double split-ring resonators: Analytical modeling and numerical simulations. *Electromagnetics*, 24(5):317–338, 2004.

[19] Hongcang Guo, Na Liu, Liwei Fu, Todd P Meyrath, Thomas Zentgraf, Heinz Schweizer, and Harald Giessen. Resonance hybridization in double split-ring resonator metamaterials. *Optics express*, 15(19):12095–12101, 2007.

[20] Basudev Lahiri. *Split ring resonator (srr) based metamaterials*, PhD thesis, University of Glasgow, 2010.

[21] James Leno Vedral. *Analysis, Characterization and Application of Microwave Metamaterials*. PhD thesis, University of Colorado Colorado Springs. Kraemer Family Library, 2016.

[22] Chi Hyung Ahn. *Microwave Metamaterial Applications using Complementary Split Ring Resonators and High Gain Rectifying Reflectarray for Wireless Power Transmission*. PhD thesis, Doctoral dissertation, Texas A & M University, 2010.

[23] Juan Domingo Baena et al. Equivalent-circuit models for split-ring resonators and complementary split-ring resonators coupled to planar transmission lines. *IEEE transactions on microwave theory and techniques*, 53(4):1451–1461, 2005.

[24] M Gokkavas, K Guven, I Bulu, K Aydin, R S Penciu, M Kafesaki, C M Soukoulis, and E Ozbay. Experimental demonstration of

a left-handed metamaterial operating at 100 ghz. *Physical Review B*, 73(19):193103, 2006.

[25] Tie Jun Cui, Zhang-Cheng Hao, Xiao Xing Yin, Wei Hong, and Jin Au Kong. Study of lossy effects on the propagation of propagating and evanescent waves in left-handed materials. *Physics Letters A*, 323(5-6):484–494, 2004.

[26] F J Rachford, D L Smith, P F Loschialpo, and D W Forester. Calculations and measurements of wire and/or split-ring negative index media. *Physical Review E*, 66(3):036613, 2002.

[27] R S Penciu, M Kafesaki, T F Gundogdu, E N Economou, and C M Soukoulis. Theoretical study of left-handed behavior of composite metamaterials. *Photonics and Nanostructures-Fundamentals and Applications*, 4(1):12–16, 2006.

[28] Ekmel Ozbay, Koray Aydin, Ertugrul Cubukcu, and Mehmet Bayindir. Transmission and reflection properties of composite double negative metamaterials in free space. *IEEE Transactions on Antennas and Propagation*, 51(10):2592–2595, 2003.

[29] Ricardo Marqués, Ferran Martin, and Mario Sorolla. *Metamaterials with negative parameters: theory, design, and microwave applications*, volume 183. John Wiley & Sons, 2011.

[30] Martin Schueler, Christian Mandel, Margarita Puentes, and Rolf Jakoby. Metamaterial inspired microwave sensors. *IEEE Microwave Magazine*, 13(2):57–68, 2012.

[31] Valentina Giorgis, Pierfrancesco Zilio, Gianluca Ruffato, Michele Massari, Gabriele Zacco, and Filippo Romanato. Resonance properties of thick plasmonic split ring resonators for sensing applications. *Optics express*, 22(22):26476–26486, 2014.

[32] Muharrem Karaaslan and Mehmet Bakir. Chiral metamaterial based multifunctional sensor applications, *Progress In Electromagnetics Research*, 149:55–67, 2014.

[33] Evren Ekmekci and Gonul Turhan-Sayan. Multi-functional metamaterial sensor based on a broad-side coupled srr topology with a multi-layer substrate. *Applied Physics A*, 110(1):189–197, 2013.

[34] Kepeng Qiu, Jianqiang Jin, Zijun Liu, Fuli Zhang, and Weihong Zhang. A novel thermo-tunable band-stop filter employing a conductive rubber split-ring resonator. *Materials & Design*, 116:309–315, 2017.

[35] Evren Ekmekci and Gonul Turhan-Sayan. Metamaterial sensor applications based on broadside-coupled srr and v-shaped resonator structures. In *2011 IEEE International Symposium on Antennas and Propagation (APSURSI)*, pages 1170–1172. IEEE, 2011.

[36] Hasanul Kairm et al. Concept and model of a metamaterial-based passive wireless temperature sensor for harsh environment applications. *IEEE Sensors Journal*, 15(3):1445–1452, 2014.

[37] Yongyao Chen, Haijun Liu, Michael Reilly, Hyungdae Bae, and Miao Yu. Enhanced acoustic sensing through wave compression and pressure amplification in anisotropic metamaterials. *Nature communications*, 5:5247, 2014.

[38] R Marqués, J D Baena, M Beruete, F Falcone, T Lopetegi, M Sorolla, F Martin, and J Garcia. Ab initio analysis of frequency selective surfaces based on conventional and complementary split ring resonators. *Journal of Optics A: Pure and Applied Optics*, 7(2):S38, 2005.

[39] Joe Kizhakooden, Jovia Jose, Nees Paul, Sreedevi P Chakyar, Anju Sebastian, Sikha K Simon, K S Umadevi, C Bindu, Jolly Andrews, and V P Joseph. Broadside coupled split ring resonator based multiband

monopole patch antenna for wireless communication applications. *AIP Conference Proceedings*, 2162(1):020068, 2019.

[40] F Martın, Jordi Bonache, F al Falcone, Mario Sorolla, and R Marqués. Split ring resonator-based left-handed coplanar waveguide. *Applied Physics Letters*, 83(22):4652–4654, 2003.

[41] Guy Lipworth et al. Magnetic metamaterial superlens for increased range wireless power transfer. *Scientific reports*, 4:3642, 2014.

[42] Francesco Aieta, Patrice Genevet, Mikhail A Kats, Nanfang Yu, Romain Blanchard, Zeno Gaburro, and Federico Capasso. Aberration-free ultrathin flat lenses and axicons at telecom wavelengths based on plasmonic metasurfaces. *Nano letters*, 12(9):4932–4936, 2012.

[43] Shuyan Zhang et al. High efficiency near diffraction-limited mid-infrared flat lenses based on metasurface reflectarrays. *Optics express*, 24(16):18024–18034, 2016.

[44] Jessica Bénédicto, Emmanuel Centeno, Rémi Pollès, and Antoine Moreau. Ultimate resolution of indefinite metamaterial flat lenses. *Physical Review B*, 88(24):245138, 2013.

[45] C Bindu, Sreedevi P Chakyar, Anju Sebastian, Sikha K Simon, Jovia Jose, Nees Paul, K S Umadevi, Joe Kizhakooden, Jolly Andrews, and V P Joseph. Enhancing the resolution in imaging using folded metamaterial split ring resonator structure at microwave frequencies. In *AIP Conference Proceedings*, volume 2162, page 020067. AIP Publishing, 2019.

[46] Koray Aydin, Irfan Bulu, and Ekmel Ozbay. Subwavelength resolution with a negative-index metamaterial superlens. *Applied physics letters*, 90(25):254102, 2007.

[47] Nathan Landy and David R Smith. A full-parameter unidirectional

metamaterial cloak for microwaves. *Nature materials*, 12(1):25, 2013.

[48] Hongsheng Chen, Bae-Ian Wu, Baile Zhang, and Jin Au Kong. Electromagnetic wave interactions with a metamaterial cloak. *Physical Review Letters*, 99(6):063903, 2007.

[49] Hui Feng Ma and Tie Jun Cui. Three-dimensional broadband ground-plane cloak made of metamaterials. *Nature communications*, 1:21, 2010.

[50] Ricardo Marqués, Francisco Mesa, Jesus Martel, and Francisco Medina. Comparative analysis of edge-and broadside-coupled split ring resonators for metamaterial design-theory and experiments. *IEEE Transactions on antennas and propagation*, 51(10):2572–2581, 2003.

[51] K S Umadevi, Sreedevi P Chakyar, Sikha K Simon, Jolly Andrews, and V P Joseph. Split ring resonators made of conducting wires for performance enhancement. *EPL (Europhysics Letters)*, 118(2):24002, 2017.

[52] Juan D Baena, Ricardo Marqués, Francisco Medina, and Jesús Martel. Artificial magnetic metamaterial design by using spiral resonators. *Physical review B*, 69(1):014402, 2004.

[53] Pradeep Anju. *Investigations on metamaterial based spiral inductors for compact microwave devices*, PhD thesis, Cochin University of Science and Technology, 2014.

[54] K Yang, H Wang, Z Lei, Y Xie, and H Lai. Cpw-fed slot antenna with triangular srr terminated feedline for wlan/wimax applications. *Electronics Letters*, 47(12):685–686, 2011.

[55] P Menon Ragi, K S Umadevi, Paul Nees, Jovia Jose, M V Keerthy, and V P Joseph. Flexible split-ring resonator metamaterial structure at microwave frequencies. *Microwave and Optical Technology Letters*, 54(6):1415–1416, 2012.

[56] Sergei Tretyakov. *Analytical modeling in applied electromagnetics*. Artech House, 2003.

[57] Nigel P Johnson, Ali Z Khokhar, Harold M Chong, Richard M De La Rue, Tomasz J Antosiewicz, and Scott McMeekin. A review of size and geometrical factors influencing resonant frequencies in metamaterials. *Opto-Electronics Review*, 14(3):187–191, 2006.

[58] David M Allen. The principles and practice of photochemical machining and photoetching. *Adam Hilger, Techno House, Redcliffe Way, Bristol BS 1 6 NX, UK*, 1986.

[59] N Katsarakis, T H Koschny, M Kafesaki, E N Economou, and C M Soukoulis. Electric coupling to the magnetic resonance of split ring resonators. *Applied physics letters*, 84(15):2943–2945, 2004.

[60] Ricardo Marqués, Francisco Medina, and Rachid Rafii-El-Idrissi. Role of bianisotropy in negative permeability and left-handed metamaterials. *Physical Review B*, 65(14):144440, 2002.

[61] J García-García, Ferran Martín, J D Baena, R Marques, and Lukas Jelinek. On the resonances and polarizabilities of split ring resonators. *Journal of Applied Physics*, 98(3):033103, 2005.

[62] David R Smith, Jonah Gollub, Jack J Mock, Willie J Padilla, and David Schurig. Calculation and measurement of bianisotropy in a split ring resonator metamaterial. *Journal of Applied Physics*, 100(2):024507, 2006.

[63] Koray Aydin, Irfan Bulu, Kaan Guven, Maria Kafesaki, Costas M Soukoulis, and Ekmel Ozbay. Investigation of magnetic resonances for different split-ring resonator parameters and designs. *New journal of physics*, 7(1):168, 2005.

[64] Stefan Linden, Christian Enkrich, Martin Wegener, Jiangfeng Zhou,

Thomas Koschny, and Costas M Soukoulis. Magnetic response of metamaterials at 100 terahertz. *Science*, 306(5700):1351–1353, 2004.

[65] N Katsarakis, G Konstantinidis, A Kostopoulos, R S Penciu, T F Gundogdu, M Kafesaki, E N Economou, T H Koschny, and C M Soukoulis. Magnetic response of split-ring resonators in the far-infrared frequency regime. *Optics Letters*, 30(11):1348–1350, 2005.

[66] Sreedevi P Chakyar, Sikha K Simon, C Bindu, Jolly Andrews, and V P Joseph. Complex permittivity measurement using metamaterial split ring resonators. *Journal of Applied Physics*, 121(5):054101, 2017.

[67] Evren Ekmekci and Gonul Turhan-Sayan. Comparative investigation of resonance characteristics and electrical size of the double-sided srr, bc-srr and conventional srr type metamaterials for varying substrate parameters. *Progress In Electromagnetics Research*, 12:35–62, 2009.

[68] Sreedevi P Chakyar, Jolly Andrews, and V P Joseph. Temperature dependence of relative permittivity: A measurement technique using split ring resonators. *World Academy of Science, Engineering and Technology, International Journal of Mechanical, Aerospace, Industrial, Mechatronic and Manufacturing Engineering*, 10(6):1030–1033, 2016.

[69] Samuel Y Liao. *Microwave devices and circuits*. Pearson Education India, 1989.

[70] Lin-Feng Chen, C K Ong, CP Neo, VV Varadan, and Vijay K Varadan. *Microwave electronics: measurement and materials characterization*. John Wiley & Sons, 2004.

[71] Mi Lin, Megan H Duane, and Mohammed N Afsar. Cavity-perturbation measurement of complex permittivity and permeability of common ferrimagnetics in microwave-frequency range. *IEEE Transactions on mag-*

netics, 42(10):2885–2887, 2006.

[72] Dinesh C Dube, Michael T Lanagan, J H Kim, and S J Jang. Dielectric measurements on substrate materials at microwave frequencies using a cavity perturbation technique. *Journal of applied physics*, 63(7):2466–2468, 1988.

[73] Il Sung Seo, Woo Seok Chin et al. Characterization of electromagnetic properties of polymeric composite materials with free space method. *Composite Structures*, 66(1):533–542, 2004.

[74] R A Waldron. Perturbation theory of resonant cavities. *Proceedings of the IEE-Part C: Monographs*, 107(12):272–274, 1960.

[75] K T Mathew and U Raveendranath. Waveguide cavity perturbation method for measuring complex permittivity of water. *Microwave and Optical Technology Letters*, 6(2):104–106, 1993.

[76] K T Mathew and U Raveendranath. Cavity perturbation techniques for measuring dielectric parameters of water and other allied liquids. *Sensors Update*, 7(1):185–210, 2000.

[77] Anand Parkash, J K Vaid, and Abhai Mansingh. Measurement of dielectric parameters at microwave frequencies by cavity-perturbation technique. *IEEE transactions on microwave theory and techniques*, 27(9):791–795, 1979.

[78] S Biju Kumar, Honey Hohn, Rani Joseph, M Hajian, L P Ligthart, and K T Mathew. Complex permittivity and conductivity of poly aniline at microwave frequencies. *Journal of the European Ceramic Society*, 21(15):2677–2680, 2001.

[79] D X Gouveia, L C Costa, and M A Valente. Resonant cavity for the measurement of microwave magnetic permeability using the small perturbation theory. *Microwave and Optical Technology Letters*,

50(2):399–402, 2008.

[80] Hideki Shirakawa, Alan McDiarmid, and Alan Heeger. Twenty-five years of conducting polymers. *Chemical Communications*, 2003(1):1–4, 2003.

[81] Alan J Heeger. Semiconducting and metallic polymers: the fourth generation of polymeric materials (nobel lecture). *Angewandte Chemie International Edition*, 40(14):2591–2611, 2001.

[82] Hideki Shirakawa, Edwin J Louis, Alan G MacDiarmid, Chwan K Chiang, and Alan J Heeger. Synthesis of electrically conducting organic polymers: halogen derivatives of polyacetylene,(ch) x. *Journal of the Chemical Society, Chemical Communications*, (16):578–580, 1977.

[83] H K Chaudhari and D S Kelkar. Investigation of structure and electrical conductivity in doped polyaniline. *Polymer international*, 42(4):380–384, 1997.

[84] Jin-Chih Chiang and Alan G MacDiarmid. polyaniline: Protonic acid doping of the emeraldine form to the metallic regime. *Synthetic Metals*, 13(1-3):193–205, 1986.

[85] V T Truong, S Z Riddell, and R F Muscat. Polypyrrole based microwave absorbers. *Journal of Materials Science*, 33(20):4971–4976, 1998.

[86] Bruno Scrosati. Conducting polymers: advanced materials for new design, rechargeable lithium batteries. *Polymer international*, 47(1):50–55, 1998.

[87] Manju Gerard, Asha Chaubey, and B D Malhotra. Application of conducting polymers to biosensors. *Biosensors and bioelectronics*, 17(5):345–359, 2002.

[88] A G MacDiarmid, J C Chiang, A F Richter, Epstein, and A J. Polyani-

line: a new concept in conducting polymers. *Synthetic Metals*, 18(1-3):285–290, 1987.

[89] Krishna Naishadham and Prasad K Kadaba. Measurement of the microwave conductivity of a polymeric material with potential applications in absorbers and shielding. *IEEE Transactions on Microwave Theory and Techniques*, 39(7):1158–1164, 1991.

[90] Yangyong Wang and Xinli Jing. Intrinsically conducting polymers for electromagnetic interference shielding. *Polymers for advanced technologies*, 16(4):344–351, 2005.

[91] P T C Wong, B Chambers, A P Anderson, and P V Wright. Large area conducting polymer composites and their use in microwave absorbing material. *Electronics letters*, 28(17):1651–1653, 1992.

[92] Y B Wankhede, S B Kondawar, S R Thakare, and P S More. Synthesis and characterization of silver nanoparticles embedded in polyaniline nanocomposite. *Adv. Mater. Lett*, 4:89–93, 2013.

[93] Safenaz M Reda and Sheikha M Al-Ghannam. Synthesis and electrical properties of polyaniline composite with silver nanoparticles. *Advances in materials Physics and Chemistry*, 2(2):75, 2012.

[94] Yong Cao, Paul Smith, and Alan J Heeger. Counter-ion induced processibility of conducting polyaniline. *Synthetic Metals*, 57(1):3514–3519, 1993.

[95] Honey John, Rinku M Thomas, Joe Jacob, K T Mathew, and Rani Joseph. Conducting polyaniline composites as microwave absorbers. *Polymer composites*, 28(5):588–592, 2007.

[96] Alan G MacDiarmid and Arthur J Epstein. Polyanilines: a novel class of conducting polymers. *Faraday Discussions of the Chemical Society*, 88:317–332, 1989.

[97] N J Pinto, P D Shah, P K Kahol, and B J McCormick. Dielectric constant and ac conductivity in polyaniline derivatives. *Solid state communications*, 97(12):1029–1031, 1996.

[98] Sylvain Fauveaux and Jean-Louis Miane. Broadband electromagnetic shields using polyaniline composites. *Electromagnetics*, 23(8):617–627, 2003.

[99] Swati Unde, J Ganu, and S Radhakrishnan. Conducting polymer-based chemical sensor: Characteristics and evaluation of polyaniline composite films. *Advanced Materials for Optics and Electronics*, 6(3):151–157, 1996.

[100] Shigesou Hashida, Hitoshi Namio, and Susumu Hirakawa. Surface morphology and crystalline orientation of uniaxially drawn polytetrafluoroethylene films. *Journal of applied polymer science*, 37(10):2897–2906, 1989.

[101] P N Adams, P J Laughlin, A P Monkman, and A M Kenwright. Low temperature synthesis of high molecular weight polyaniline. *Polymer*, 37(15):3411–3417, 1996.

[102] R G Gilbert and J Stejskal. Polyaniline. preparation of a conducting polymer (iupac technical report). *Pure and applied chemistry*, 74(5):857–868, 2002.

[103] Nees Paul, Sreedevi P Chakyar, K S Umadevi, Simon K Sikha, Joe Kizhakooden, Jolly Andrews, and V P Joseph. Humidity sensitive flexible microwave absorbing sheet using polyaniline–polytetrafluoroethylene composite. *Arabian Journal for Science and Engineering*, 44(1):553–560, 2019.

[104] Sisi Deng and Guang Li. Structural features and microwave absorbing propertiesof polyaniline-montmorillonite composites prepared by

in-situ. *Journal of Fiber Bioengineering and Informatics*, 6(1):33–40, 2013.

[105] Juhua Luo, Yang Xu, Wei Yao, Cuifeng Jiang, and Jianguang Xu. Synthesis and microwave absorption properties of reduced graphene oxide-magnetic porous nanospheres-polyaniline composites. *Composites Science and Technology*, 117:315–321, 2015.

[106] H C Pant, M K Patra, S C Negi, A Bhatia, S R Vadera, and N Kumar. Studies on conductivity and dielectric properties of polyaniline-zinc sulphide composites. *Bulletin of Materials Science*, 29(4):379–384, 2006.

[107] R A P O D'Amorim, M I Teixeira, L V E Caldas, and S O Souza. Physical, morphological and dosimetric characterization of the Teflon agglutinator to thermoluminescent dosimetry. *Journal of Luminescence*, 136:186–190, 2013.

[108] P J Rae and D M Dattelbaum. The properties of poly (tetrafluoroethylene)(PTFE) in compression. *Polymer*, 45(22):7615–7625, 2004.

[109] R Mishra, S P Tripathy, K K Dwivedi, D T Khathing, S Ghosh, M Müller, and D Fink. Effect of electron irradiation on polytetrafluoro ethylene. *Radiation measurements*, 37(3):247–251, 2003.

[110] Suk-Hye Son, Hae-Joon Lee, Young-Jun Park, and Jung-Hyun Kim. Preparation of conducting polymer composites: effects of porosity on electrical conductivity. *Polymer international*, 46(4):308–312, 1998.

[111] James Baker-Jarvis, Eric J Vanzura, and William A Kissick. Improved technique for determining complex permittivity with the transmission/reflection method. *IEEE Transactions on microwave theory and techniques*, 38(8):1096–1103, 1990.

[112] Xudong Chen, Tomasz M Grzegorczyk, Bae-Ian Wu, Joe Pacheco Jr, and Jin Au Kong. Robust method to retrieve the constitutive effective

parameters of metamaterials. *Physical Review E*, 70(1):016608, 2004.

[113] Deepak K Ghodgaonkar, Vasundara V Varadan, and Vijay K Varadan. A free-space method for measurement of dielectric constants and loss tangents at microwave frequencies. *IEEE Transactions on Instrumentation and measurement*, 38(3):789–793, 1989.

[114] D K Ghodgaonkar, VV Varadan, and V K Varadan. Free-space measurement of complex permittivity and complex permeability of magnetic materials at microwave frequencies. *IEEE Transactions on instrumentation and measurement*, 39(2):387–394, 1990.

[115] Il Sung Seo et al. Characterization of electromagnetic properties of polymeric composite materials with free space method. *Composite Structures*, 66(1-4):533–542, 2004.

[116] William B Weir. Automatic measurement of complex dielectric constant and permeability at microwave frequencies. *Proceedings of the IEEE*, 62(1):33–36, 1974.

[117] Anjali Sharma and Mohammed N Afsar. Accurate permittivity and permeability measurement of composite broadband absorbers at microwave frequencies. In *2011 IEEE International Instrumentation and Measurement Technology Conference*, pages 1–6. IEEE, 2011.

[118] Hao Zhou, Guizhen Lu, Yanfei Li, Song Wang, and Yue Wang. An improved method of determining permittivity and permeability by s parameters. *PIERS Proceedings, Beijing, China*, pages 768–773, 2009.

[119] Y B Feng, T Qiu, and C Y Shen. Absorbing properties and structural design of microwave absorbers based on carbonyl iron and barium ferrite. *Journal of Magnetism and Magnetic Materials*, 318(1):8–13, 2007.

[120] Jin-Bong Kim, Sang-Kwan Lee, and Chun-Gon Kim. Comparison study on the effect of carbon nano materials for single-layer microwave

absorbers in x-band. *Composites Science and Technology*, 68(14):2909–2916, 2008.

[121] Han-Shin Cho and Sung-Soo Kim. M-hexaferrites with planar magnetic anisotropy and their application to high-frequency microwave absorbers. *IEEE Transactions on magnetics*, 35(5):3151–3153, 1999.

[122] H J Kwon, J Y Shin, and J H Oh. The microwave absorbing and resonance phenomena of y-type hexagonal ferrite microwave absorbers. *Journal of Applied Physics*, 75(10):6109–6111, 1994.

[123] J Y Shin and J H Oh. The microwave absorbing phenomena of ferrite microwave absorbers. *IEEE Transactions on Magnetics*, 29(6):3437–3439, 1993.

[124] S Vinayasree, M A Soloman, Vijutha Sunny, P Mohanan, Philip Kurian, P A Joy, and M R Anantharaman. Flexible microwave absorbers based on barium hexaferrite, carbon black, and nitrile rubber for 2–12 ghz applications. *Journal of Applied Physics*, 116(2):024902, 2014.

[125] Chok Hung Chai. *Design a high performance absorber to improve an anechoic chamber performance*. PhD thesis, Universiti Malaysia Sarawak, UNIMAS, 2010.

[126] Rajanroop Kaur, Gagan Deep Aul, and Vikas Chawla. Improved reflection loss performance of dried banana leaves pyramidal microwave absorbers by coal for application in anechoic chambers. *Progress In Electromagnetics Research M*, 43:157–164, 2015.

[127] Hassan Nornikman, F Malek, Ping Jack Soh, and A A H Azremi. Reflection loss performance of hexagonal base pyramid microwave absorber using different agricultural waste material. In *Antennas and Propagation Conference (LAPC), 2010 Loughborough*, pages 313–316.

IEEE, 2010.

[128] M R Meshram, Nawal K Agrawal, Bharoti Sinha, and P S Misra. Characterization of m-type barium hexagonal ferrite-based wide band microwave absorber. *Journal of Magnetism and Magnetic Materials*, 271(2):207–214, 2004.

[129] Anil Ohlan, Kuldeep Singh, Amita Chandra, and S K Dhawan. Microwave absorption properties of conducting polymer composite with barium ferrite nanoparticles in 12.4–18 ghz. *Applied Physics Letters*, 93(5):053114, 2008.

[130] Satoshi Sugimoto, Kazuaki Haga, Toshio Kagotani, and Koichiro Inomata. Microwave absorption properties of ba m-type ferrite prepared by a modified coprecipitation method. *Journal of magnetism and magnetic materials*, 290:1188–1191, 2005.

[131] A Verma, R G Mendiratta, T C Goel, and D C Dube. Microwave studies on strontium ferrite based absorbers. *Journal of Electroceramics*, 8(3):203–208, 2002.

[132] Lan Zhang, Hong Zhu, Yuan Song, Yongming Zhang, and Yi Huang. The electromagnetic characteristics and absorbing properties of multi-walled carbon nanotubes filled with er 2 o 3 nanoparticles as microwave absorbers. *Materials Science and Engineering: B*, 153(1):78–82, 2008.

[133] Ki-Yeon Park, Jae-Hung Han, Sang-Bok Lee, Jin-Bong Kim, Jin-Woo Yi, and Sang-Kwan Lee. Fabrication and electromagnetic characteristics of microwave absorbers containing carbon nanofibers and nife particles. *Composites Science and Technology*, 69(7):1271–1278, 2009.

[134] Xiangxuan Liu, Zeyang Zhang, and Youpeng Wu. Absorption properties of carbon black/silicon carbide microwave absorbers. *Composites Part B: Engineering*, 42(2):326–329, 2011.

[135] Rajesh Kumar Srivastava, TN Narayanan, AP Reena Mary, MR Anantharaman, Anchal Srivastava, Robert Vajtai, and Pulickel M Ajayan. Ni filled flexible multi-walled carbon nanotube–polystyrene composite films as efficient microwave absorbers. *Applied Physics Letters*, 99(11):113116, 2011.

[136] Hassan Nornikman, Ping Jack Soh, Abdullah Al-Hadi Azremi, and M S Anuar. Performance simulation of pyramidal and wedge microwave absorbers. In *Modelling & Simulation, 2009. AMS'09. Third Asia International Conference on*, pages 649–654. IEEE, 2009.

[137] W Emerson. Electromagnetic wave absorbers and anechoic chambers through the years. *IEEE Transactions on Antennas and Propagation*, 21(4):484–490, 1973.

[138] Hans Severin. Nonreflecting absorbers for microwave radiation. *IRE Transactions on Antennas and Propagation*, 4(3):385–392, 1956.

[139] A Simmons and W Emerson. An anechoic chamber making use of a new broadband absorbing material. In *1958 IRE International Convention Record*, volume 1, pages 34–41. IEEE, 1966.

[140] Yang Bo, Huiyan Yang, Ying Hu, Tianming Yao, and Shasheng Huang. A novel electrochemical dna biosensor based on graphene and polyaniline nanowires. *Electrochimica Acta*, 56(6):2676–2681, 2011.

[141] Larisa Florea, Cormac Fay, Emer Lahiff, Thomas Phelan, Noel E O'Connor, Brian Corcoran, Dermot Diamond, and Fernando Benito-Lopez. Dynamic ph mapping in microfluidic devices by integrating adaptive coatings based on polyaniline with colorimetric imaging techniques. *Lab on a Chip*, 13(6):1079–1085, 2013.

[142] Zimple Matharu, G Sumana, Sunil K Arya, S P Singh, Vinay Gupta, and B D Malhotra. Polyaniline langmuir- blodgett film based choles-

terol biosensor. *Langmuir*, 23(26):13188–13192, 2007.

[143] Himani Sharma. *Conducting Polymers: Polyaniline, Its State of the Art and Applications*. PhD thesis, Thapar Institute of Engineering and Technology, Deemed University, Punjab, 2006.

[144] Wei Fan, Chao Zhang, Weng Weei Tjiu, Kumari Pallathadka Pramoda, Chaobin He, and Tianxi Liu. Graphene-wrapped polyaniline hollow spheres as novel hybrid electrode materials for supercapacitor applications. *ACS applied materials & interfaces*, 5(8):3382–3391, 2013.

[145] Rahul R Salunkhe, Shao-Hui Hsu, Kevin C W Wu, and Yusuke Yamauchi. Large-scale synthesis of reduced graphene oxides with uniformly coated polyaniline for supercapacitor applications. *ChemSusChem*, 7(6):1551–1556, 2014.

[146] Kai Zhang, Li Li Zhang, X S Zhao, and Jishan Wu. Graphene/polyaniline nanofiber composites as supercapacitor electrodes. *Chemistry of Materials*, 22(4):1392–1401, 2010.

[147] Ertugrul Cubukcu, Shuang Zhang, Yong-Shik Park, Guy Bartal, and Xiang Zhang. Split ring resonator sensors for infrared detection of single molecular monolayers. *Applied Physics Letters*, 95(4):043113, 2009.

[148] T Driscoll, G O Andreev, D N Basov, S Palit, S Y Cho, N M Jokerst, and D R Smith. Tuned permeability in terahertz split-ring resonators for devices and sensors. *Applied Physics Letters*, 91(6):062511, 2007.

[149] Hee-Jo Lee and Jong-Gwan Yook. Biosensing using split-ring resonators at microwave regime. *Applied Physics Letters*, 92(25):254103, 2008.

[150] Hee-Jo Lee, Hyun-Seok Lee, Kyung-Hwa Yoo, and Jong-Gwan Yook. Dna sensing using split-ring resonator alone at microwave regime. *Journal of Applied Physics*, 108(1):014908, 2010.

[151] A B Shvartsburg, V Ya Pecherkin, L M Vasilyak, S P Vetchinin, and V E Fortov. Resonant microwave fields and negative magnetic response, induced by displacement currents in dielectric rings: theory and the first experiments. *Scientific reports*, 7(1):2180, 2017.

[152] Nees Paul, Joe Kizhakooden, Jovia Jose, Jolly Andrews, and V P Joseph. Metamaterial split ring resonators made of polyaniline-polytetrafluoroethylene at microwave frequencies. In *2019 Thirteenth International Congress on Artificial Materials for Novel Wave Phenomena (Metamaterials)*, pages X–305. IEEE, 2019.

[153] Hongcang Guo, Na Liu, Liwei Fu, Heinz Schweizer, Stefan Kaiser, and Harald Giessen. Thickness dependence of the optical properties of split-ring resonator metamaterials. *physica status solidi (b)*, 244(4):1256–1261, 2007.

[154] Abdul-Nafiu Abiodun Jabita. *Design of singly split single ring resonator for measurement of dielectric constant of materials using resonant method*, PhD thesis, University of Gavle, 2013.

[155] Andrew R Fulford and Stuart M Wentworth. Conductor and dielectric-property extraction using microstrip tee resonators. *Microwave and Optical Technology Letters*, 47(1):14–16, 2005.

[156] Nees Paul, Sikha K Simon, C Bindu, Jolly Andrews, and V P Joseph. Thin film metamaterial split ring resonators at microwave frequencies. In *2019 Thirteenth International Congress on Artificial Materials for Novel Wave Phenomena (Metamaterials)*, pages X–035. IEEE, 2019.

LIST OF PUBLICATIONS

1. *Paul N.*, Chakyar S.P., Umadevi K.S., Sikha S.K., Kizhakooden J., Andrews J. and Joseph V.P., Humidity Sensitive Flexible Microwave Absorbing Sheet Using Polyaniline-Polytetrafluoroethylene Composite, Arabian Journal for Science and Engineering, 44(1), pp.553-560, 2019.

2. *Nees Paul*, Joe Kizhakooden, Jovia Jose, Jolly Andrews, and VP Joseph, Metamaterial split ring resonators made of Polyaniline-Polytetrafluoroethylene at microwave frequencies, In 2019 Thirteenth International Congress on Artificial Materials for Novel Wave Phenomena (Metamaterials),IEEE, pages X305, 2019.

3. *Nees Paul*, Sikha K Simon, C Bindu, Jolly Andrews, and VP Joseph, Thin film metamaterial split ring resonators at microwave frequencies, In 2019 Thirteenth International Congress on Artificial Materials for Novel Wave Phenomena (Metamaterials), IEEE, pages X035,2019.

4. *Paul N.*, Janet Jimmy, Sreedevi P. Chakyar, Sikha K. Simon, Joe Kizhakooden, C. Bindu, Anju Sebastian, K. S. Umadevi, Jovia Jose, Jolly Andrews and V. P. Joseph, Microwave absorption properties of flexible zinc oxide sheet, AIP Conference Proceedings 2162, 020070, 2019.

5. Jose Jovia, K. Simon Sikha, Kizhakooden Joe, Sebastian Anju, Chakyar Sreedevi, *Paul Nees*, C Bindu, Andrews Jolly, V. P. Joseph, Frequency Dependent Radiation Properties of Negative Permittivity Metamaterial Reflector Antenna, Physica Scripta, 94, 105811, pp.9-12, 2019.

6. J. Jose, S. K. Simon, J. Kizhakooden, A. Sebastian, S. P. Chakyar, *N. Paul*, C. Bindu, J. Andrews, and V. P. Joseph, Interaction of a sine wave with an artificial negative permittivity medium using nonstandard FDTD, PIER, Vol. 83, pp. 1-5, 2019.

7. Joe Kizhakooden, Jovia Jose, *Nees Paul*, Sikha K Simon, Sreedevi P Chakyar, Jolly Andrews and V. P. Joseph, Metamaterial inspired feather light artificial plasma horn antenna for astronomical and communication applications, Wiley, Vol 61(3), pp.777 780, 2019.

8. K Joe, J Jovia, *P Nees*, J Andrews, and V. P. Joseph, Frequency tunable monopole patch antenna using broadside coupled split ring resonator for wireless communication applications, In 2019 Thirteenth International Congress on Artificial Materials for Novel Wave Phenomena (Metamaterials), IEEE, pages X200, 2019.

9. Anju Sebastian, Denet Davis, Sikha K. Simon, Sreedevi P. Chakyar, Jovia Jose, Joe Kizhakooden, *Nees Paul*, C. Bindu, V. P. Joseph and Jolly Andrews, Non-destructive method for thickness measurement of dielectric films using metamaterial resonator, AIP Conference Proceedings 2162, 020141, 2019.

10. C. Bindu, Sreedevi P. Chakyar, Anju Sebastian, Sikha K. Simon, Jovia Jose, *Nees Paul*, K. S. Umadevi, Joe Kizhakooden, Jolly Andrews and V. P. Joseph, Enhancing the resolution in imaging using folded metamaterial split ring resonator structure at microwave frequencies, AIP Conference Proceedings 2162, 020067, 2019.

11. Joe Kizhakooden, Jovia Jose, *Nees Paul*, Sreedevi P. Chakyar, Anju Sebastian, Sikha K. Simon, K. S. Umadevi, C. Bindu, Jolly Andrews and V. P. Joseph, Broadside coupled split ring resonator based multiband monopole patch antenna for wireless communication applications, AIP Conference Proceedings 2162, 020068, 2019.

12. Jovia Jose, Sikha K. Simon, Anju Sebastian, Sreedevi P. Chakyar, Joe Kizhakooden, *Nees Paul*, C. Bindu, K. S. Umadevi, Jolly Andrews and

V. P. Joseph, Scattering from artificial plasma cylinder using nonstandard FDTD, AIP Conference Proceedings 2162, 020069, 2019.

13. Sreedevi P. Chakyar, Shanto T. A., Aathira Murali, Sikha K. Simon, *Nees Paul*, Jolly Andrews, Joseph V.P., Measurement of dielectric constant of waxes at different temperatures using Split Ring Resonator structure, Proceedings of IEEE MTTS International Microwave and RF Conference 2016 978-1-5090-4685-0/16, 2016.

14. Ragi P.M., Umadevi K.S., *Nees P*, Jose J., Keerthy M.V. and Joseph V.P., Flexible Split Ring Resonator metamaterial structure at microwave frequencies, Microwave and Optical Technology Letters, 54(6), pp.1415-1416, 2012.

CONFERENCE PRESENTATIONS

1. Metamaterial Split Ring Resonators made of Polyaniline- Polytetrafluoroethylene at Microwave Frequencies, 13th International Congress on Artificial Materials for Novel Wave Phenomena Metamaterials, Italy, Rome, 16-19 September 2019.

2. Resonance Properties of Split Ring Resonators made of Polyaniline based Conducting Polymer, OSI-International Symposium on Optics, IIT Kanpur, 20-22 September 2018.

3. A Novel flexible negative permeability metamaterial structure made of conducting wires, 3rd International Conference on Competency Building Strategy in Business And Technology for Sustainable Development, Sri Ganesh school of Business Management, Coimbatore, 25 February 2014.

4. Microwave absorption properties of flexible zinc oxide sheets, International Conference on Advanced Materials, Nirmalagiri College, Kannur, 12-14 June 2019.

5. Frequency tunable split ring resonators based on PolyanlinePolytetrafluoroethylene hybrid composite, International conference on Materials for the Millennium, CUSAT, Kochi, 14-16 March 2019.

6. Humidity sensitive ring resonators for microwave applications, Christ College, Thrissur, 24-25 January 2019.

7. Microwave characterization of Polyaniline powder for humidity sensitive absorbers, National Conference on Science and Applications of Functional Materials, St. Josephs College, Thrissur, 7 December 2018.

8. Polyaniline-Polytetrafluroethylene Hybrid Flexible Sheet as Humidity Sensor at Microwave Frequencies, National seminar on Nanophotonics, St. Thomas College, Thrissur, 10 January 2017.

9. Effect of substrate dielectric constant on the resonant frequency of Broadside-Coupled Split Ring Resonator metamaterial structure, Electroceramics, St. Aloysius College, Thrissur, 24-25 February 2014.

SELECTED PUBLICATIONS

Humidity Sensitive Flexible Microwave Absorbing Sheet Using Polyaniline–Polytetrafluoroethylene Composite

Nees Paul, Sreedevi P. Chakyar, K. S. Umadevi, Simon K. Sikha, Joe Kizhakooden, Jolly Andrews & V. P. Joseph

Arabian Journal for Science and Engineering

ISSN 2193-567X

Arab J Sci Eng
DOI 10.1007/s13369-018-3402-0

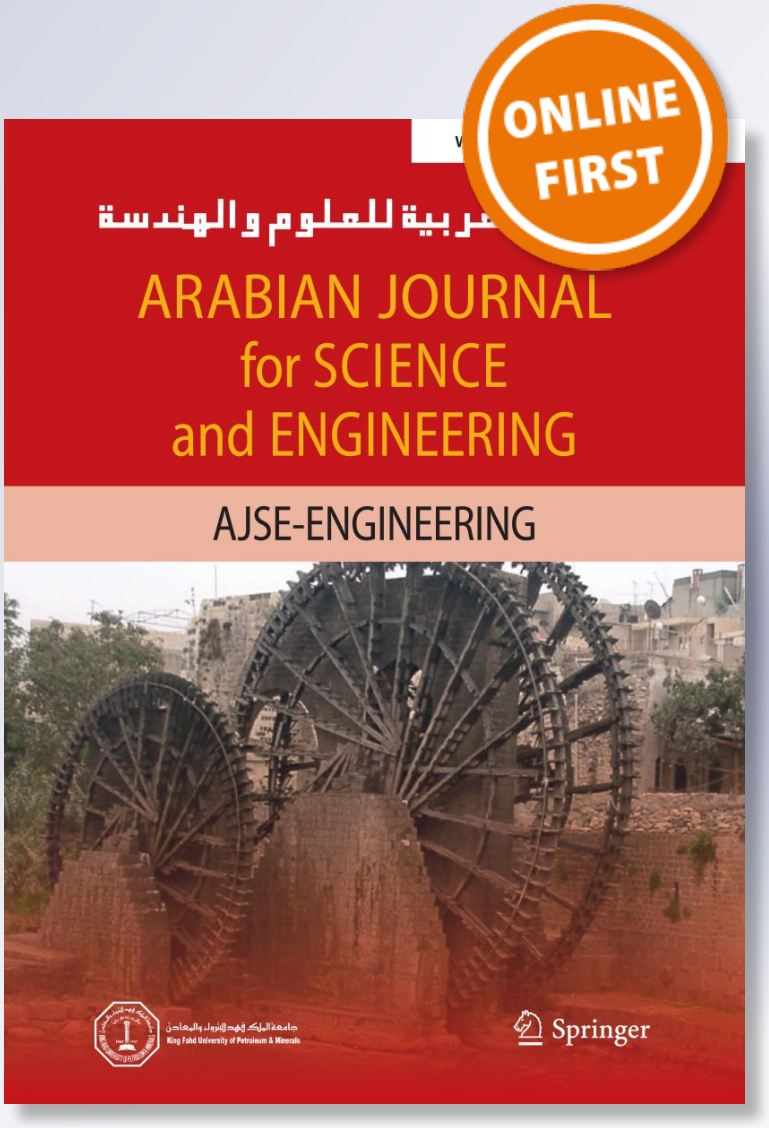

Springer

Arabian Journal for Science and Engineering
https://doi.org/10.1007/s13369-018-3402-0

RESEARCH ARTICLE - PHYSICS

Humidity Sensitive Flexible Microwave Absorbing Sheet Using Polyaniline–Polytetrafluoroethylene Composite

Nees Paul[1,2] · Sreedevi P. Chakyar[1] · K. S. Umadevi[3,4] · Simon K. Sikha[1] · Joe Kizhakooden[1,2] · Jolly Andrews[1] · V. P. Joseph[1]

Received: 9 March 2018 / Accepted: 7 June 2018

Abstract
Pelletized or powdered polyaniline composite, a potential candidate for microwave absorbers, was synthesized in the sheet form for the first time, and its absorption characteristics along with structural, electrical and mechanical properties are presented. Enhanced microwave absorption behavior of this novel, thin, flexible, lightweight sheet in hydrous environment was analyzed for various humidity-dependent sensor and electromagnetic applications. The preparation method of protonated chlorine-doped polyaniline (PANI), and its synthesis in the sheet form using polytetrafluoroethylene (PTFE) are discussed. The surface and structural morphology were characterized by XRD and SEM, which reveal the granular, macro-porous and polycrystalline structure of the material. A transmission–reflection-based waveguide technique was used for obtaining the permittivity of sheets in the frequency range of 3–9 GHz by employing the Nicholson–Ross algorithm, and it was verified by cavity perturbation method. The temperature stability of the PANI–PTFE conducting sheet was checked using four-probe method. Conductivity enhancement of the sheet in hydrous environment was studied using a humidity chamber. The microwave absorption studies at various humidity conditions were carried out using waveguide method which also illustrated its potentiality as a humidity sensor. The mechanical strength of the proposed conducting polymer sheet was tested by standard load–extension procedure. To make this PANI–PTFE polymer material suitable for anechoic chamber-like applications, it was impregnated in polyurethane foam and its humidity-related microwave absorption studies were carried out using free space method.

Keywords Flexible composites · Polyaniline · Microwave absorber · Humidity sensor

1 Introduction

Microwave absorbers were of great importance even during the initial stages of research and development of electromagnetic devices and diversification of their applications. Nowadays, the relevance and the importance of these absorbers have increased manifold due to the exponential increase in the types and quality of electromagnetic gadgets. Owing to the high density of electromagnetic (EM) users added care has to be taken for avoiding the issues related to electromagnetic interference (EMI), which is of prime importance in communication systems and in various industrial, scientific, and medical (ISM) applications. Another major concern is health hazard confusions related to overexposure of microwave radiations which demand some sort of protective measures for the safe use of these advanced technologies. Such scenario demands intense research for the development of novel type of microwave absorbers having added advantages over conventional types in order to address the emerging issues related to state-of-the-art microwave technology.

Microwave absorbers are broadly classified based on the principle of electromagnetic absorption caused by conductivity and electric/magnetic losses owing to its hysteresis nature. The boundary mismatch, a major concern in connection with any type of microwave absorbers can be tailored

✉ V. P. Joseph
drvpjo@gmail.com

1 Department of Physics, Christ College (Autonomous), University of Calicut, Thrissur, Kerala, India

2 Department of Physics, St. Thomas' College (Autonomous), University of Calicut, Thrissur, Kerala, India

3 Department of Physics, Newman College, Mahatma Gandhi University, Thodupuzha, Kerala, India

4 Department of Electronics, Prajyothi Nikethan College, University of Calicut, Thrissur, Kerala, India

Published online: 22 June 2018

by proper adjustment of permittivity (ε) and permeability (μ) and also by using various trigonometric shapes for the absorbing medium [1]. Most commonly used absorbents are carbonyl ions (e.g., carbon black, graphite powders, carbon nanoparticles) [2,3] and ferrites [4–6] usually mixed inside the polymers like plastic and rubber made in different variants like sheet and foam [1,7]. Polyurethane and polystyrene are widely used foam-type material as microwave absorber in 1–40 GHz region [8,9]. Carbon with neoprene binders is normally used nowadays to prepare microwave absorber foams for anechoic chambers [10–12]. Another group of cost-effective microwave absorbers for the range of 1–20 GHz are proposed by different researchers which uses agricultural wastes and rice husk in pyramidal and sheet forms, respectively. Though these absorbers are lightweight, they are rigid and require complicated synthesis process [13,14].

Another class of microwave absorbers use conducting polymers as the matrix in which different dielectric and magnetic fillers are added for enhancing the absorption characteristics. Some of the commonly used absorbents are barium titanate ($BaTiO_3$) [15–17], strontium ferrites [18], erium oxide (Er_2O_3) [19], iron-nickel alloy (NiFe) [20] and silicon carbides [21] which find wide range of applications in broadband microwave absorption and shielding. Development of these materials has opened up an entirely new dimension of polymer technology which finds uses in various fields like dynamic pH-sensing in micro-fluidic devices [22], amperometric cholesterol and alcohol biosensors [23,24], electrochemical microsensors [25] and super capacitor applications [26–28]. These polymers are also proposed in flexible forms like graphene sheet (GS)/polyaniline nanofiber composite [29] and free-standing graphene with polyaniline [30] which may find application in the development of low-cost electrode materials for storage devices. These conducting polymer composites are ideal for situations requiring high-degree microwave absorption levels. They have added advantages of selecting absorption levels and frequency ranges by suitable choice of fillers.

For moderate absorption purposes, conducting polymers can be used without any dielectric or magnetic fillers [31–33]. Polyaniline (PANI) and polypyrroles (PPy) are two such stable conducting polymers proposed to have applications in microwave shields and absorbers. Troung et al. [34] proposed a moderate conductivity tunable microwave absorber for use at 12–18 GHz where added care has to be taken to protect the original fiber shape of the polypyrrole. John et al. [35] proposed conducting polyaniline as a choice for microwave absorber and analyzed the environmental stability and absorption characteristics. The conductivity and the complex permittivity of polyaniline are analyzed in detail for pelletized and powdered form for selected frequencies [36].

In this paper, we present a self-standing, lightweight and flexible polyaniline-based microwave absorber in the form of a thin sheet. It shows enhanced microwave absorption properties in comparison with already reported powder and pellet forms of polyaniline. This novel polycrystalline sheet was prepared from polyaniline by embedding it in polytetrafluoroethylene (PTFE) matrix. It shows an added characteristic of high sensitivity to humidity-based microwave absorption. Absorption characteristic studies of this polyaniline-based foam-type microwave absorber are also presented.

2 Methods and Measurements

2.1 Material Preparation

Protonated chlorine-doped polyaniline was prepared by the standard chemical oxidation method [35,37,38]. Polyaniline in powder form was synthesized at room temperature from aniline in the presence of 1 M ammonium peroxydisulphate (APS) as oxidant, and 1 M HCl as dopant in the ratio 1:6:12 and polymerization continued for 5 h. The filtrate was then washed with acetone and diluted HCl solutions to remove the unreacted aniline and was air-dried to get polyaniline powder.

In order to prepare polyaniline-based microwave absorber sheet, this conducting polymer powder was used as filler in PTFE matrix. The lightweight PTFE adhesive was chosen as matrix to provide flexibility and to enhance the conductivity of PANI due to the closer arrangement of constituent particles. For this, the polyaniline powder (in gm) was dispersed in de-mineralized water (in ml) in the ratio 1:10 in a ultrasonicator. 7 wt% of polytetrafluoroethylene in aqueous solution was added to the above mixture and stirred for 1 h using a magnetic stirrer, and the suspension was filtered. The filtrate was air-dried at room temperature and ground to fine powder using a mortar. By adding a few drops of isopropyl alcohol, it was made into dough which was rolled into PANI–PTFE hybrid flexible sheets. During the synthesis of the sheet, it was observed that the increase or the decrease in the wt% of the PTFE in solution taken reduces the feasibility of transforming the composite into sheet form. Two such sheets of 0.4 and 0.9 mm were prepared by the above procedure. Figure 1 shows the photograph of PANI–PTFE hybrid sheet of thickness 0.9 mm.

Since many ISM applications prefer foam-type microwave absorbers, polyaniline-based foam sheets were also synthesized. Finely crushed 2 gm of polyaniline powder was dispersed in a mixture of 10 ml distilled water and 7 wt% PTFE solution. Then, it was continuously stirred for 1 h to get uniform PANI–PTFE dispersion which acts as a dielectric filler inside the foam. Polyurethane foam of 25 cm × 25 cm × 2.5 cm dimension was then impregnated with the above dispersion and air-dried at room temperature to obtain PANI–PTFE foam-type microwave absorber.

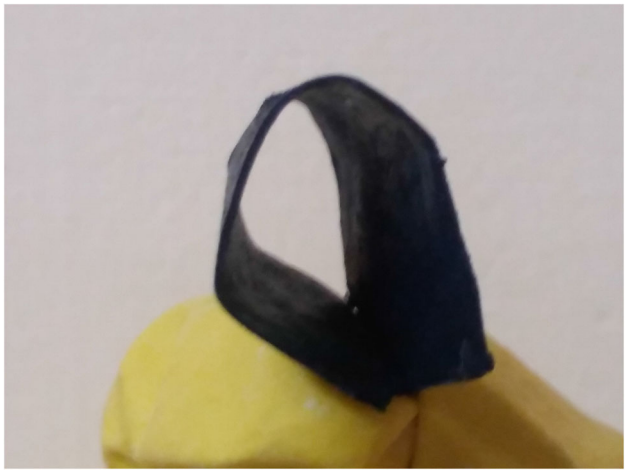

Fig. 1 Photograph of polyaniline–polytetrafluoroethylene (PANI–PTFE) hybrid sheet of thickness 0.9 mm

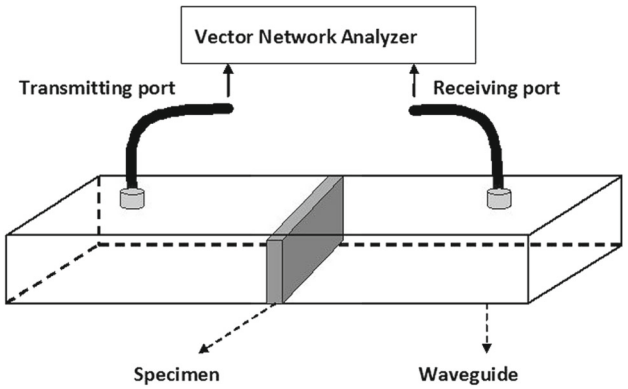

Fig. 2 Waveguide setup for measuring the transmission (S_{21}) and reflection (S_{11}) coefficients of polyaniline powder and PANI–PTFE hybrid sheets

2.2 Measurement Techniques

The microwave absorption characteristics of the PANI–PTFE hybrid sheet was analyzed at room temperature and room humidity by evaluating its permittivity from the reflection and the transmission coefficients which were obtained by waveguide method. Measurements were taken for polyaniline in powder form also. The absorption power level was normalized to 0 dB before taking measurements. For powdered sample, this procedure was done by keeping low loss polyvinylchloride (PVC) sample holders with a filling space of thickness 3 mm inside the rectangular waveguide. The same procedure was repeated for powdered sample with filling space of 5 mm also. In the case of PANI–PTFE hybrid sheet, two samples of thickness 0.4 and 0.9 mm were used. In both cases, the sample was placed inside the waveguide covering the entire cross section with the plane of absorber perpendicular to the propagation direction. The transmission (S_{21}) and reflection (S_{11}) coefficients of the samples were done in 3–9 GHz frequencies using suitable waveguide sections connected to a Vector Network Analyzer (VNA). Figure 2 represents a schematic diagram of the experimental setup.

Since polyaniline is a conducting non-magnetic material, its effective permeability (μ_r) is assumed to be 1. The real and imaginary parts of the permittivity were calculated from the hybrid parameters using Nicholson–Ross Algorithm [39–45] with the help of equations

$$\frac{\mu_r}{\varepsilon_r} = \left(\frac{1+\Gamma}{1-\Gamma}\right)^2 \tag{1}$$

and

$$\mu_r \varepsilon_r = -\left[\frac{c}{\omega d} ln\left(\frac{1}{P}\right)\right]^2 \tag{2}$$

where d is the thickness of the sample, ω is the angular frequency, P is the propagation factor, Γ is the reflection coefficient, and c is the velocity of light. The results obtained were verified using standard cavity perturbation technique [36].

The humidity sensitive microwave absorption properties of the PANI–PTFE were analyzed by taking the S_{21} curve for various humidity conditions. For this, a rectangular humidity chamber was constructed using perspex sheet and humidity was regulated using an atomizer-circulating fan setup. The possible changes in the D.C. conductivity in relation to various humidity conditions were measured by keeping the sheet inside a humidity chamber setup as shown in Fig. 3. For microwave absorption studies at different relative humidity (RH) values between 30 and 90%, the PANI–PTFE sheet was immediately shifted from the humidity chamber to the microwave setup and S_{21} curves were taken. To analyze the temperature stability of the newly fabricated sheet, conductivity–temperature study was carried out using standard four-probe method.

The surface morphology of the sheet was investigated using Scanning Electron Microscope (SEM, JSM-6390LA). Crystalline nature of the PANI powder and PANI–PTFE sheet samples was analyzed using XRD equipped with CuK_α ($\lambda = 1.54$ Å). Mechanical strength and the Young's modulus of the prepared PANI–PTFE were evaluated using the conventional load–extension technique. Microwave absorption characteristics of PANI–PTFE foam was analyzed using free space method by placing the foam in between two wide-band standard gain horn antennas connected to VNA [46]. Photograph of the experimental setup placed inside an anechoic test box is given in Fig. 4.

3 Results and Discussion

SEM images of hybrid sheet show macro-porous structure with clusters of PANI–PTFE granules. Figure 5 depicts the

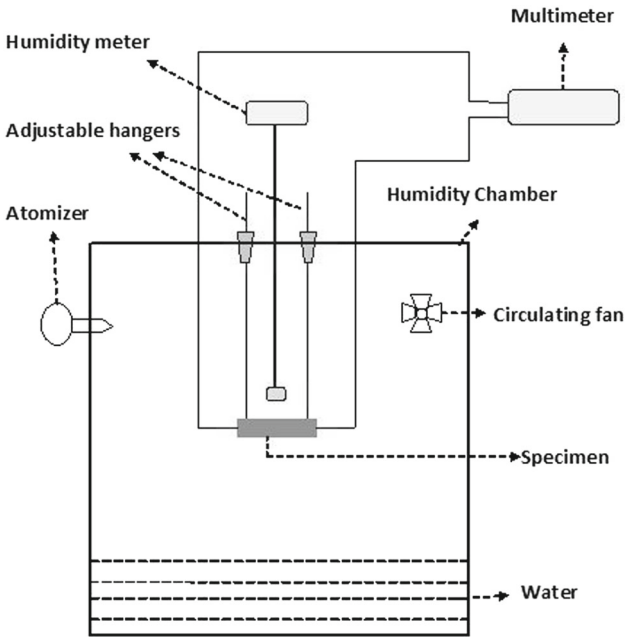

Fig. 3 Pictorial representation of atomizer-circulating fan setup for humidity varying measurements

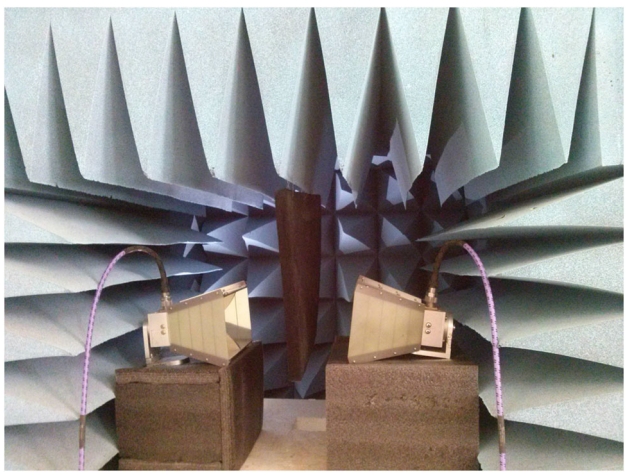

Fig. 4 Free space measurement setup of PANI–PTFE foam-type absorber

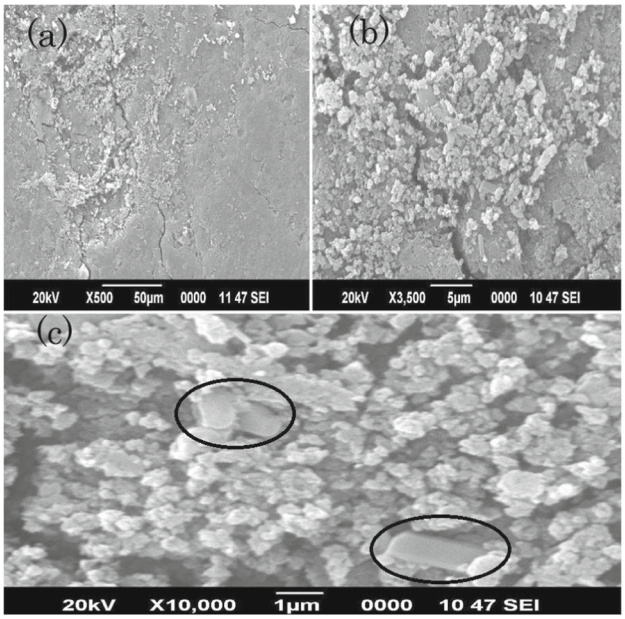

Fig. 5 SEM images of PANI–PTFE hybrid sheet of thickness 0.9 mm at different resolutions **(a, b, c)**, where unglued PTFE granules are shown within elliptical rings **(c)**

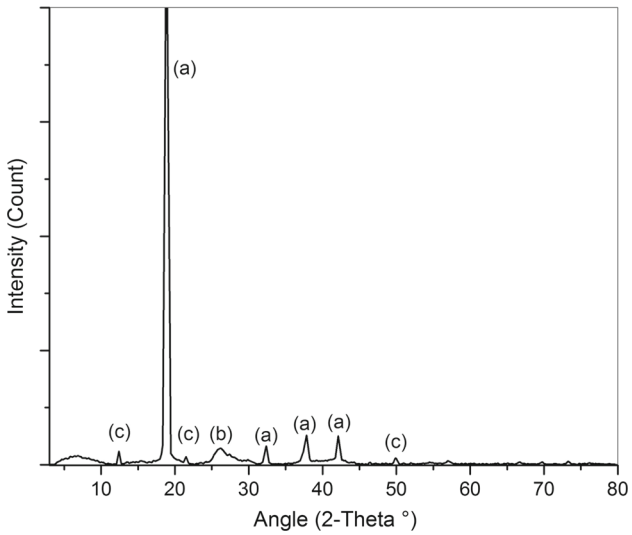

Fig. 6 X-ray diffraction pattern of PANI–PTFE hybrid sheet

images obtained for a sample of thickness 0.9 mm. The cylinder-shaped inclusions seen scattered in Fig. 5c are the unglued molecules of PTFE.

The XRD pattern of polyaniline powder shows it as amorphous in nature [47–49], while PTFE shows neither a fully amorphous nor a fully crystalline structure [50–52]. The insertion of PANI into PTFE matrix was examined by XRD and Fig. 6 shows the spectra of PANI–PTFE conducting polymer sheet. The spectrum shows a polycrystalline structure due to the presence of peaks marked as 'a' at angles (2θ) 18.869°, 32.396°, 37.835° and 42.108° with spacing (d) 4.70055, 2.76133, 2.37595 and 2.14420 Å, respectively which is due to the presence of PTFE [50,51]. The broad peak marked as 'b' at an angle 26.5° in the spectrum is due to the PANI [47,48]. The binding process of PANI with PTFE is also resulted in other peaks marked as 'c' at angles 12.401°, 21.509° and 49.914° with spacing 7.13174, 4.12805 and 1.82563 Å, respectively, depicts the enhanced crystalline nature.

Conductivity property of the prepared sheets was analyzed using four-probe method, and variation of conductivity with temperature is given in Fig. 7. The graph shows relatively steady conductance around room temperature (305 K)

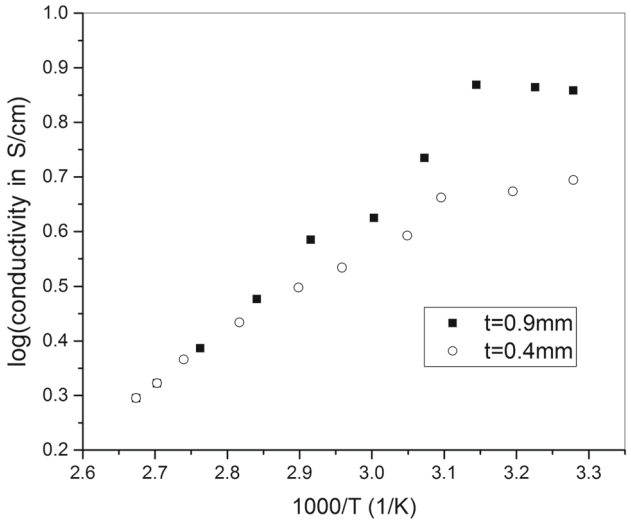

Fig. 7 Conductivity–temperature curve of PANI–PTFE sheet of 0.9 and 0.4 mm thickness measured using four-probe setup at 30% RH

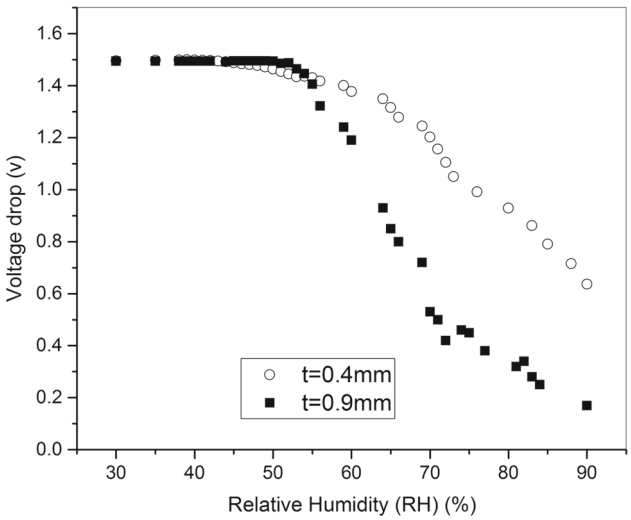

Fig. 8 Humidity response on the voltage drop measured between two points of 1 cm apart for the PANI–PTFE hybrid sheet of 0.9 and 0.4 mm thickness at 30 °C

for both samples and shows gradual decrease in conductivity with increase in temperature, which clearly indicates the conducting behavior for our PANI–PTFE sheets. However, the thick sheet ($t = 0.9$ mm) shows higher conductivity at low temperatures compared to thin sheet ($t = 0.4$ mm) as expected. The conductivity dependence on humidity in terms of voltage drop was measured for both sheets and is depicted in Fig. 8. It is quite evident from the graph that as relative humidity increases beyond 50% RH, the conductivity of both sheets shows marked enhancement. From the figure, it is clear that for the thick sheet voltage drop is lower than the thin sheet for higher humidity values owing to the lower resistance of the thick sample.

Table 1 Readings from cavity perturbation method

Parameters	Frequency (GHz) at	
	7.869	8.784
Real part of permittivity (ε')	3.449	3.2478
Imaginary part of permittivity (ε'')	1.4007	0.6659
Conductivity (σ), S/m	0.6129	0.3254
Skin depth (ρ), m	0.0073	0.0094
Dielectric heating coefficient, J	0.7139	1.5017
Absorption coefficient	136.9863	106.383

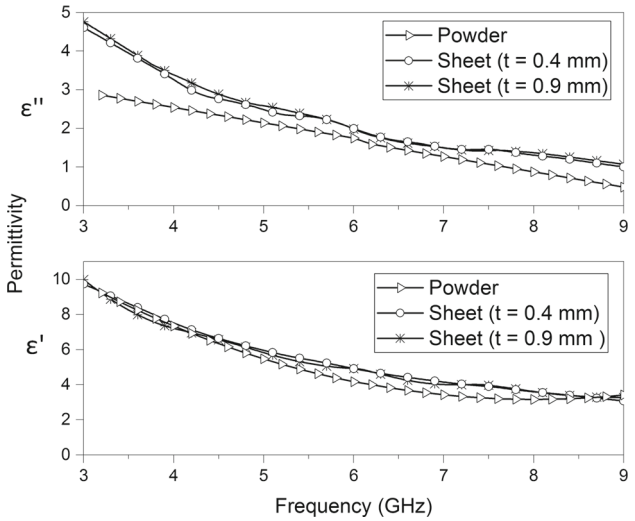

Fig. 9 Real (ε') and imaginary (ε'') parts of permittivity of polyaniline powder and PANI–PTFE hybrid sheets

The real and imaginary parts of permittivity of the polyaniline powder and PANI–PTFE sheets of thickness $t = 0.4$ mm and $t = 0.9$ mm were evaluated using Nicholson–Ross algorithm [Eqs. (1) and (2)] and are given in Fig. 9. Both parts of permittivity show gradual decrease with frequency. There is a difference for the permittivity between powder and sheet forms for both real and imaginary components. The difference due to the thickness of the sheet is observed to be negligible. The variation for imaginary part of the permittivity between powder and sheet form is noticeably high in the lower and higher frequencies of the experimental region, whereas for the real part this deviation is observed in the intermediate frequency regions. This markable variation in the imaginary part of permittivity is indicative of the prepared sheets ability to show more conductivity which may enhance its microwave absorption properties. The permittivity values were also verified for the PANI–PTFE hybrid sheet ($t = 0.9$ mm) using cavity perturbation method for selected frequencies and values obtained are given in Table 1. Table 1 also shows some other related parameters like conductivity, skin depth, dielectric heating and absorption coefficients which were also obtained by the cavity method.

The microwave absorption studies of the PANI–PTFE hybrid sheets of thickness $t = 0.4$ mm and $t = 0.9$ mm were studied for dry and wet forms by measuring its reflection and transmission coefficients for frequency range 3–9 GHz. The dry sheet is at room humidity of 30% RH and wet one is at high humidity level of 90% RH. Figure 10a, b shows S_{11} and S_{21} obtained for thickness $t = 0.4$ mm, whereas Fig. 10c, d shows the results for $t = 0.9$ mm. It is evident from Fig. 10a, c that S_{11} values show a slight increase in reflection with increase in frequency. Both wet and dry sheets irrespective of thickness show the same results indicating that reflection mainly depends on the surface smoothness and not on the thickness and the moisture condition of the sheet. From Fig. 10b, d, following inferences can be drawn. As the frequency increases, the average absorption level decreases, but not in a linear manner. The absorption level is observed to be dependent on thickness of the sheet more prominently on the upper half of the experimental frequency band. In both cases, we find an enhanced absorption for the wet sheets which clearly indicate a higher microwave absorption property of the humid sheet. For the thin sheet ($t = 0.4$ mm), the difference between the absorption levels of the wet and dry sheets is around 3 dB at lower frequency region (3–6 GHz), whereas at higher frequency region (6–9 GHz) it is around 12 dB. But in the case of thick sheets, the difference between the wet and dry sheet is around 6 dB irrespective of the interacting frequency. The potentiality of using this PANI–PTFE hybrid polymer sheet as a good choice of microwave absorbing material is quite evident from the above figure. Increase in thickness and humidity of the PANI–PTFE sheets results to a good extent in the enhancement of microwave absorption which may be useful in various electromagnetic absorbing and shielding applications. The possibility of metallic inclusions during preparation of PANI–PTFE sheets can be explored for further enhancement of absorption levels.

For analyzing the flexibility of our newly formed PANI–PTFE sheet, the elasticity in terms of Young's modulus Y was calculated from its load–extension graph (Fig. 11) and the average value (loading–unloading) was found to be around 4.5 GN/m^2. This value is in the range of a typical nylon fiber which makes our hybrid sheet flexible as well as a durable one for different applications.

In order to use newly formulated PANI–PTFE material as a novel microwave absorber in applications like anechoic chamber, we examined the absorption characteristics of PANI–PTFE impregnated inside the polyurethane foam. The transmission coefficients obtained for the dry (30% RH) and humid (90% RH) conditions measured using free space method is presented in Fig. 12. A noticeable increase in

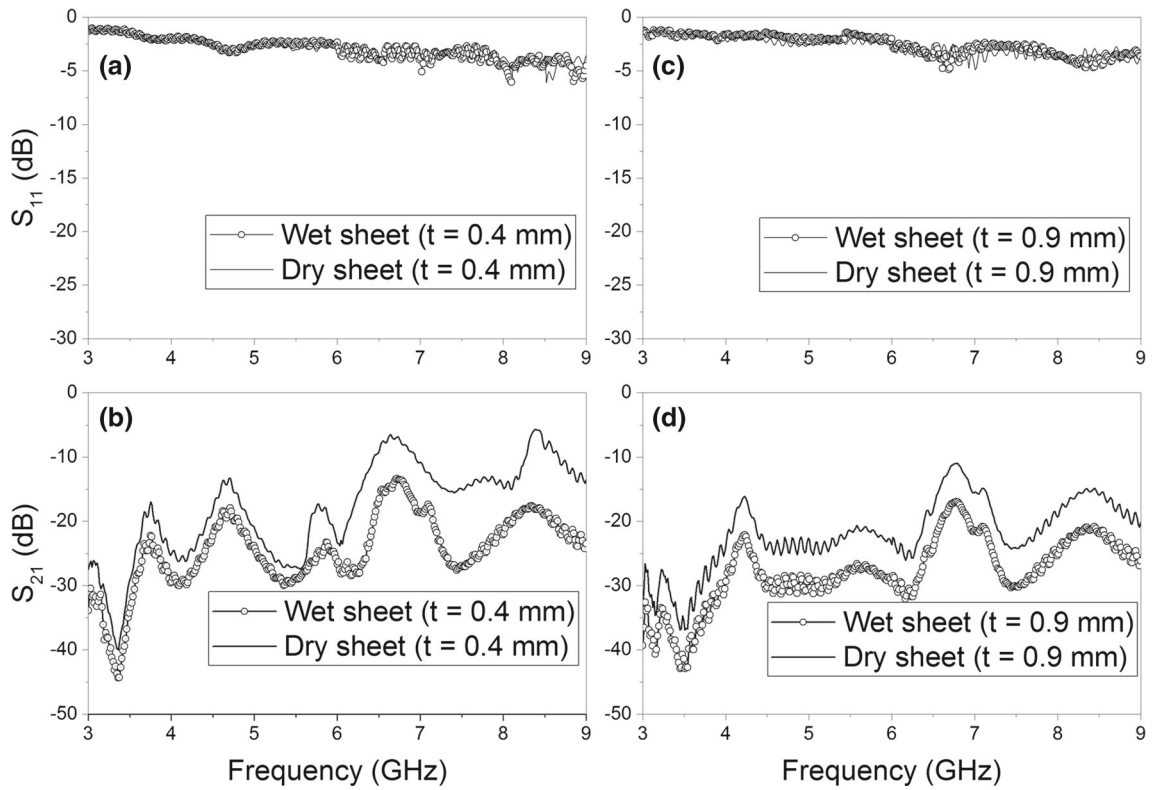

Fig. 10 Transmission (S_{21}) and reflection coefficients (S_{11}) of PANI–PTFE hybrid sheets of different thickness at different humid conditions in 3–9 GHz frequency range. **a**, **c** S_{11} for $t = 0.4$ and 0.9 mm, respectively, **b**, **d** S_{21} for $t = 0.4$ and 0.9 mm, respectively

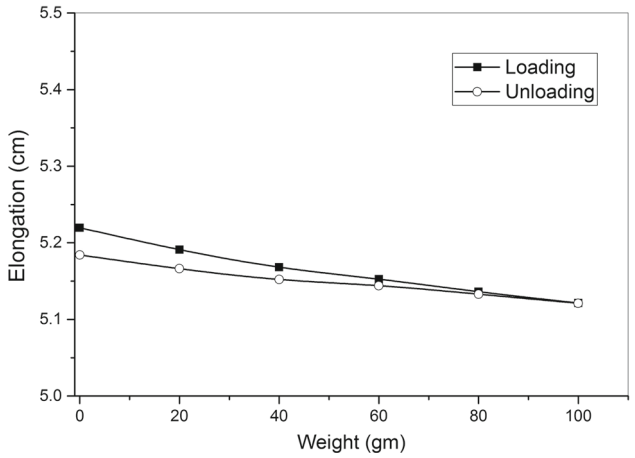

Fig. 11 Load–extension graph for PANI–PTFE hybrid sheet of dimension 6.8 cm × 1.5 cm × 0.13 cm

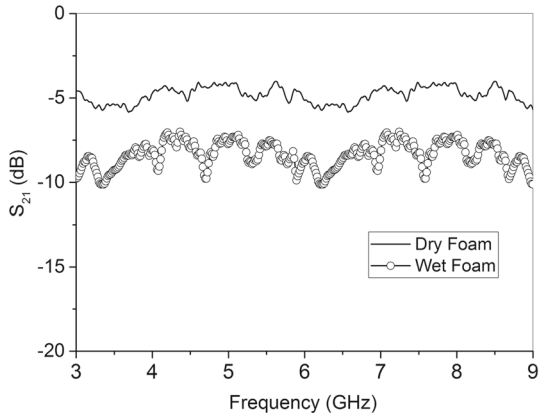

Fig. 12 Plot of transmission (S_{21}) coefficient of PANI–PTFE embedded foam in dry (30% RH) and humid (90% RH) conditions

absorption level of around 5 dB for the wet foam in the entire frequency range is observed.

4 Conclusions

Polyaniline–polytetrafluoroethylene (PANI–PTFE) hybrid sheet synthesized had a polycrystalline structure. This thin, flexible and lightweight sheet had excellent microwave absorption characteristics along with an added property of showing marked variation in absorption level with different humidity content, which makes this sheet an ideal candidate for humidity-based microwave sensors and other electromagnetic applications. The studies on mechanical strength and temperature stability of this PANI–PTFE sheet predict that it is suitable for state-of-the-art microwave technology. This cost-effective microwave absorber was also fabricated in thick foam form which makes it suitable for anechoic chamber-type applications.

References

1. Vinayasree, S.; Soloman, M.; Sunny, V.; Mohanan, P.; Kurian, P.; Joy, P.; Anantharaman, M.: Flexible microwave absorbers based on barium hexaferrite, carbon black, and nitrile rubber for 2–12 GHz applications. J. Appl. Phys. **116**(2), 024902 (2014)
2. Feng, Y.; Qiu, T.; Shen, C.: Absorbing properties and structural design of microwave absorbers based on carbonyl iron and barium ferrite. J. Magn. Magn. Mater. **318**(1), 8 (2007)
3. Kim, J.B.; Lee, S.K.; Kim, C.G.: Comparison study on the effect of carbon nano materials for single-layer microwave absorbers in X-band. Compos. Sci. Technol. **68**(14), 2909 (2008)
4. Cho, H.S.; Kim, S.S.: M-hexaferrites with planar magnetic anisotropy and their application to high-frequency microwave absorbers. IEEE Trans. Magn. **35**(5), 3151 (1999)
5. Kwon, H.; Shin, J.; Oh, J.: The microwave absorbing and resonance phenomena of y-type hexagonal ferrite microwave absorbers. J. Appl. Phys. **75**(10), 6109 (1994)
6. Shin, J.; Oh, J.: The microwave absorbing phenomena of ferrite microwave absorbers. IEEE Trans. Magn. **29**(6), 3437 (1993)
7. Chai, C.H.: Design a high performance absorber to improve an anechoic chamber performance. Ph.D. thesis, Universiti Malaysia Sarawak, UNIMAS (2010)
8. Kumar Srivastava, R.; Narayanan, T.; Reena Mary, A.; Anantharaman, M.; Srivastava, A.; Vajtai, R.; Ajayan, P.M.: Ni filled flexible multi-walled carbon nanotube-polystyrene composite films as efficient microwave absorbers. Appl. Phys. Lett. **99**(11), 113116 (2011)
9. Nornikman, H., Soh, P.J., Azremi, A.A.H., Anuar, M.: In: Third Asia International Conference on Modelling and Simulation, AMS'09 (IEEE, 2009), pp. 649–654 (2009)
10. Emerson, W.: Electromagnetic wave absorbers and anechoic chambers through the years. IEEE Trans. Antennas Propag. **21**(4), 484 (1973)
11. Severin, H.: Nonreflecting absorbers for microwave radiation. IRE Trans. Antennas Propag. **4**(3), 385 (1956)
12. Simmons, A.; Emerson, W.: In: 1958 IRE International Convention Record, vol. 1 (IEEE, 1966) pp. 34–41 (1966)
13. Kaur, R.; Aul, G.D.; Chawla, V.: Improved reflection loss performance of dried banana leaves pyramidal microwave absorbers by coal for application in anechoic chambers. Prog. Electromagn. Res. **43**, 157 (2015)
14. Nornikman, H., Malek, F., Soh, P.J., Azremi, A.H.: In: Antennas and Propagation Conference (LAPC), 2010 Loughborough (IEEE, 2010). pp. 313–316 (2010)
15. Meshram, M.; Agrawal, N.K.; Sinha, B.; Misra, P.: Characterization of m-type barium hexagonal ferrite-based wide band microwave absorber. J. Magn. Magn. Mater. **271**(2), 207 (2004)
16. Ohlan, A.; Singh, K.; Chandra, A.; Dhawan, S.: Microwave absorption properties of conducting polymer composite with barium ferrite nanoparticles in 12.4–18 GHz. Appl. Phys. Lett. **93**(5), 053114 (2008)
17. Sugimoto, S.; Haga, K.; Kagotani, T.; Inomata, K.: Microwave absorption properties of ba m-type ferrite prepared by a modified coprecipitation method. J. Magn. Magn. Mater. **290**, 1188 (2005)
18. Verma, A.; Mendiratta, R.; Goel, T.; Dube, D.: Microwave studies on strontium ferrite based absorbers. J. Electroceram. **8**(3), 203 (2002)
19. Zhang, L.; Zhu, H.; Song, Y.; Zhang, Y.; Huang, Y.: The electromagnetic characteristics and absorbing properties of multi-walled carbon nanotubes filled with Er 2 O 3 nanoparticles as microwave absorbers. Mater. Sci. Eng. B **153**(1), 78 (2008)
20. Park, K.Y.; Han, J.H.; Lee, S.B.; Kim, J.B.; Yi, J.W.; Lee, S.K.: Fabrication and electromagnetic characteristics of microwave

absorbers containing carbon nanofibers and nife particles. Compos. Sci. Technol. **69**(7), 1271 (2009)
21. Liu, X.; Zhang, Z.; Wu, Y.: Absorption properties of carbon black/silicon carbide microwave absorbers. Compos. B Eng. **42**(2), 326 (2011)
22. Florea, L.; Fay, C.; Lahiff, E.; Phelan, T.; O'Connor, N.E.; Corcoran, B.; Diamond, D.; Benito-Lopez, F.: Dynamic pH mapping in microfluidic devices by integrating adaptive coatings based on polyaniline with colorimetric imaging techniques. Lab Chip **13**(6), 1079 (2013)
23. Matharu, Z.; Sumana, G.; Arya, S.K.; Singh, S.; Gupta, V.; Malhotra, B.: Polyaniline Langmuir–Blodgett film based cholesterol biosensor. Langmuir **23**(26), 13188 (2007)
24. Sharma, H.: Conducting polymers: polyaniline, its state of the art and applications. Ph.D. thesis, Thapar Institute of Engineering and Technology, Deemed University, Punjab (2006)
25. Bo, Y.; Yang, H.; Hu, Y.; Yao, T.; Huang, S.: A novel electrochemical DNA biosensor based on graphene and polyaniline nanowires. Electrochim. Acta **56**(6), 2676 (2011)
26. Fan, W.; Zhang, C.; Tjiu, W.W.; Pramoda, K.P.; He, C.; Liu, T.: Graphene-wrapped polyaniline hollow spheres as novel hybrid electrode materials for supercapacitor applications. ACS Appl. Mater. Interfaces **5**(8), 3382 (2013)
27. Salunkhe, R.R.; Hsu, S.H.; Wu, K.C.; Yamauchi, Y.: Large-scale synthesis of reduced graphene oxides with uniformly coated polyaniline for supercapacitor applications. ChemSusChem **7**(6), 1551 (2014)
28. Zhang, K.; Zhang, L.L.; Zhao, X.; Wu, J.: Graphene/polyaniline nanofiber composites as supercapacitor electrodes. Chem. Mater. **22**(4), 1392 (2010)
29. Spinks, G.M.; Dominis, A.J.; Wallace, G.G.; Tallman, D.E.: Electroactive conducting polymers for corrosion control. J. Solid State Electrochem. **6**(2), 85 (2002)
30. Belaabed, B.; Wojkiewicz, J.L.; Lamouri, S.; El Kamchi, N.; Lasri, T.: Synthesis and characterization of hybrid conducting composites based on polyaniline/magnetite fillers with improved microwave absorption properties. J. Alloys Compd. **527**, 137 (2012)
31. Naishadham, K.; Kadaba, P.K.: Measurement of the microwave conductivity of a polymeric material with potential applications in absorbers and shielding. IEEE Trans. Microw. Theory Tech. **39**(7), 1158 (1991)
32. Wang, Y.; Jing, X.: Intrinsically conducting polymers for electromagnetic interference shielding. Polym. Adv. Technol. **16**(4), 344 (2005)
33. Wong, P.; Chambers, B.; Anderson, A.; Wright, P.: Large area conducting polymer composites and their use in microwave absorbing material. Electron. Lett. **28**(17), 1651 (1992)
34. Truong, V.T.; Riddell, S.; Muscat, R.: Polypyrrole based microwave absorbers. J. Mater. Sci. **33**(20), 4971 (1998)
35. John, H.; Thomas, R.M.; Jacob, J.; Mathew, K.; Joseph, R.: Conducting polyaniline composites as microwave absorbers. Polym. Compos. **28**(5), 588 (2007)
36. Kumar, S.B.; Hohn, H.; Joseph, R.; Hajian, M.; Ligthart, L.; Mathew, K.: Complex permittivity and conductivity of poly aniline at microwave frequencies. J. Eur. Ceram. Soc. **21**(15), 2677 (2001)
37. Adams, P.; Laughlin, P.; Monkman, A.; Kenwright, A.: Low temperature synthesis of high molecular weight polyaniline. Polymer **37**(15), 3411 (1996)
38. Gilbert, R.; Stejskal, J.: Polyaniline, preparation of a conducting polymer (IUPAC technical report). Pure Appl. Chem. **74**(5), 857 (2002)
39. Baker-Jarvis, J.; Vanzura, E.J.; Kissick, W.A.: Improved technique for determining complex permittivity with the transmission/reflection method. IEEE Trans. Microw. Theory Tech. **38**(8), 1096 (1990)
40. Chen, X.; Grzegorczyk, T.M.; Wu, B.I.; Pacheco Jr., J.; Kong, J.A.: Robust method to retrieve the constitutive effective parameters of metamaterials. Phys. Rev. E **70**(1), 016608 (2004)
41. Ghodgaonkar, D.K.; Varadan, V.V.; Varadan, V.K.: A free-space method for measurement of dielectric constants and loss tangents at microwave frequencies. IEEE Trans. Instrum. Meas. **38**(3), 789 (1989)
42. Ghodgaonkar, D.; Varadan, V.; Varadan, V.: Free-space measurement of complex permittivity and complex permeability of magnetic materials at microwave frequencies. IEEE Trans. Instrum. Meas. **39**(2), 387 (1990)
43. Seo, I.S.; Chin, W.S.; et al.: Characterization of electromagnetic properties of polymeric composite materials with free space method. Compos. Struct. **66**(1–4), 533 (2004)
44. Smith, D.R.; Schultz, S.; Markoš, P.; Soukoulis, C.: Determination of effective permittivity and permeability of metamaterials from reflection and transmission coefficients. Phys. Rev. B **65**(19), 195104 (2002)
45. Weir, W.B.: Automatic measurement of complex dielectric constant and permeability at microwave frequencies. Proc. IEEE **62**(1), 33 (1974)
46. Seo, I.S.; Chin, W.S.; et al.: Characterization of electromagnetic properties of polymeric composite materials with free space method. Compos. Struct. **66**(1), 533 (2004)
47. Deng, S.; Li, G.: Structural features and microwave absorbing propertiesof polyaniline-montmorillonite composites prepared by in-situ. J. Fiber Bioeng. Inform. **6**(1), 33 (2013)
48. Luo, J.; Xu, Y.; Yao, W.; Jiang, C.; Xu, J.: Synthesis and microwave absorption properties of reduced graphene oxide-magnetic porous nanospheres-polyaniline composites. Compos. Sci. Technol. **117**, 315 (2015)
49. Pant, H.; Patra, M.; Negi, S.; Bhatia, A.; Vadera, S.; Kumar, N.: Studies on conductivity and dielectric properties of polyaniline–zinc sulphide composites. Bull. Mater. Sci. **29**(4), 379 (2006)
50. D'Amorim, R.; Teixeira, M.I.; Caldas, L.V.E.; Souza, S.O.: Physical, morphological and dosimetric characterization of the Teflon agglutinator to thermoluminescent dosimetry. J. Lumin. **136**, 186 (2013)
51. Rae, P.J.; Dattelbaum, D.M.: The properties of poly(tetrafluoroethylene) (PTFE) in compression. Polymer **45**(22), 7615 (2004)
52. Mishra, R.; Tripathy, S.; Dwivedi, K.; Khathing, D.; Ghosh, S.; Müller, M.; Fink, D.: Effect of electron irradiation on polytetrafluoro ethylene. Radiat. Meas. **37**(3), 247 (2003)

Microwave absorption properties of flexible zinc oxide sheet

Cite as: AIP Conference Proceedings **2162**, 020070 (2019); https://doi.org/10.1063/1.5130280
Published Online: 29 October 2019

Nees Paul, Janet Jimmy, Sreedevi P. Chakyar, Sikha K. Simon, Joe Kizhakooden, C. Bindu, Anju Sebastian, K. S. Umadevi, Jovia Jose, Jolly Andrews, and V. P. Joseph

Microwave Absorption Properties of Flexible Zinc Oxide Sheet

Nees Paul[1, 2], Janet Jimmy[2], Sreedevi P Chakyar[1], Sikha K Simon[1], Joe Kizhakooden[1, 2], C. Bindu[1,3], Anju Sebastian[1], K. S. Umadevi[4], Jovia Jose[1,5], Jolly Andrews[1] and V. P. Joseph[1, a)]

[1]*Christ College (Autonomous), Irinjalakuda, Thrissur, University of Calicut, Kerala, 680125, India.*
[2]*St. Thomas' College (Autonomous), Thrissur, University of Calicut, Kerala, 680001, India.*
[3]*Govt. College, Chittur, Palakkad, University of Calicut, Kerala, 678104, India.*
[4]*Prajyothi Nikethan College, Pudukad, Thrissur, University of Calicut, Kerala, 680301, India.*
[5]*Vimala College (Autonomous), Cheroor, Thrissur, University of Calicut, Kerala, 680009, India*

[a)]Corresponding author: vpj@christcollegeijk.edu.in

Abstract. This paper presents the fabrication and microwave absorption properties of low-cost flexible light-weight zinc oxide (ZnO) sheet. The elastomers, films and foams used as microwave absorbers are made of lossy materials impregnated on low density matrixes which are thicker, heavier and expensive in wide frequency ranges. The prepared ZnO sheet in polytetrafluoroethylene (PTFE) matrix and isopropyl alcohol (IPA) as binder is characterized using XRD which showed the crystalline structure of ZnO in the sample. The microwave characterization is done using waveguide method by placing the sheet samples of different thickness (1 mm and 2 mm) perpendicular to the direction of propagation of power inside the rectangular wave-guides with operating frequency ranges of 5 - 7 GHz and 7 - 9 GHz connected to a Vector Network Analyzer (VNA). Transmission (S_{21}) and reflection (S_{11}) coefficients are analyzed in the above frequency ranges. The reflection coefficients show no remarkable variation throughout the measured frequency range whereas the transmission coefficients exhibit noticeable drop in the transmitted power around 5 - 15 dB at certain frequencies. As the thickness of the sample increases, the absorption level also increases. The absorption of microwave power is observed to be maximum at 8 - 9 GHz frequency range. Absorption properties of conducting ZnO sheet may find applications in the design of novel type of microwave absorbers.

INTRODUCTION

Research and development of microwave absorbers are of great importance in various electromagnetic gadgets and applications which may have immense industrial and technological prospects. The relevance and the importance of these absorbers have renewed the interest in the selection and fabrication of materials for the realization of these frequency selective surfaces of high quality. The health related hazards associated with the tremendous increase of electromagnetic (EM) machineries in various ISM (industrial, scientific, and medical) applications have led to a greater demands of advanced technologies. So high quality microwave absorbers with advances in device processing methods can address the above issues related to state-of-the-art microwave technology.

The conductivity and electric/magnetic losses owing to the hysteresis nature of the absorbing material is mainly used to characterize the quality of microwave absorbers. Proper tailoring of electromagnetic parameters like permittivity (ε) and permeability (μ) can fuel and fan the boundary mismatch, which is a major concern in connection with any type of microwave absorber [1]. Carbonyl ions, ferrites and conductive polymers are now-a-days used as reliable absorbent materials for sheet type microwave absorbers [2, 3, 4, 5, 6, 7]. The use of agricultural wastes and rice husk in pyramidal and sheet forms respectively had also been proposed by researchers, but they are rigid and require complicated synthesis process [8, 9].

Proceedings of the International Conference on Advanced Materials
AIP Conf. Proc. 2162, 020070-1–020070-4; https://doi.org/10.1063/1.5130280
Published by AIP Publishing. 978-0-7354-1907-0/$30.00

Recently scientific community has considered zinc oxide (ZnO) as a 'future material' with potential applications in piezoelectric transducers, varistors, phosphors and transparent conducting films [10]. ZnO also affords superior radiation hardness enhancing the usefulness of this material for space applications [11, 12].

In this paper we present a self-standing, lightweight and flexible zinc oxide based microwave absorber for the first time in the form of a thin sheet. It shows enhanced microwave absorption properties in the specific frequency regions. This sheet is prepared from zinc oxide by embedding it in polytetrafluoroethylene (PTFE) matrix with isopropyl alcohol (IPA) binder. The sheet is characterized using XRD which revealed the crystalline nature of ZnO in the sample. The microwave characterization is done using waveguide method [13] by placing the sheet samples of different thickness (1 mm and 2 mm) parallel to the plane of electric field vector inside rectangular waveguides which is excited with a TE_{10} with operating frequency ranges of 5 - 7 GHz and 7 - 9 GHz connected to a Vector Network Analyzer (VNA). ZnO, which is a transparent conducting oxide, are ideal for situations requiring high degree of microwave absorption levels with added advantages of frequency selective properties.

EXPERIMENTAL

In order to prepare ZnO based microwave absorber sheet, this transparent conducting oxide powder is used as filler in polytetrafluoroethylene (PTFE) matrix [2]. The light weight PTFE adhesive is chosen as matrix to provide flexibility. The ZnO powder (in gm) and de-mineralized water (in ml) is mixed in an ultrasonicator in the ratio of 1:10. PTFE (7 wt. %) in aqueous solution is added to the above mixture which is magnetically stirred for around one hour and is then filtered. The air dried filtrate is then ground to fine powder with help of a mortar. Using a few drops of IPA, the filtrate is made into dough which is then rolled to form ZnO sheets [2]. Two such sheets of thicknesses 1 mm and 2 mm are prepared by the above procedure. Figure 1 shows the photograph of flexible ZnO sheet of thickness 2 mm.

FIGURE 1. Photograph of flexible zinc oxide sheet of thickness 2 mm.

MEASUREMENT TECHNIQUES

The microwave absorption characteristics of the ZnO sheet are analyzed at room temperature by evaluating the transmission and reflection coefficients which are obtained by waveguide method. By calibration the absorption power level is normalized to 0 dB before taking measurements. Here ZnO sheet of thickness 1 mm and 2 mm are

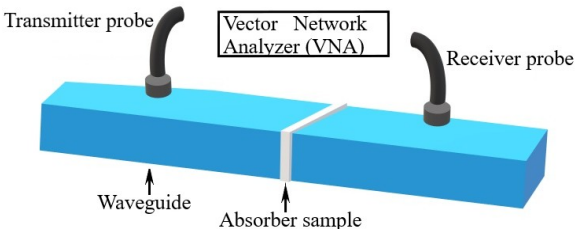

FIGURE 2. Schematic diagram of experimental set up, for the measurement of transmission and reflection coefficients, using waveguide method showing the ZnO sheet specimen.

used. In both cases, the sample is placed inside the waveguide covering the entire cross section with the plane of sheet perpendicular to the direction of propagation. The transmission (S_{21}) and reflection (S_{11}) coefficients of the samples are taken from 5 - 9 GHz frequencies using suitable waveguide to coaxial adapters connected to a Vector Network Analyzer (VNA). Figure 2 represents a schematic diagram of the experimental set up with the absorber sheet sample. Crystalline nature of the ZnO sheet sample is analyzed using XRD equipped with CuK_{α} ($\lambda = 1.54\ A^0$).

RESULTS AND DISCUSSIONS

The crystalline nature of ZnO powder is already established [14]. After the insertion of ZnO in PTFE matrix the XRD is taken and Fig. 3 shows the spectra of the sample. The ZnO sheet maintains the crystalline structure showing the peaks as in ZnO powder. All the distinct peaks observed for ZnO sheet matches with that of ZnO powder (JCPDS #043-0002) except the one at an angle around 18^0 corresponds to PTFE (JCPDS #47-2217) [15, 16].

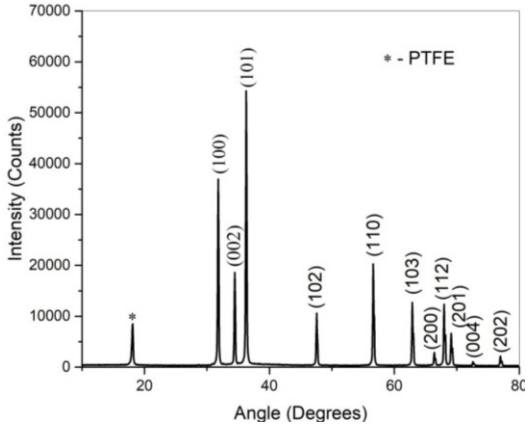

FIGURE 3. X-ray diffraction pattern of zinc oxide sheet with peaks indexed.

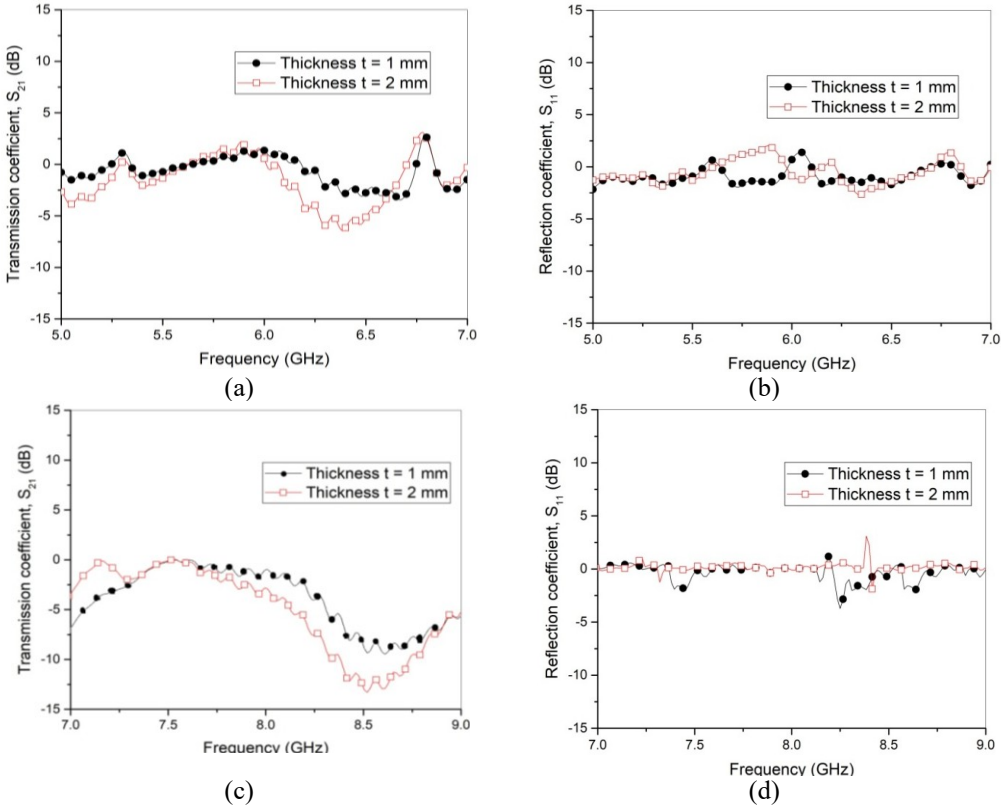

FIGURE 4. Transmission (S_{21}) and reflection coefficients (S_{11}) of ZnO sheets of different thickness at different frequency ranges[(a) & (b) in 5 - 7 GHz and (b) & (d) in 7 – 9 GHz].

CONCLUSION

The proposed zinc oxide (ZnO) sheet is thin, flexible and lightweight which has excellent microwave absorption characteristics. The frequency selective absorption properties of this sheet find applications in band stop filters and for other EMI (electromagnetic interference) applications. The low and high temperature electrical stability of ZnO extend its potentiality to use in any climatic conditions. This suggests that ZnO is an ideal candidate which can be used as an efficient microwave absorbing material.

REFERENCES

1. Vinayasree, S., M. A. Soloman, Vijutha Sunny, P. Mohanan, Philip Kurian, P. A. Joy, and M. R. Anantharaman, Jour. of Appl. Phys. **116**(2), 024902 (2014).
2. Paul Nees, Sreedevi P. Chakyar, K. S. Umadevi, Simon K. Sikha, Joe Kizhakooden, Jolly Andrews, and V. P. Joseph, AJSE, **44**(1), 553-560 (2019).
3. Sunny, Vijutha, Philip Kurian, P. Mohanan, P. A. Joy, and M. R. Anantharaman, Jour. of Alloys and Compounds, **489**(1), 297-303 (2010).
4. Akman, O., H. Kavas, A. Baykal, Muhammet S. Toprak, Ali Çoruh, and B. Aktaş, Jour. of Magnetism and Magnetic Materials, **327**, 151-158 (2013).
5. Kwon, H. J., J. Y. Shin, and J. H. Oh., Jour. of Appl. Phys **75**(10), 6109-6111(1994).
6. Park, Ki-Yeon, Jae-Hung Han, Sang-Bok Lee, Jin-Bong Kim, Jin-Woo Yi, and Sang-Kwan Lee, Composites Science and Technology, **69**(7- 8), 1271-1278 (2009).
7. Sugimoto, Satoru, S. Kondo, Kaori Okayama, H. Nakamura, David Book, Toshio Kagotani, M. Homma, H. Ota, M. Kimura, and R. Sato,IEEE Transactions on Magnetics, **35**(5), 3154-3156 (1999).
8. Nornikman, Hassan, Mohd Fareq Bin Abd Malek, Ping Jack Soh, Azremi Abdullah Al-Hadi, Fwen Hoon Wee, and A. Hasnain. Piers, 145-166 (2010).
9. Nornikman, H., P. J. Soh, A. A. H. Azremi, F. H. Wee, and M. F. Malek, Piers Online, **5**(6), (2009).
10. Coleman, V. A., and C. Jagadish, Zinc oxide bulk, thin films and nanostructures (Elsevier Science Ltd, 2006), pp. 1-20.
11. Xu, P. S., Y. M. Sun, C. S. Shi, F. Q. Xu, and H. B. Pan, Nuclear Instruments and Methods in Physics Research Section B: Beam Interactions with Materials and Atoms, **199**, 286-290 (2003).
12. Pearton, S. J., D. P. Norton, K. Ip, Y. W. Heo, and T. Steiner, Journal of Vacuum Science & Technology B: Microelectronics and Nanometer Structures Processing, Measurement, and Phenomena, **22**(3), 932-948 (2004).
13. Chen, Lin-Feng, C. K. Ong, C. P. Neo, V. V. Varadan, and Vijay K. Varadan, Microwave electronics: measurement and materials characterization, (John Wiley & Sons, 2004), pp. 452 - 454.
14. Xu HaiYan, Hao Wang, YongCai Zhang, WenLiang He, ManKang Zhu, Bo Wang, and Hui Yan. Ceramics International, **30**(1), 93-97 (2004).
15. Nason, T. C., J. A. Moore, and T-M. Lu. Appl. Phys. Letters, **60**(15), 1866-1868 (1992).
16. Rae P. J., and D. M. Dattelbaum, Polymer, **45**(22), 7615-7625 (2004).

13th International Congress on Artificial Materials for Novel Wave Phenomena - Metamaterials 2019
Rome, Italy, Sept. 16$^{\text{th}}$ - Sept. 21$^{\text{th}}$ 2019
doi:10.1109/MetaMaterials.2019.8900920

Thin Film Metamaterial Split Ring Resonators at Microwave Frequencies

Nees Paul[1,2], Sikha K. Simon [1], Bindu C.[1,3], Jolly Andrews[1] and V. P. Joseph[1]

[1] Dept. of Physics, Christ College (Autonomous), University of Calicut, Thrissur, 680125, Kerala, India.
[2]Dept. of Physics, St.Thomas' College (Autonomous), University of Calicut, Thrissur, 680001, Kerala, India.
[3]Dept. of Physics, Government College, University of Calicut, Chittur, 678104, Kerala, India.
jmalieckkal123@gmail.com

Abstract – **In this paper we present a metamaterial Split Ring Resonator (SRR) made of thin films of nanometer thickness working in microwave frequencies. Since the thickness of nano-film used for fabricating metamaterial structures is below the skin depth, unique resonance behavior is observed in comparison to the resonance curves of its conventional counterpart made with thick films. At thickness less than skin depth, the film becomes resistive which in turn results in a wide band magnetic resonance. Silver thin film resonators of thickness 350 nm, 550 nm and 750 nm prepared on glass substrates using RF sputtering technique are used for the study. Absorption characteristics of the SRR and Broad-side Coupled SRR (BCSRR) are analyzed.**

I. Introduction

This era has witnessed intense research in thin film technologies to meet the need for miniaturization and quality enhancement of devices and gadgets. Metamaterials, owing to their exotic and unique characteristics, are extending their applications into diverse fields of technology searching for new horizons in the state of the art. In this paper, we report a new addition to the metamaterial resonators realized using thin films working in microwave frequencies.

The highly conducting metals like silver, gold and copper are mainly used for making SRRs so as to produce maximum magnetic resonance in the system[1, 2]. Here we discuss the resonance properties of metallic Split Ring Resonators (SRRs) made with silver thin films of thickness below the skin depth. The films are prepared by RF sputtering technique and the transmission spectra of this novel resonator is measured using Vector Network Analyzer (VNA) in the frequency range of 3 - 9 GHz.

II. Materials and methods

The thin film silver SRRs of different thickness are prepared using RF magnetron sputtering technique. The glass substrate is cleaned using traditional cleaning techniques with ultrasonic bath and isopropyl alcohol. Then one side of the oven-dried slide is covered with high temperature resistant kapton tape. The resonator structure is then stenciled on the tape and is then fixed in the sample holder of the sputtering chamber facing the target. The silver target used is 50 mm diameter and 99.99% pure. The plasma was activated by a 13.56 MHz RF power of 25 W in argon pressure of 3 X 10^{-3} Torr with argon flow of 20 sccm. After coating, the mask (kapton tape) is carefully removed to get the ring resonators on the glass substrate. SRR and BCSRR structures of thickness 350 nm, 550 nm and 750 nm in square shape are prepared using this technique by varying the sputtering duration. Figure 1 gives the photograph of thin film SRR fabricated on a glass substrate. For the BCSRR, rings are fabricated on both sides of glass substrate of thickness 1.3 mm. The resonators are then placed between the monopole antennas connected to the transmitting and receiving probes of a Vector Network Analyzer (VNA) for the transmission measurement[3, 4].

doi:10.1109/MetaMaterials.2019.8900920

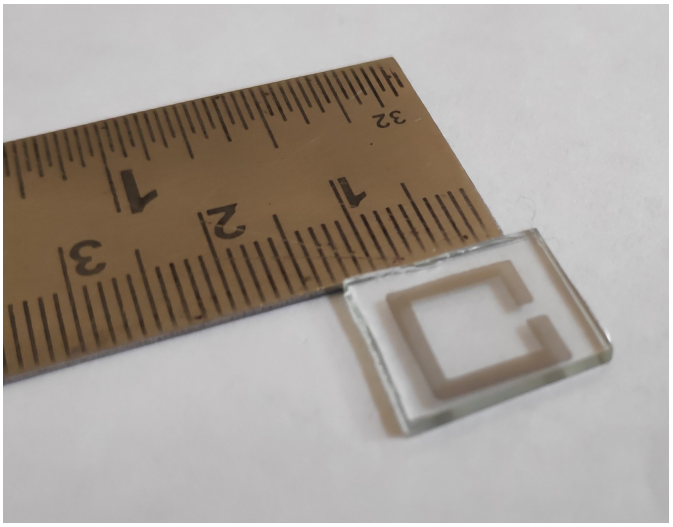

Fig. 1: Photograph of the thin film SRR fabricated on a glass substrate.

III. Results and Discussions

The magnetic resonance in SRRs are analyzed from the transmission spectra obtained from VNA. The resonance absorption spectra of SRRs of different thickness are presented in Fig. 2. As the thickness of the film increases, the frequency shifts toward the lower values. It is quite evident from the graph that resonance curve is of wide-band nature owing to the resistive nature of the resonator due to the lowering of thickness below skin depth, which is around 1 μm at the resonating frequency. We also observe a shift in resonant frequency towards higher end as the thickness decreases which may be due to the increase of the evanescent field with the corresponding reduction in thickness. For thicknesses beyond the skin depth the resonance frequency remains the same with a reduced narrow bandwidth owing to the disappearance of observed resistive component. Figure 3 shows the transmission spectra for the BCSRR made using thickness t = 750 nm along with the resonance observed for its single ring. We observe a reasonable shift in resonance frequency for the BCSRR in comparison with the resonant frequency of its single ring due to the mutual coupling between the rings.

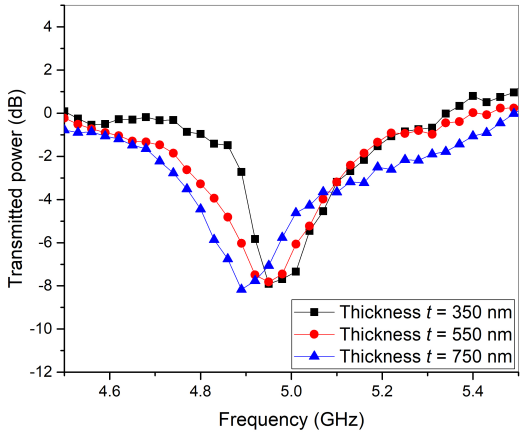

Fig. 2: Magnetic resonance in single square ring SRRs of different thicknesses t of 350 nm, 550 nm and 750 nm respectively made on glass substrate with dimensions - length l= 10 mm, width w = 2 mm and split width s = 1 mm.

doi:10.1109/MetaMaterials.2019.8900920

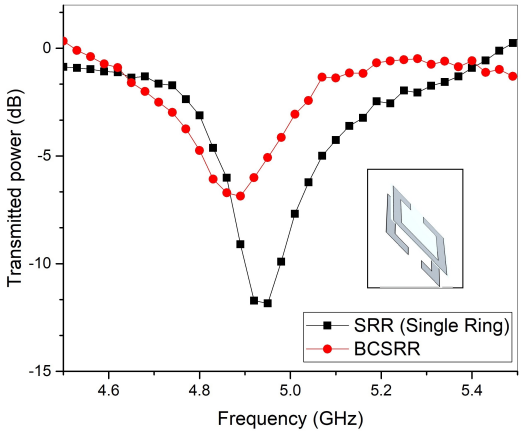

Fig. 3: Magnetic resonance in BCSRR of thickness t = 750 nm made on glass substrate with dimensions length l = 10 mm, width w = 2 mm, split width s = 1 mm and separation between rings d = 1.3 mm along with the resonance curve for a single SRR with same values of l, w and s.

IV. Conclusion

Thin film metamaterial Split Ring Resonator structure working at microwave frequency is fabricated for the first time and its resonant behavior is analyzed. It is observed that this novel SRR made in nanometer thickness, a value lower than the skin depth, exhibits wide band resonance characteristics. Since the accompanying evanescent wave component is higher for this type of SRR, the possibility of actualizing ultra sensitive sensors can be realized using this novel SRR. This resonant structure exhibits all the advantages of thin film technology such as miniaturization, enhanced quality etc. and hence it may find a lot of potential applications in various microwave related fields.

Acknowledgement

Sikha K. Simon wish to acknowledge the financial support from the Government of India through UGC Maulana Azad National Fellowship (MANF).

References

[1] H. Guo, N. Liu, L. Fu, T.P. Meyrath, T. Zentgraf, H. Schweizer, H. Giessen, "Resonance hybridization in double split-ring resonator metamaterials," *Optics express* vol. 15(19),p. 12095, 2007.

[2] R. Marqués, F. Mesa, J. Martel, F. Medina,"Comparative analysis of edge- and broadside- coupled split ring resonators for metamaterial design - theory and experiments," *IEEE Transactions on antennas and propagation*, vol. 51(10), p. 2572, 2003.

[3] Chakyar SP, K Simon S, Bindu C, Andrews J, Joseph V,"Complex permittivity measurement using metamaterial split ring resonators",*Journal of Applied Physics*, vol. 121(5),p.054101, 2017.

[4] Umadevi K, Chakyar SP, Simon SK, Andrews J, Joseph V, "Split ring resonators made of conducting wires for performance enhancement",*EPL (Europhysics Letters)*, vol. 118(2), p.24002, 2017.

13th International Congress on Artificial Materials for Novel Wave Phenomena - Metamaterials 2019
Rome, Italy, Sept. 16$^{\text{th}}$ - Sept. 21$^{\text{th}}$ 2019
doi:10.1109/MetaMaterials.2019.8900824

Metamaterial Split Ring Resonators made of Polyaniline - polytetrafluoroethylene at Microwave Frequencies

Nees Paul[1,2], **Joe Kizhakooden**[1,2], **Jovia Jose** [1,3] **Jolly Andrews**[1] **and V. P. Joseph**[1]

[1] Dept. of Physics, Christ College (Autonomous), University of Calicut, Thrissur, 680125, Kerala, India.
[2]Dept. of Physics, St.Thomas' College (Autonomous), University of Calicut, Thrissur, 680001, Kerala, India.
[3]Dept. of Physics, Vimala College (Autonomous), University of Calicut, Thrissur, 680009, Kerala, India.
neeslinto@gmail.com

***Abstract* – We present the observance of magnetic resonance for the first time in Split Ring Resonators (SRRs) made of polyaniline - based conducting polymer and verify our experimental result through simulation. The magnetic resonance behavior of Closed Ring Resonator (CRR) and SRR of polyaniline - polytetrafluoroethylene (Pani - PTFE) are presented. The humidity sensitive conducting Pani - PTFE ring behaves like low loss conducting ring with wide-band magnetic resonance whereas the CRR does not show any resonant response as is expected. The results are analyzed using simulation studies for copper rings of similar dimensions. Magnetic resonance observed in Broad-side Coupled Split Ring Resonator (BCSRR) made of Pani - PTFE is also presented, highlighting its role in metamaterial based applications. Realization of metamaterial resonating structures using conducting polymers opens a new realm with immense possibilities in microwave and terahertz technologies.**

I. INTRODUCTION

Conducting polymers has emerged as one of the key areas of research during the last decade in the field of electromagnetic sensors and absorbers. Apart from using conducting polymers for slightly modifying the environmental conditions of the Split Ring Resonator (SRR), no other works are seen reported in the literature[1]. In this work, for the first time, we have fabricated the metamaterial based Broad-side Coupled Split Ring Resonator (BCSRR) structure using polyaniline - polytetrafluoroethylene (Pani - PTFE) conducting polymer and have analyzed its magnetic resonance behavior. This paper also addresses the observance of the widening of resonance curve in relation to the comparatively less conductivity of the proposed polymer with respect to the conventional metallic resonators. During the course of development of BCSRR, we have also analyzed the magnetic resonant behavior of Closed Ring Resonator (CRR) and SRR fabricated using conducting polymer. Experimental results are verified using high frequency simulation software and excellent agreement are observed.

II. MATERIALS AND METHODS

For metallic resonators, the inductive contribution of the resonant frequency exclusively depends on the conduction current flowing through the ring. But since Pani - PTFE is a material having lower conductivity, the displacement current term which is a property of dielectric counterpart of the resonator should also be included in the calculation of the resonant frequency. The effective length of the resonating ring l_1 along with the resonant frequency Ω are given[2] by

$$l_1 = \ln[8R/r] - 7/4 \tag{1}$$

$$\Omega = \omega_o\sqrt{1 + 2\varepsilon k} \tag{2}$$

where ω_o is given by

$$\omega_0^2 = 2c^2/\varepsilon r^2 l_1 \tag{3}$$

doi:10.1109/MetaMaterials.2019.8900824

where c is the velocity of light, ε permittivity of the material of the ring, R outer radius of the ring, r inner radius of the ring, s is the split spacing and $k = s/2\pi R$.

The preparation process of Pani - PTFE conducting polymer used for fabricating SRRs is described below. Protonated chlorine doped polyaniline (Pani) is formed from aniline and ammonium peroxydisulphate (APS) using a chemical oxidation method. The powdered polyaniline is then made to a sheet form by mixing it in the matrix polytetrafluoroethylene (PTFE) so as to form polyaniline - polytetrafluoroethylene (Pani - PTFE) hybrid sheet[3]. The prepared sheets possessing greater conductivity in humid conditions are then cut into rings of specific dimensions. The schematic representation of the experimental set up along with the photograph of prepared Pani- PTFE sheet together with the drawings of CRR, SRR and BCSRR are shown in Fig. 1. In order to determine the resonant behavior, the polymer resonator is placed between the transmitting and receiving probes connected to a Vector Network Analyzer (VNA).

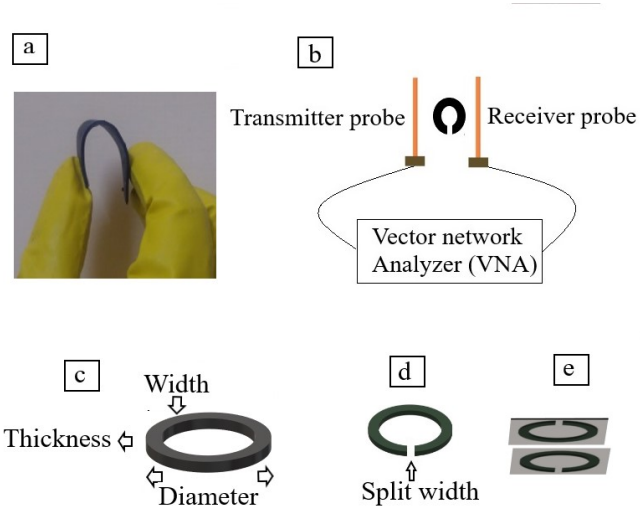

Fig. 1: (a) Photograph of the prepared Pani- PTFE conducting polymer sheet; (b) schematic representation of the resonant frequency measurement setup; (c), (d) and (e) labeled diagram of CRR, SRR and BCSRR.

III. Results and discussions

Figure 2 shows the experimental magnetic resonance curves obtained for SRR and CRR of circular geometry made of Pani - PTFE along with the simulation results. The simulated result of the circular copper ring with the same dimension is also shown in the figure for comparison. The wide-band resonance behavior of the Pani - PTFE ring in comparison with its metallic counterpart is due to the lower conductivity of the polymer. A small shift in the resonance frequency between Pani - PTFE and copper ring may be explained in terms of the higher contribution of displacement current due to the non-ignorable dielectric behavior of Pani - PTFE material (Eq. 1, 2 and 3). The absence of magnetic resonance for CRR is also noticed.

Figure 3 shows the resonant frequency curve of Pani - PTFE BCSRR along with the resonance of individual rings used to construct this resonator. Similar to a metallic BCSRR, the resonance frequency of Pani - PTFE resonator is shifted to the lower frequency region due to the coupling effects. The reason for slight enhancement in power above 0 dB for experimental resonance curves of Fig. 2 and 3 needs further investigation.

IV. Conclusion

In this work, we have presented a novel type of metamaterial resonator made of conducting polymer Pani - PTFE. We investigated the resonances in single ring SRR made from conducting polymer. The presence of magnetic resonance in the structure is confirmed using CRR resonance. By coupling two rings suitably, a metamaterial

doi:10.1109/MetaMaterials.2019.8900824

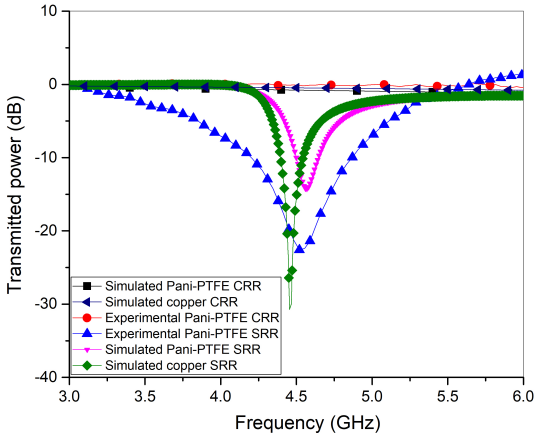

Fig. 2: Simulated and experimental resonant curves of copper and Pani-PTFE CRR and SRR rings of diameter 10 mm, width 1 mm, thickness 3 mm and split width 1 mm.

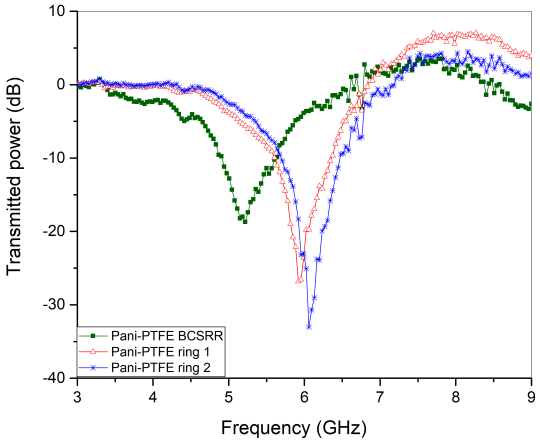

Fig. 3: Magnetic resonances observed in Pani - PTFE BCSRR of dimensions diameter 10 mm, width 1 mm, thickness 1 mm, split width 0.35 mm and separation between the rings 1 mm.

BCSRR structure is materialized and its resonance curves are analyzed in terms of lower conductivity and displacement current effects. Since the proposed material has humidity dependent conductivity properties, this new SRR can have added advantage in humidity sensing applications. The magnetic response of this polymer with tunable conductivity makes it a new candidate for the realization of left-handed materials with attractive features.

REFERENCES

[1] M. Mayy, G. Zhu, Y.A. Barnakov, M. Noginov, "Development of composite silver-polymer metamaterials, "*Journal of Applied Physics* vol. 105(8), p. 084318, 2009

[2] A. Shvartsburg, V.Y. Pecherkin, L. Vasilyak, S. Vetchinin, V. Fortov,"Resonant microwave fields and negative magnetic response, induced by displacement currents in dielectric rings: theory and the first experiments," *Scientific reports*,vol 7(1),p. 2180, 2017

doi:10.1109/MetaMaterials.2019.8900824

[3] N. Paul, S.P. Chakyar, K. Umadevi, S.K. Sikha, J. Kizhakooden, J. Andrews, V. Joseph,"Humidity Sensitive Flexible Microwave Absorbing Sheet Using PolyanilinePolytetrafluoroethylene Composite," Arabian Journal for Science and Engineering, vol 44(1), p. 553, 2018